

INFORMATION TO USERS

This manuscript has been reproduced from the microfilm master. UMI films the text directly from the original or copy submitted. Thus, some thesis and dissertation copies are in typewriter face, while others may be from any type of computer printer.

The quality of this reproduction is dependent upon the quality of the copy submitted. Broken or indistinct print, colored or poor quality illustrations and photographs, print bleedthrough, substandard margins, and improper alignment can adversely affect reproduction.

In the unlikely event that the author did not send UMI a complete manuscript and there are missing pages, these will be noted. Also, if unauthorized copyright material had to be removed, a note will indicate the deletion.

Oversize materials (e.g., maps, drawings, charts) are reproduced by sectioning the original, beginning at the upper left-hand corner and continuing from left to right in equal sections with small overlaps. Each original is also photographed in one exposure and is included in reduced form at the back of the book.

Photographs included in the original manuscript have been reproduced xerographically in this copy. Higher quality 6" x 9" black and white photographic prints are available for any photographs or illustrations appearing in this copy for an additional charge. Contact UMI directly to order.

UMI

A Bell & Howell Information Company
300 North Zeeb Road, Ann Arbor MI 48106-1346 USA
313/761-4700 800/521-0600

University of Alberta

Fractionation of Nylon Fibres

by

Xiaocai (Joyce) Chen



**A thesis submitted to the Faculty of Graduate Studies and Research in partial fulfillment
of the requirement for the degree of**

Master of Science

Department of Chemical and Material Engineering

Edmonton, Alberta

Spring 1998



**National Library
of Canada**

**Acquisitions and
Bibliographic Services**

395 Wellington Street
Ottawa ON K1A 0N4
Canada

**Bibliothèque nationale
du Canada**

**Acquisitions et
services bibliographiques**

395, rue Wellington
Ottawa ON K1A 0N4
Canada

Your file Votre référence

Our file Notre référence

The author has granted a non-exclusive licence allowing the National Library of Canada to reproduce, loan, distribute or sell copies of this thesis in microform, paper or electronic formats.

The author retains ownership of the copyright in this thesis. Neither the thesis nor substantial extracts from it may be printed or otherwise reproduced without the author's permission.

L'auteur a accordé une licence non exclusive permettant à la Bibliothèque nationale du Canada de reproduire, prêter, distribuer ou vendre des copies de cette thèse sous la forme de microfiche/film, de reproduction sur papier ou sur format électronique.

L'auteur conserve la propriété du droit d'auteur qui protège cette thèse. Ni la thèse ni des extraits substantiels de celle-ci ne doivent être imprimés ou autrement reproduits sans son autorisation.

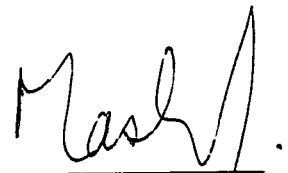
0-612-28927-3

Canada

University of Alberta

Faculty of Graduate Studies and Research

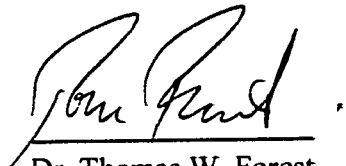
The undersigned certify that they have read, and recommend to the Faculty of Graduate Studies and Research for acceptance, a thesis entitled Fractionation of Nylon Fibres by Xiaocai (Joyce) Chen in partial fulfillment of the requirement for the degree of Master of Science.



Dr. Jacob H. Masliyah
(Supervisor)



Dr. Philip A. J. Mees



Dr. Thomas W. Forest

**This thesis is dedicated to my dear husband Mr. Wei Li and my parents Mrs. Shizhong
Zhou and Mr. Wenrui Chen for their endless love and encouragement**

ABSTRACT

The objective of this study was to determine whether fibre fractionation is due to difference in fibre length or diameter. Nylon fibres, having the same diameter but different lengths of 1 mm and 3 mm, were used in the fractionation study. Two fractionation methods were used: a vertical settler and a rotating cone fractionator.

Based on theoretical analysis, a vertical settler should fractionate fibres according to length and diameter, when the fibres have an orientation parallel to the flow direction. Fractionation experiments confirm the theoretical prediction. Under extreme dilution used in this study there is no effect of feed consistency and the performance of fibre fractionation decreases with an increase in the overflow stream flow rate. Fibre fractionation performance improves for larger fibre diameter. A theoretical model was developed to simulate fractionation in the vertical settler and it agrees fairly well with the experimental results.

Rotating cone fractionator also proved to be capable of fractionating nylon fibres of the same diameter by their length difference. The performance of fibre fractionation increases with a decrease in feed consistency, and there is little effect of feed flow rate on fractionation performance. It is also found that the rotational cone speed, the location of feed distributor and cone size have some effect on fibre fractionation. Based on the literature studies, a possible fractionation mechanism is proposed.

ACKNOWLEDGEMENTS

I would like to thank my supervisor Dr. Jacob H. Masliyah for his excellent guidance and immense encouragement throughout the course of this project.

A special thanks goes to Dr. Vilas Rewatkar for his continuous technical support and tremendous effort on thesis correction.

I would also like to thank Dr. William Eckert, Mr. Artin Afacan and my other colleagues and the staff in the department for their support and help.

Finally, I would like to thank the Natural Sciences and Engineering Research Council of Canada (NSERC) and the Networks of Centres of Excellence (NCE) in Mechanical and Chemi-mechanical Wood-pulps Network for providing the funding which made this thesis possible.

TALBE OF CONTENTS

Chapter 1

Introduction	1
1.1 Fibre fractionation	1
1.2 Objective of present work	6

Chapter 2

Measurements	9
2.1 Fibre length measurements	9
2.2 Properties of nylon fibres	11
2.3 Consistency measurements	12

Chapter 3

Vertical settler	16
3.1 Introduction	16
3.1.1 Sedimentation of spherical particles	17
3.1.2 Sedimentation of axisymmetric particles	18
3.2 Mathematical model	19

3.2.1 Settling velocities of individual fibres	20
3.2.1.1 Cross flow	20
3.2.1.2 Axial flow	22
3.2.2 Fibre orientation in a vertical settler	23
3.2.3 Model development	28
3.3 Experimental set-up	32
3.4 Results and discussions	34
3.4.1 Effect of split ratio	34
3.4.2 Effect of feed flow rate	40
3.4.3 Effect of feed consistency	49
3.4.4 Effect of fibre diameter	53
3.5 Conclusions	57

Chapter 4

Rotating cone fractionator	59
4.1 Introduction	59
4.2 Experimental set-up and procedure	63
4.2.1 Experimental set-up	63
4.2.2 Experimental procedure	65
4.3 Visual observations	66
4.4 Possible fractionation mechanism	67
4.5 Results and discussions	71
4.5.1 Variation of average fibre length and amount of fibres with collection zone.....	71
4.5.2 Effect of surface roughness	72
4.5.3 Effect of radial location of feed distributor	83
4.5.4 Effect of feed flow rate	87
4.5.5 Effect of rotational cone speed	87

4.5.6 Effect of feed consistency	93
4.5.7 Effect of cone size	95
4.6 Conclusions	99

Chapter 5

Summary	100
---------------	-----

Chapter 6

Recommendations for future work	102
---------------------------------------	-----

References	103
------------------	-----

Appendix I

Data for all the figures included in this thesis	107
--	-----

Appendix II

Conversion for term $\alpha_{so}/(\alpha_{so} + \alpha_{lo})$	114
---	-----

NOMENCLATURE

A	cone angle, (degree), as shown in Fig 4.2
A_L	fibre arithmetic mean length, (mm or m)
C_D	drag coefficient, dimensionless, as defined in equation 3.3
C_v	volumetric concentration of fibres
d	fibre coarseness, (denier, g/9000m)
D	fibre diameter, (μm , mm or m)
$F(\Phi_z)$	cumulative distribution function, as defined in equation 3.12
F_A	gravitational force on the cylindrical fibre, (N), as defined in equation 3.2
F_D	drag force on the cylindrical fibre in cross flow, (N), as defined in equation 3.1
F_Z	drag force on fibre in axial flow, (N), as defined in equation 3.10
g	acceleration due to gravity, (m/s^2)
h_f	vertical location of feed distributor from cone surface, (mm), as shown in Fig 4.2
L	fibre length, (mm or m)
L_L	length weighted mean length, (mm or m)
L_w	weight weighted mean length, (mm or m)
M	crowding factor, dimensionless, as defined in equation 4.1
N	rotational cone speed, (rev/m), as shown in Fig 4.2
n	fibre count
Q_F	feed flow rate, (m^3/s), as shown in Fig 3.2.3 and Table 4.2.2
Q_O	overflow rate, (m^3/s), as shown in Fig 3.2.3

Q_U	underflow rate, (m^3/s), as shown in Fig 3.2.3
R	radius of rotating cone, (mm), as shown in Fig 4.2
r_e	effective aspect ratio of the particles, dimensionless
Re	Reynolds number
r_f	radial location of feed distributor from axis of rotation, (mm), as shown in Fig 4.2
S	cross-section area of the vertical settler, (m^2)
T	fibre cell wall thickness, (mm)
U_A	terminal settling velocity of fibres in axial flow, (m/s), as defined in equation 3.11
U_c	terminal settling velocity of fibres in cross flow, (m/s), as defined in equation 3.9
U_f	velocity of fluid in a vertical settler, (m/s), as shown in Fig 3.2.3
U_l	velocity of long fibres in a vertical settler, (m/s), as shown in Fig 3.2.3
U_L	radial velocity of long fibres over a cone surface, (m/s), as shown in Fig 4.4b
U_s	velocity of short fibres in a vertical settler, (m/s), as shown in Fig 3.2.3
U_S	radial velocity of short fibres over a cone surface, (m/s), as shown in Fig 4.4b
V_L	tangential velocity of long fibres over a cone surface, (m/s), as shown in Fig 4.4b
V_S	tangential velocity of shorts fibre over a cone surface, (m/s), as shown in Fig 4.4b
W_L	radial component of velocity of long fibres, as shown in Fig 4.4b
W_S	radial component of velocity of short fibres, as shown in Fig 4.4b
W_{SU}	weight of fibre suspension, (gram or kg)
X	consistency of fibre suspension, (w/w, %)

Greek Letters

α_f	volume fraction of fluid in the source zone, as shown in Fig 3.2.3
α_l	volume fraction of long fibres in the source zone, as shown in Fig 3.2.3
α_s	volume fraction of short fibres in the source zone, as shown in Fig 3.2.3
$\Delta\rho$	density difference between fibre and continuous phase, (kg/m^3)
Φ_z	orientation angle from 0° to 180° with 90° being the direction of the flow, (degrees)
$\dot{\gamma}$	shear rate, ($1/\text{s}$)
μ	viscosity of the continuous phase, ($\text{Pa}\cdot\text{s}$)
θ_z	spherical polar co-ordinate with Z, as shown in Fig 3.2.2a
ρ_c	density of the continuous phase, (kg/m^3)
ρ_f	density of fibres, (kg/m^3)
ρ_w	density of water, (kg/m^3)
τ	shear stress in simple shear flow, (N/m^2)

Subscripts

f	fluid
F	feed suspension
l	long fibre in VS method
L	long fibre in RCF method
O	overflow
s	short fibre in VS method
S	short fibre in RCF method
U	underflow
w	water

LIST OF FIGURES, TABLES AND PHOTOGRAPHS

Figures

- Figure 1.1 Effect of biological age on average fibre length for typical softwood and hardwood
- Figure 1.2 Length distributions of nylon fibres and hardwood fibres
- Figure 2.2 Fibre length distributions
- Figure 3.2.2a Cylindrical fibre coordinates with respect to the polar axes
- Figure 3.2.2b Cumulative distribution of nylon fibre orientations
- Figure 3.2.3 Schematic of a vertical settler used for the mathematical model
- Figure 3.3 Vertical settler experimental set-up
- Figure 3.4.1a Variation of average fibre length in the overflow and underflow streams with split ratio
- Figure 3.4.1b Overflow fibre length distributions at different split ratios
- Figure 3.4.2a Variation of the arithmetic average fibre length with split ratio at different feed flow rates
- Figure 3.4.2b Variation of the length weighted average fibre length with split ratio at different feed flow rates
- Figure 3.4.2c Variation of the average fibre length at different upward fluid velocities
- Figure 3.4.2d Comparison between theoretical model and experimental data for a feed flow rate of $9.077 \times 10^{-6} \text{ m}^3/\text{s}$
- Figure 3.4.2e Comparison between theoretical model and experimental data for a feed flow rate of $4.657 \times 10^{-6} \text{ m}^3/\text{s}$

- Figure 3.4.2f Comparison between theoretical model and experimental data for a feed flow rate of $2.819 \times 10^{-6} \text{ m}^3/\text{s}$
- Figure 3.4.3a Variation of average fibre length at different feed consistencies
- Figure 3.4.3b Comparison between theoretical model and experimental data for two feed consistencies
- Figure 3.4.4a Variation of average fibre length with split ratio for a $20 \text{ }\mu\text{m}$ fibre diameter
- Figure 3.4.4b Variation of average fibre length with split ratio for a $14 \text{ }\mu\text{m}$ fibre diameter
- Figure 3.4.4c Variation of the settling velocity of individual fibre in axial flow with fibre diameter for 1 mm and 3 mm long fibres
- Figure 4.1 Axial zone collection of particle cloud near a rotating vaneless disk
- Figure 4.2 RCF experimental set-up
- Figure 4.3 Three different atomization modes for RCF
- Figure 4.4a Flow of fibre suspension over the cone surface showing radial and tangential velocity profile
- Figure 4.4b Schematic view of fibre migration velocities over a conical surface
- Figure 4.5.1a Variation of average fibre length at different collection zones
- Figure 4.5.1b Length distributions of suspension from different collection zones
- Figure 4.5.1c Variation of percentage of fibre weight with collection zone
- Figure 4.5.2a Reproducibility test for a smooth surface cone
- Figure 4.5.2b Reproducibility test for a 20-mesh surface cone
- Figure 4.5.3a Variation of average fibre length at different radial locations of feed distributor
- Figure 4.5.3b Effect of radial location of feed distributor on flow pattern
- Figure 4.5.3c Variation of average fibre length at different rotational cone speeds at $r_f = 25.5 \text{ mm}$
- Figure 4.5.4 Variation of average fibre length at different feed flow rates
- Figure 4.5.5 Variation of average fibre length at different rotational cone speeds

Figure 4.5.6 Variation of average fibre length at different feed consistencies

Figure 4.5.7a Variation of average fibre length at different cone radii at $N = 450$ rpm

Figure 4.5.7b Variation of average fibre length at different cone radii at $N = 670$ rpm

Photographs

Photograph 3.2.2 Photograph showing nylon fibre alignment in the direction of the flow in a vertical settler

Photograph 3.4.3 Fibre suspensions of at different consistencies of 0.01%, 0.05% and 0.15%

Photograph 4.5.2 Photograph of suspension flow on a rough surface cone

Photograph 4.5.4 Photographs of suspension flow at two different feed flow rates

Photograph 4.5.5 Photographs of suspension flow at three different rotational cone speeds

Photograph 4.5.7 Photographs of flow pattern at two different cone radii

Tables

Table 1.1a Properties of north American pulpwoods

Table 1.1b General classification of pulping processes

Table 2.2 Properties of nylon fibres

Table 3.4.1 Approximate consistency and average fibre length for each overflow sample corresponding to various split ratios at $Q_F = 2.819 \times 10^{-6} \text{ m}^3/\text{s}$

Table 4.1 Literature survey on fibre fractionation using a plate atomizing wheel

Table 4.2.2 Range of parameters studied for RCF

Table 4.5.2a Details of wire size and openings of the different screens

Table 4.5.2b Experimental conditions for reproducibility tests

CHAPTER 1

INTRODUCTION

1.1 FIBRE FRACTIONATION

Although common pulping techniques are utilized in the pulp and paper industry, the properties and qualities of paper can vary over a wide range. This is due to different physical and chemical characteristics of fibrous and non-fibrous raw material. For example, generally the length of softwood fibre is longer than that of hardwood. Both softwood and hardwood include numerous various wood species (Table 1.1a). The biological age of the species can also influence the length of fibre (Figure 1.1). For the same wood species, the final properties of fibres depend on the pulping process (Table 1.1b), e.g., mechanical pulping, chemical pulping and combination of both.

Species	Fibre length (mm)	Fibre Diameter (μm)	Ratio L/T	Coarseness mg/100m
Birch	1.8	20-36	500	5-8
Red Gum	1.7	20-40	300	8-10
Black Spruce	3.5	25-30	700	14-19
Red Cedar	3.5	30-40	1400	15-17
Southern Pine	4.6	35-45	700	20-30
Douglas-Fir	3.9	35-45	700	25-32
Redwood	6.1	50-65	1700	25-35

Table 1.1a Properties of north American pulpwoods, L/T is the ratio of pulp fibre length to cell wall thickness.

Mechanical	Hybrid	Chemical
Pulping by mechanical energy (small amount of chemicals and heat)	Pulping with combinations of chemical and mechanical treatments	Pulping with chemicals and heat (little or no mechanical energy)
High yield (85-95%)	Intermediate yield (55-85%)	Low yield (40-55%)
Short, impure fibres <ul style="list-style-type: none"> • weak • unstable 	"Intermediate" pulp properties (some unique properties)	Long, strong fibres: <ul style="list-style-type: none"> • strong • stable
Good print quality		Poor print quality
Examples: <ul style="list-style-type: none"> • stone groundwood • refiner mechanical pulp • thermomechanical pulp 	Examples: <ul style="list-style-type: none"> • neutral sulfite semichemical • high-yield kraft • high-yield sulfite 	Examples: <ul style="list-style-type: none"> • kraft • sulfite • soda

Table 1.1b General classification of pulping processes

(Smook, 1992)

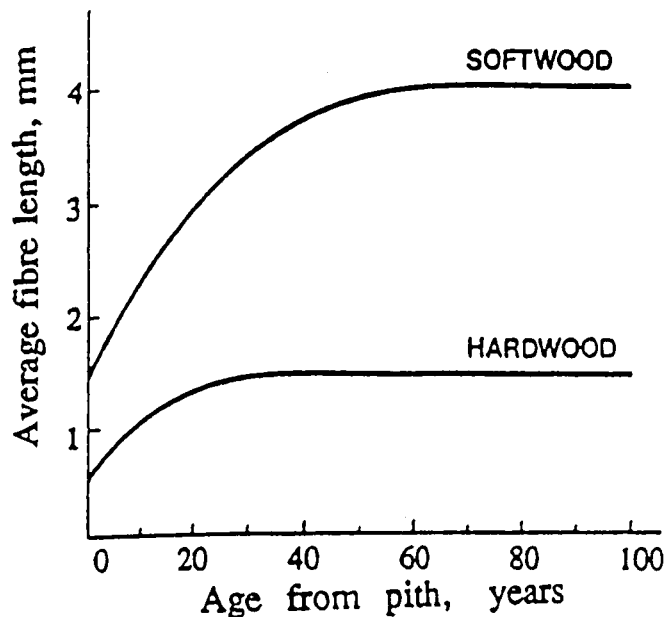


Figure 1.1 Effect of biological age on average fibre length for typical softwood and hardwood (*Smook, 1992*)

Due to environmental protection and shortage of wood fibre resources, mechanical and secondary pulps are becoming more and more used in the pulp and paper industry, since mechanical pulping has much higher yield than chemical pulping, and valuable fibres can be reused by recycling. However, the application is limited due to their low pulp quality. For example, mechanical pulp has a high percentage of lignin and fines, and recycle pulp includes various fibres such as new and old fibres, reuseable and non-reuseable, even unwanted contaminants. With the endeavor of many researchers, it is found that fibre fractionation, which is to fractionate fibres into several fractions that can each be used in a separate product, is as an efficient solution not only for improving product quality and increasing recycling, but also for raw-material shortage, environmental protection demands, and

decreasing energy costs. Four general applications for pulp fractionation were summarized by Moller et al. (1979). Fractionation optimizes the usage of fibre resource by separating them into different groups to:

- suit different requirement for the final product;
- suit different machines, or individual machine characteristics;
- suit different beating conditions;
- reuse the valuable pulp from waste;

There are also some other applications, such as removing good fibres from black liquor, upgrading white water overflow to shower water and deinking recycling.

Generally, the fibres are fractionated according to their size, such as, length, diameter or both. Among them, fractionation by length is highly needed because fibre length influences the properties of a final product. Forgacs (1963) reviewed the literature on pulp characterization and concluded that fibre length, fibre-specific surface, and some sorts of fibre shape factor are important parameters controlling the finished product properties. His results indicted that the burst factor, breaking length, and tear factor increase with an increase in the specific surface. However, at a given specific surface, the properties related to burst factor, breaking length, and tear factor improve as the fibre length is increased. The studies by Clark (1942, 1962) showed that for constant fibre coarseness (mass per unit length), the tensile length of a sheet made from relatively unbeaten pulp (other factors being the same) varies as $L^{1/2}$, the burst varies as L , the fold varies as L^5 , and tear as $L^{3/2}$.

Demands for raw-material shortage, environmental protection, and minimizing energy costs prompted the development of the technique of fibre

fractionation. Based on different principles, various equipment has been invented, patented and later applied to the pulp and paper industry. Recently, Rewatkar and Masliyah (1996) summarized the different equipment used for fibre fractionation:

- Screens (based on perforation barrier).
- Hydrocyclones (based on difference in shear force due to density difference).
- Plate atomizing wheel (based on separation due to strong shear field within a film flowing over big-speed spinning wheel).
- Liquid column flow (based on the development of a concentration gradient in a fibre suspension flowing in the form of slugs).
- Spouted bed (based on different spouting velocity of fibre flocs).
- Jacqueline apparatus (based on the tendency of formation of fibre flocs due to centrifugal force).

Recently, two new fibre fractionation techniques are reported in the literature:

- Flotation cell by Eckert et al. (1997) (based on the different drainage rate of fibres within the froth).
- Rotating Cone Fractionator by Rewatkar and Masliyah (1997) (based on the similar principle to plate atomizing wheel using collection assembly).

Fibre fractionation by various works was carried out to separate a mixture of pulps produced by different pulping processes or originating from different wood species. Consequently, it is difficult to compare the performance of the different fractionating equipment. Screens are used in the majority of pulp industries, fractionating fibres mainly according to their length. Hydrocyclones primarily separate fibres on the basis of specific surface. Liquid column flow and Johnson fractionator fractionate are based on fibre length like the screens. All of the fractionation techniques can only deal with very low consistency of feed suspension of about 0.25%. However, it is reported that plate atomizing wheel, which separates

fibres according to their diameter, can fractionate fibre suspension with consistency as high as 6%. However, there are some disadvantages of plate atomization wheel in that it requires high rotating speed, plate with a smooth surface, vibrationless disk rotation, etc. The newly designed equipment, rotating cone fractionator (RCF), overcomes those shortcomings by its unique features, off-centre feed introduction and angular collection assembly. Details for RCF are given in chapter 4. Another newly developed technique, flotation cell, inspired by the deinking method, is found to be a successful technique for recovering long fibres from a pulp suspension.

1.2 OBJECTIVE OF PRESENT WORK

The principal objective of this study is to determine whether fibres can be fractionated by length or by diameter. Although a large number of studies have been conducted on wood fibre fractionation, it is not clear as yet whether fractionation occurs according to fibre length or diameter. This is particularly important because length and diameter of natural wood fibres vary independently. In order to avoid use of natural wood fibres, nylon fibres are used in the present study, because the size distribution of the nylon fibres (Figure 1.2 (a)) is much more uniform than that of the polydisperse natural wood pulps (Figure 1.2 (b)).

Two different methods are used in this project: vertical settler (VS) and rotating cone fractionator (RCF). The properties of nylon fibres are given in chapter 2. Various measurement techniques are also described in chapter 2. In chapter 3, the details of VS set-up and experiment procedure are presented. Based on the

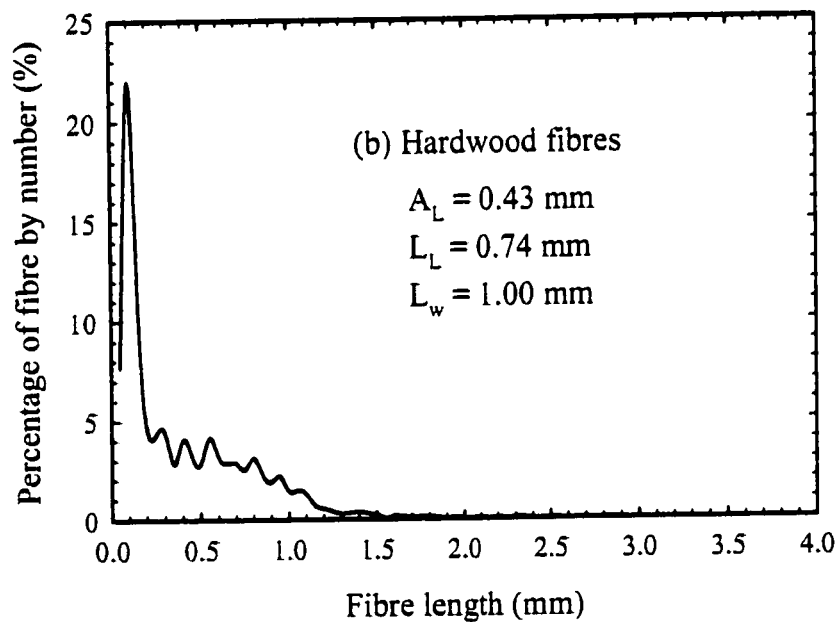
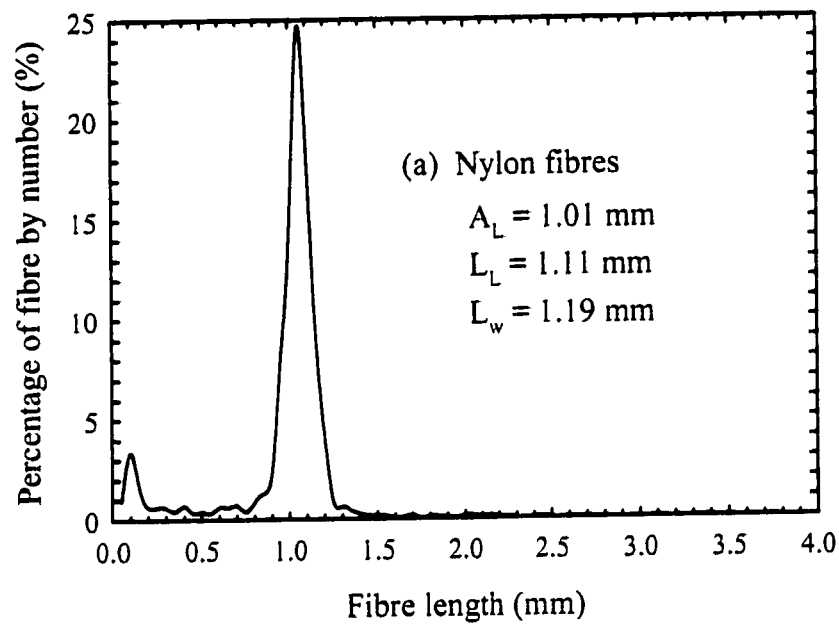


Figure 1.2 Length distributions of nylon fibres and hardwood fibres

principle discussed, the theoretical model is checked by comparing it with the experimental results. The effect of various parameters such as feed flow rate split ratio and feed consistency on fractionation is studied. In Chapter 4, the details of RCF are investigated, which include experimental set-up, possible mechanism and conclusions. Various parameters are studied, such as roughness of the cone surface, location of feed distributor, feed flow rate, rotational cone speed, feed consistency and cone size.

CHAPTER 2

MEASUREMENTS

2.1 FIBRE LENGTH MEASUREMENTS

The fibre length measurements are well covered in “handbook for pulp and paper technologists” by Smook (1992). Traditionally, there are two different measurement techniques: screening and microscopic. In the screening method, a dilute suspension of fibres is made to flow at high velocity parallel to screen slots, while at a much slower velocity through the slots. The pulp sample is typically divided into two fibre length fractions. In the microscopic method, the magnified image of a known weight of fibres is projected onto a calibrated grid pattern; fibre length is measured to produce a length distribution and the average fibre length is calculated mathematically. Recently, these methods have been replaced by modern

optical counting devices, such as Kajaani analyzer (FS-100 and FS-200) and Fibre Quality Analyzer (FQA).

In the present study, a fibre quality analyzer (FQA) was used to measure the average fibre length, fibre length distribution and percentage of fines ($L < 0.2\text{mm}$) present in the fibre suspension. There are three ways to represent the fibre mean length.

First, arithmetic mean length (A_L), which is the average contour length of all detected fibres in a given sample.

$$A_L = \frac{\sum n_i L_i}{\sum n_i}$$

where $i = 1, 2, \dots, n$; n = fibre count; L = fibre length.

The presence of fines will significantly affect this value.

Second, the length weighted mean length, which is defined as follows:

$$L_L = \frac{\sum n_i L_i^2}{\sum n_i L_i}$$

Fines do not have a significant effect on L_L .

Third, the weight weighted mean length:

$$L_w = \frac{\sum n_i L_i^3}{\sum n_i L_i^2}$$

Long fibres have a significant impact on L_w .

In the present study, the first two measures were used to represent the mean lengths of fibre suspensions. During all the fibre length measurements, 4000 fibres were counted.

2.2 PROPERTIES OF NYLON FIBRES

The nylon fibres used in this study were received from the Pulp and Paper Centre at University of British Columbia. Their characteristics are listed in Table 2.2.

Length (A_L , mm)	Diameter (D , μm)	Density (ρ_p , kg/m^3)	Coarseness (d , denier, or g/9000m)
0.95	14	1.13×10^3	1.5
2.18	14	1.13×10^3	1.5
1.01	20	1.13×10^3	3.0
2.75	20	1.13×10^3	3.0

Table 2.2 Properties of nylon fibres

The arithmetic mean length was measured by FQA, the mean diameter was measured under a microscope and the value of coarseness was given by the supplier. The fibre density was measured according to the procedure in American standard test methods (ASTM) for density and specific gravity of plastics by displacement. Since most of the fibre lengths are about 1 mm and 3 mm, the fibres are named as nominal 1 mm fibre and 3 mm fibre instead of using their actual mean length.

The length distributions for these four types of nylon fibres are shown in Figure 2.2a - d. The feed suspension, containing 20% 1 mm fibres and 80% 3 mm fibres by weight, was kept constant throughout the experiments. The length distributions for two types of feed suspensions (3 denier and 1.5 denier) are also shown in Figure 2.2e & f. The majority of the experiments were carried out using the 3 denier nylon fibres. The 1.5 denier nylon fibres are only used to study the effect of fibre diameter in section 3.4.4 in the vertical settler. In the following section, the word "fibres" always means the 3 denier fibres unless specifically stated otherwise.

All the length measurements were based on 4000 fibres counted by FQA. The percentage of the fibre is based on fibre number count. From fibre length distribution of the feed suspension, it can be observed that the areas of the two peaks, representing the two fibre populations, are similar although the ratio of their weights is 1:4.

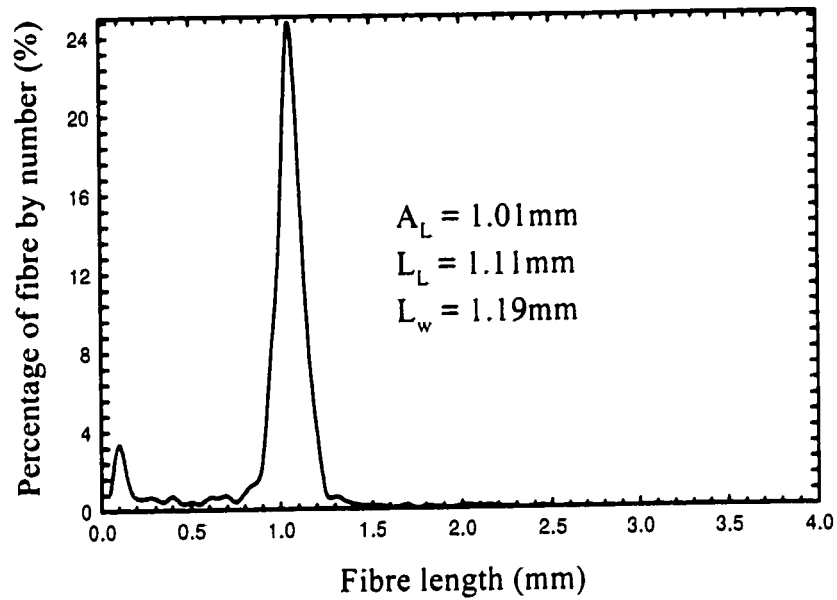
2.3 CONSISTENCY MEASUREMENTS

In order to compare quantitatively fractionation performance, one needs the consistency of feed suspension used and different fractions collected. Since the range of the feed consistency used in the experiments was very small (0.01% - 0.1%), it was difficult to obtain direct consistency measurement by a conventional measurement technique, i.e. TAPPI standard. In order to obtain an estimate, an alternative technique was used. The stepwise procedure is as follows:

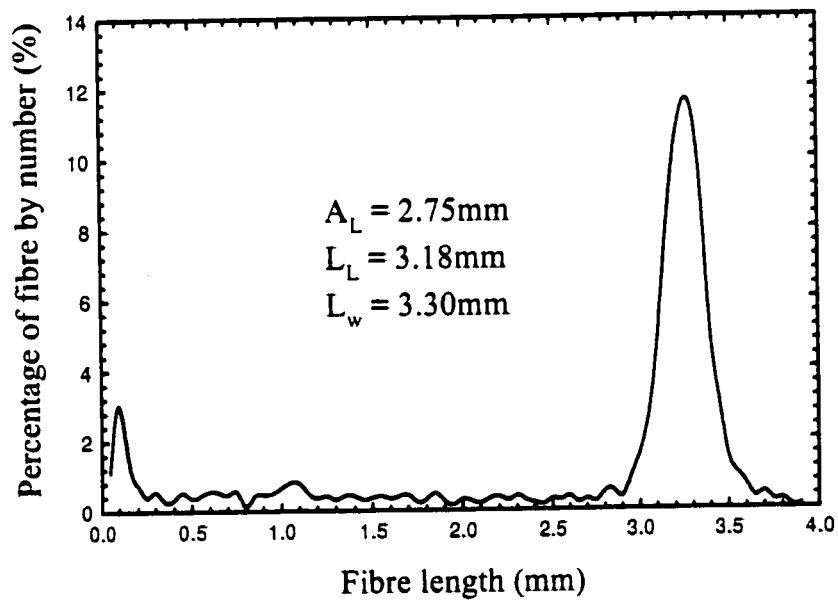
1. Weigh the fibre suspension (W_{SU}),
2. Pass all the fibre suspension through the FQA,
3. Collect the data of the arithmetic mean length (A_L) and the total fibre number (n),
4. The consistency of fibre suspension (X) can be calculated as follows:

$$X = \frac{n A_L d}{W_{SU}} \times 100\%, \text{ where the units of } A_L \text{ and } W_{SU} \text{ are m and gram, respectively,}$$

and the value of d (denier or g/9000m), is shown in Table 2.2.

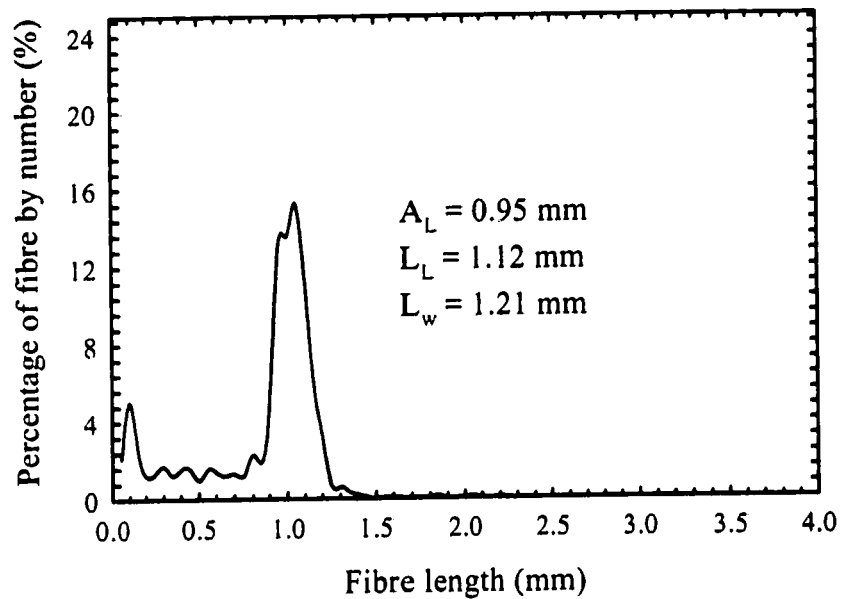


(a) 1 mm nylon fibre with 3 denier coarseness

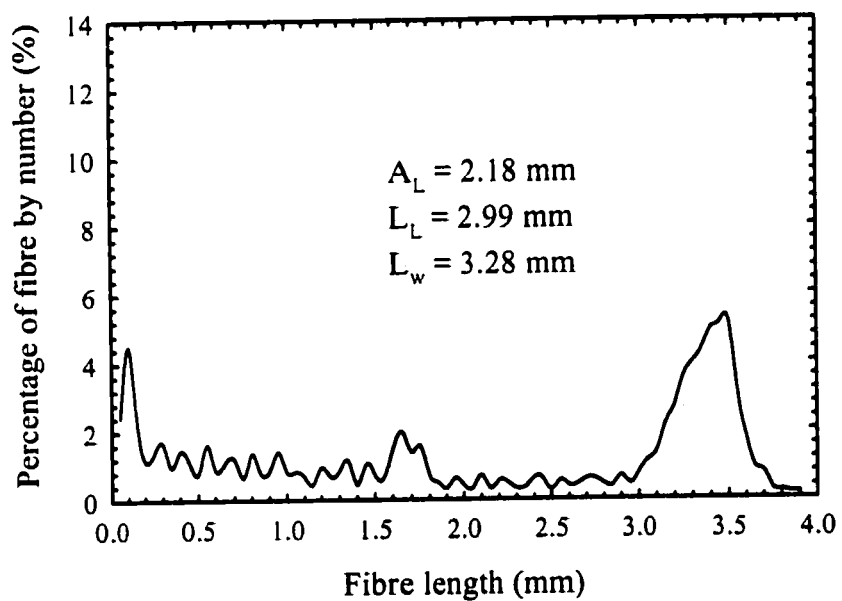


(b) 3 mm nylon fibre with 3 denier coarseness

Figure 2.2 Fibre length distributions

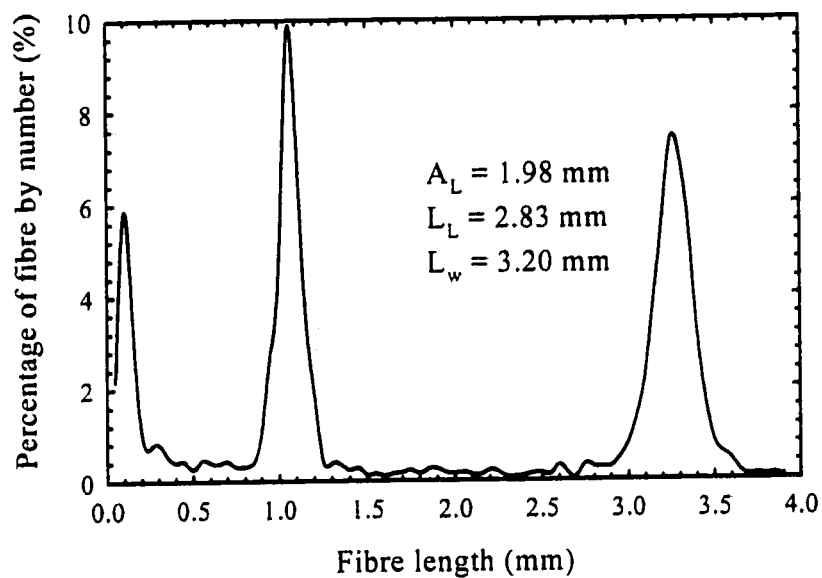


(c) 1 mm nylon fibre with 1.5 denier coarseness

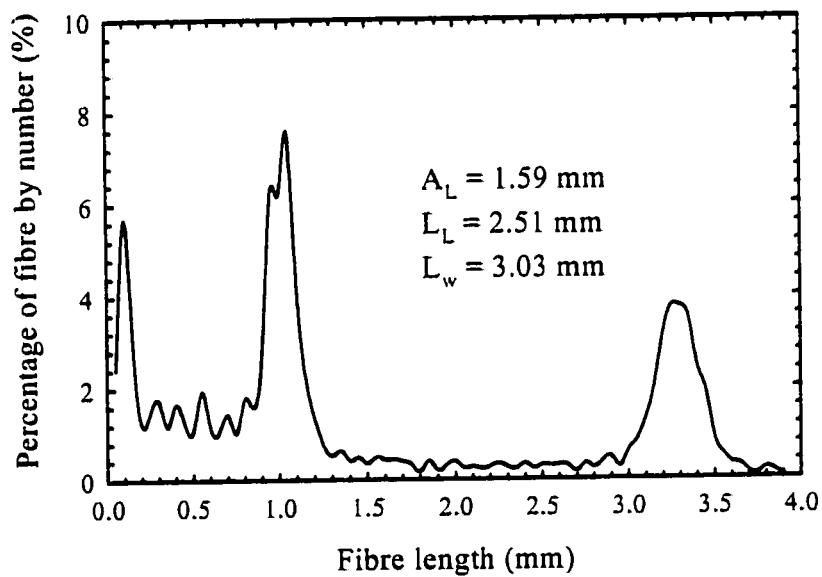


(d) 3 mm nylon fibre with 1.5 denier coarseness

Figure 2.2 Fibre length distributions



(e) Feed suspension of 3 denier fibres
including 20% 1mm and 80% 3mm (w/w)



(f) Feed suspension of 1.5 denier fibres
including 20% 1mm and 80% 3mm (w/w)

Figure 2.2 Fibre length distributions

CHAPTER 3

VERTICAL SETTLER

3.1 INTRODUCTION

Vertical settlers (VS) are commonly used in the sedimentation field for cleaning, thickening and size classification etc. The sedimentation performance in a vertical settler strongly depends on the settling velocities of particles and their concentration. For a given fluid and particles, the shape and orientation of the falling particles determine the performance of a vertical settler. A literature survey on sedimentation of spherical and axisymmetric particles is given below.

3.1.1 Sedimentation of spherical particles

Much research has been conducted on sedimentation processes of bidisperse suspensions of spherical particles which can be further classified into two categories: low total solids volume fraction suspensions (≤ 0.15) and high total solids volume fraction suspensions (> 0.15).

Previous results (Richardson and Meikle, 1961; Smith, 1965) for the low solids concentration regime, where no lateral heterogeneities develop, indicated that there are several distinct zones formed with clearly identifiable interfaces separating the movement of them. These zones can be modeled successfully with the aid of material balances written across the discontinuities together with the drift-flux or slip velocity correlation. Later, several theoretical models have been developed for calculating the settling velocity of the particles within a bidisperse suspension. Law et al. (1987) compared different models and proposed that models published by Masliyah (1979), Selim et al. (1983) and Patwardhan and Tien (1985) are in good agreement with experimental data.

For concentrated suspensions (Whitemore, 1955; Weiland and McPherson, 1979; Fessas and Weiland, 1982, 1984; Weiland et al. 1984; Batchelor and Van Rensburg, 1986), it was found that the settling velocities of both particle species are greatly enhanced. This is due to the lateral segregation of light and heavy particles into clusters and the formation of fingering type flow structure along the direction of the gravitational field.

Most of the theoretical studies developed for a batch system have been employed for a continuous system. Kynch (1952) developed a formal mathematical

analysis of the thickening process, which has been extended by many researchers (Talmadge and Fitch, 1955; Tarrer et al., 1974; Dixon, 1977). Masliyah et al. (1981) studied gravity separation using sand particles of various sizes. Nasr-El-Din et al. (1988) developed a mathematical model for the continuous separation of bidisperse suspension containing light and heavy species. Later, Nasr-El-Din et al. (1989) also studied continuous separation of bidisperse suspensions in inclined channels which shows an enhancement separation as compared to a vertical settler. Recently, Nasr-El-Din et al. (1989, 1990) had conducted similar work on concentrated bidisperse suspensions in both vertical settlers and inclined channels.

3.1.2 Sedimentation of axisymmetric particles

Settling velocity of axisymmetric particles often deviates significantly from spherical particles, such as fibres, clays, aggregates, iron filings, and many microorganisms. The performance of sedimentation of axisymmetric particles has been studied extensively in the past by some researchers.

Jeffery (1922) found that there are a variety of possible motions corresponding to different initial conditions of particle orientation. In 1967, Anczurowski and Mason derived formal equations for the distribution of orientations of the axes of particles and the mean value of various projections of particle dimensions in dilute suspension of prolate and oblate spheroids. Davis (1991) obtained the average sedimentation velocity in dilute suspensions for the settling of axisymmetric particles in shear flow. His results indicated that the average sedimentation velocity strongly depends on the aspect ratio of the particles, the orientation of the gravity vector relative to the flow field, and only weakly on the distribution of orbits. Romero et al. (1993) applied sedimentation method on classification of cylindrical fibres and predicted their settling velocities in a continuous-flow inclined settler. They focused on the

theoretical analyses to demonstrate the sedimentation behavior of axisymmetrical particles and the possibility of separation.

The objective of the present study is to fractionate fibres according to fibre length difference and study the effects of various operating conditions on the fractionation performance. A theoretical model has been proposed for fibre fractionation by using VS.

3.2 MATHEMATICAL MODEL

Inspired by the standard one-dimensional wave model (Kynch, 1952) for sedimentation, Nasr-El-Din et al. (1988) developed a theoretical model based on mass balance and slip velocities. They studied a continuous gravity separation of a bidisperse suspension containing lighter (polystyrene) and heavier (polymethyl methacrylate) spherical particle than the suspending fluid (salt solution) in a vertical settler. The model predicted all the observed trends and agreed fairly well with their experimental measurements.

We apply the same techniques on the nylon fibres that have the same density and diameter, but of different length. Fibres become fractionated because of the difference in their settling velocities. The settling velocities of fibres have been estimated theoretically as follows.

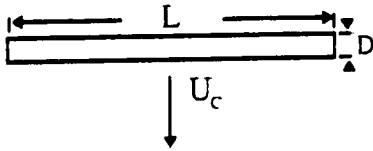
3.2.1 Settling velocities of individual fibres

The settling velocity of cylindrical fibres depends on their orientations and imposed flow field that causes the particles to rotate. Hence, we will consider two extreme settling directions: cross flow and axial flow.

3.2.1.1 Cross flow

When a cylinder falls normal to its axis, the drag experienced by the cylinder is given by:

$$F_D = C_D \cdot \frac{1}{2} \rho_c U_c^2 \cdot (\text{Projected area}) \quad (3.1)$$



Where C_D – drag coefficient, a function of the cylinder Reynolds number,

ρ_c – density of the continuous phase, (kg/m^3),

U_c – settling velocity of cylindrical particle, (m/s).

The gravitational force experienced by the cylinder is given by

$$F_A = \left(\frac{\pi}{4} D^2 L \right) \Delta \rho g \quad (3.2)$$

where D – fibre diameter, (m),

L – fibre length, (m),

$\Delta \rho$ – density difference between fibre and continuous phase, (kg/m^3),

g – acceleration due to gravity, (m/s^2).

At steady state, the drag force is equal to the gravitational force leading to:

$$C_D \cdot \frac{1}{2} \rho_c U_c^2 \cdot (\text{projected area}) = \left(\frac{\pi}{4} D^2 L \right) \Delta \rho g$$

Substituting the value of the projected area, DL, and rearranging,

$$C_D = \frac{\pi D \Delta \rho g}{2 \rho_c U_c^2} \quad (3.3)$$

Pruppacher et al. (1970) proposed an empirical expression for the drag coefficient in steady cross flow past long cylinders for various range of Reynolds number as follows:

$$C_D = C'_D (1 + 0.147 \text{Re}^{0.82}) \quad (0.1 < \text{Re} \leq 5) \quad (3.4)$$

$$C_D = C'_D (1 + 0.227 \text{Re}^{0.55}) \quad (5 < \text{Re} \leq 40) \quad (3.5)$$

$$C_D = C'_D (1 + 0.0838 \text{Re}^{0.82}) \quad (40 < \text{Re} \leq 400) \quad (3.6)$$

where $C'_D = 9.689 \text{Re}^{-0.78}$, (3.7)

$$\text{Re} = \frac{\rho_c U_c D}{\mu}, \quad (3.8)$$

D – diameter of a cylindrical particle or fibre diameter, (m),

μ – viscosity of the continuous phase, (Pa.s).

Combining equations (3.3), (3.4), (3.7) and (3.8), the terminal settling velocity for a single fibre in cross flow at low Re can be obtained as:

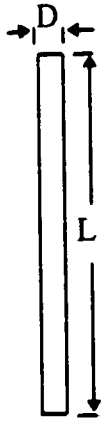
$$U_c = \left[\frac{0.162 D^{1.78} \Delta \rho g}{\mu^{0.78} \rho_c^{0.22}} \right]^{0.82} \quad (3.9)$$

From equation (3.9), it can be observed that at low Re , the settling velocity of a single fibre is independent of the fibre length in the cross flow.

Similarly, we can draw the same conclusion at high Re . In the present work, a fibre mixture of 1 mm and 3 mm can not be fractionated under cross flow condition, since the two fibres have identical settling velocities.

3.2.1.2. Axial flow

When a cylinder falls parallel to its axis, the drag force experienced by the cylinder is given by the following expression (Happel & Brenner, 1983),



$$\text{Drag force: } F_z = - \frac{2 \pi \mu L U_A}{\ln(L/D) + 0.19315} \quad (3.10)$$

where U_A is the settling velocity of fibre in axial flow.

At steady state, the drag force is equal to the gravitational force, leading to

$$\text{Then } U_A = \frac{D^2 \Delta \rho g [\ln(L/D) + 0.19315]}{8 \mu} \quad (3.11)$$

From equation (3.11), it can be observed that the terminal settling velocity for a cylindrical particle increases with an increase in fibre length at a constant fibre diameter. In the present study for the 3 denier nylon fibres, $\Delta\rho = 130 \text{ kg/m}^3$, $D = 2 \times 10^{-5} \text{ m}$, $g = 9.8 \text{ m/s}^2$, $L = 1.0 \times 10^{-3} \text{ m}$ and $3.0 \times 10^{-3} \text{ m}$, $\mu = 1.0 \times 10^{-3} \text{ Pa}\cdot\text{s}$. By substituting these values into equation (3.11), the U_A values, for a 3 mm fibre and a 1 mm in water, are calculated as $3.31 \times 10^{-4} \text{ m/s}$ and $2.61 \times 10^{-4} \text{ m/s}$. The Reynolds numbers are estimated as 0.02 and 0.016, respectively, which are in the applicability range of equation (3.11).

In our present study, water is used to prepare the fibre suspensions. As the density of fibres is higher than that of water, both fibres settle down in water. In the vertical settler method, the feed suspension is introduced into the vertical settler at its centre. With the help of a pump, the suspension can be split within the settler into two streams, overflow and underflow streams. Details will be given in Section 3.3. When the upward fluid velocity is larger than the settling velocity of the 1 mm fibres but smaller than that of the 3 mm fibres within the vertical settler, the 1 mm fibres tend to come out in overflow stream, whereas the 3 mm fibres come out in underflow stream. This indicates that a vertical settler is capable of fractionating the fibres by length, when the orientations of major axis of fibres align with the direction of the flow.

3.2.2 Fibre orientation in a vertical settler

Fibre orientation in a simple shear flow has been well studied in the literature. Jeffery (1922) suggested that prolate spheroidal particles immersed in a fluid in laminar motion tend to set themselves with their major axes perpendicular to the plane of the undisturbed motion of the fluid to minimize viscous dissipation. Davis

(1991) predicted that non-interacting particles of high aspect ratios tend to align with their axis in the flow direction, whereas particle-particle interactions cause misalignment. Davis also found that as the aspect ratio is increased, needle-shaped spheroids spend an increasing fraction of their orbits with their major axes aligned with the direction of flow. Romero et al. (1993) showed this phenomenon to be true through experimental observations.

Fibre orientation in a simple shear flow can be described by the cumulative distribution expression (3.12) derived by Anxzurowski and Mason (1967). Equation 3.12 shows the distribution of orientations of the axes of prolate spheroid and the mean value of various projections of spheroid dimensions in dilute suspensions of axisymmetrical spheroids.

$$F(\Phi_z) = \frac{1}{\pi} \tan^{-1} \left(\frac{\tan \Phi_z}{r_e} \right) \quad (3.12)$$

where Φ_z is the orientation angle from 0° to 180° with 90° being the direction of flow, shown in Figure 3.2.2a, and r_e is the effective aspect ratio of the particles. The cumulative distribution function, $F(\Phi_z)$, is defined as the fraction of particles having orientation angles less than Φ_z .

For a spheroid, the effective aspect ratios, r_e , is the same as the true aspect ratio, r , defined as the ratio of the major to minor axis lengths. For other shapes, a relationship between r_e and r must be determined by computation or experiment. According to Davis (1991), r_e are 30.5 and 84 for 1 mm fibre and 3 mm fibre, respectively. Substituting the values of r_e for the fibres used in this study into equation

(3.12), the function $F(\Phi_z)$ can be evaluated and it is shown in Figure 3.2.2b. The plots indicate that more than 90% of both nylon fibres have values of Φ_z close to 90° .

A photograph of fibre orientation was taken at the top of the vertical settler under the flow condition, of a feed flow rate of $4.657 \times 10^{-6} \text{ m}^3/\text{s}$, a split ratio of 0.26 and feed consistency of 0.01%, shown in Photograph 3.2.2. It can be observed that the majority of fibre orientation is aligned with the direction of shear flow. This phenomenon agrees well with the theoretical predictions. Therefore, we can assume that the sedimentation direction of fibres in the suspension within the vertical settler always aligns with the direction of flow, i.e. axial flow is a reasonable assumption that one can make for the model development.

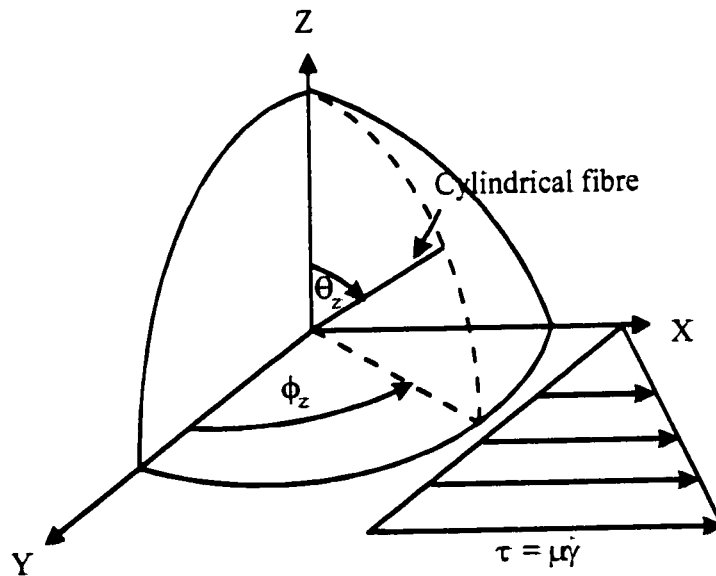


Figure 3.2.2a Cylindrical fibre coordinates with respect to the polar axes

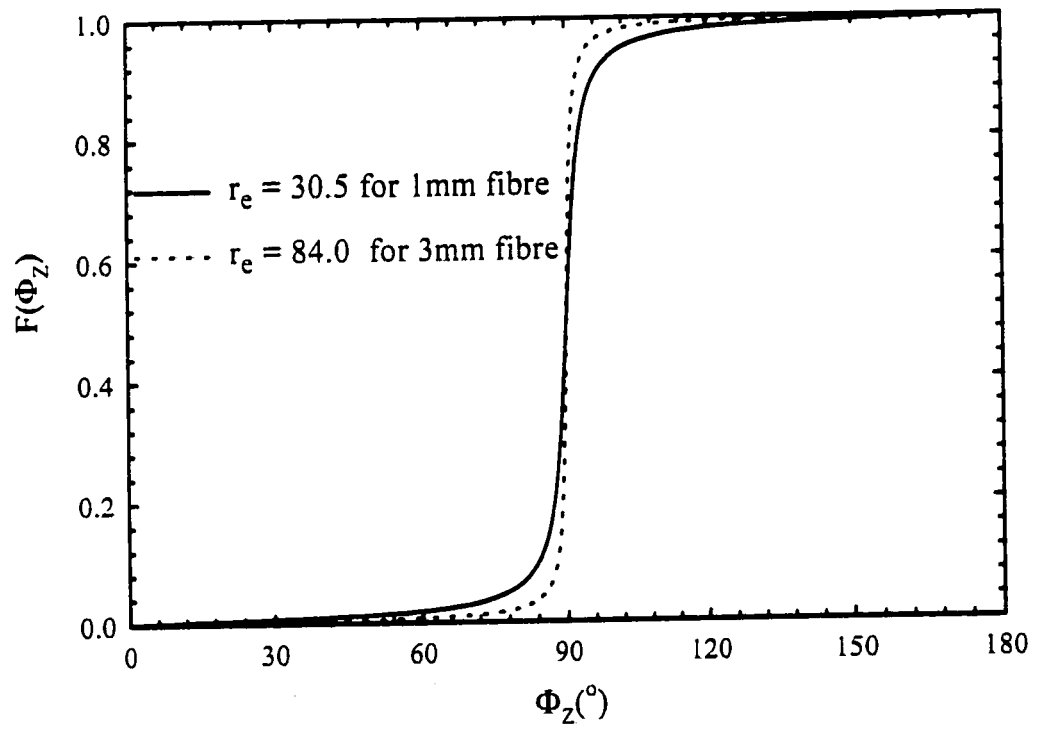
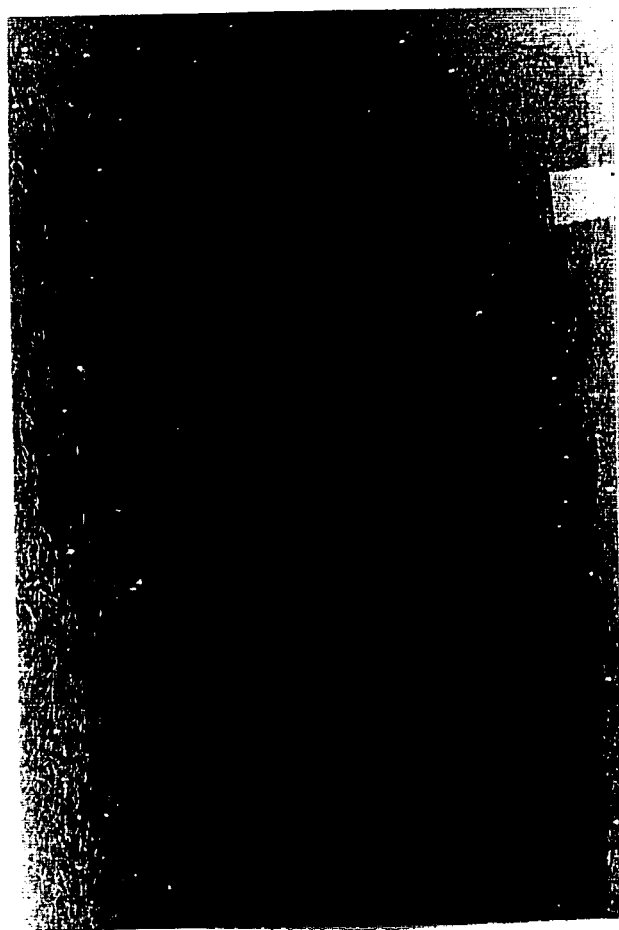


Figure 3.2.2b Cumulative distribution of nylon fibre orientations
 Φ_Z is defined from 0° -- 180° , with 90° being the direction of flow



Photograph 3.2.2 Photograph showing nylon fibre alignment in the direction of the flow in a vertical settler. Upwards is in the direction of the flow.

$Q_F = 4.657 \times 10^{-6} \text{ m}^3/\text{s}$; Split Ratio = 0.26; $X = 0.01\%$

3.2.3 Model development

The vertical settler is assumed to consist of a source zone located within the feed point of the settler as shown in Figure 3.2.3. This zone supplies the suspension to the underflow and overflow streams. The composition of this zone is not necessarily that of the feed stream. The fibre concentration within this zone is assumed to be uniform. If the upward fluid velocity is larger than the settling velocity of the fibres it can carry the fibres across the upper boundary of the source zone to report to the overflow stream. Otherwise, the fibres can only cross the lower boundary of the source zone to report to the underflow stream. These constraints are valid for both short fibres and long fibres. Flow visualization, with the continuous mode of operation, indicates that the overflow boundary appears close to the feed zone at low feed rates, however, the interface for underflow boundary is not sharp because both the long fibres and short fibres settle down naturally in a quiescent water suspension. With increasing feed flow rates and varying split ratios (i.e. fraction of feed flow rate in underflow rate) the overflow boundary can be driven to the far end of the column. Since the model is concerned only with a steady state operation, the location of the interface is immaterial. Volumetric balance for water, short fibres and long fibres over the source zone is given by

Fluid

$$Q_F \alpha_{FF} = S \alpha_f (U_{fU} - U_{fO}) \quad (3.13)$$

Short fibres

$$Q_F \alpha_{sF} = S \alpha_s (U_{sU} - U_{sO}) \quad (3.14)$$

Long fibres

$$Q_F \alpha_{lF} = S \alpha_l (U_{lU} - U_{lO}) \quad (3.15)$$

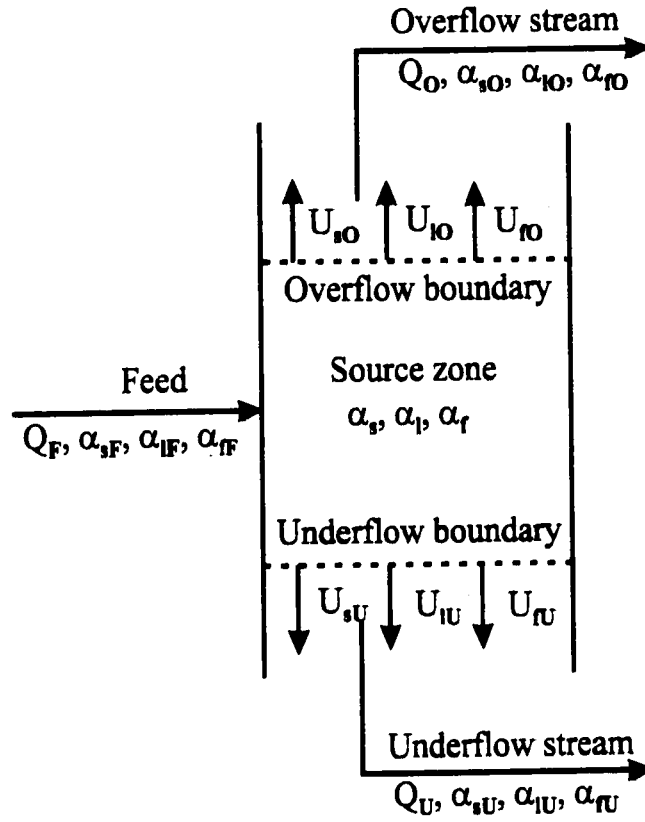


Figure 3.2.3 Schematic of a vertical settler used for the mathematical model

where Q_F is the volumetric flow rate of a feed having short and long fibres with volume fractions of α_{sF} and α_{lF} , respectively. U_{sU} and U_{sO} are the velocities of the short fibres at the underflow and overflow boundaries of the source zone, respectively. α_p , α_s and α_l are the source zone volume fractions of the fluid, short and long fibre species, respectively. S is the cross-section area of the vertical settler. The downward direction is taken as positive. The vertical velocity of the short fibre species at the overflow boundary of the source zone is given by

$$U_{sO} = \min[0, U_{fO} + U_{As}] \quad (3.16)$$

Where U_{As} is the settling velocity of short fibre in axial flow, calculated from equation (3.11). As the interaction among the fibres is negligible for low feed consistency (0.01%), it is assumed that there is no hindered settling. Similarly, the vertical velocities of the long fibres and short fibres at the underflow boundary of the source zone are respectively given by

$$U_{IU} = U_{fU} + U_{Al} \quad (3.17)$$

$$U_{sU} = U_{fU} + U_{As} \quad (3.18)$$

Similarly, the velocity of the long fibres at the overflow boundary of the source zone is given as

$$U_{IO} = \min [0, U_{fO} + U_{Al}]. \quad (3.19)$$

Equation (3.19) implies that long fibres can only leave the source zone if the upward fluid velocity is larger than the fall velocity of the long fibres, U_{IU} , but they cannot enter the source zone from the upper boundary.

In the operation of a vertical settler, one must specify the withdrawal rate of either the underflow or overflow stream. The overflow stream flow rate is given by

$$Q_O = -S (U_{sO} \alpha_s + U_{IO} \alpha_l + U_{fO} \alpha_f) \quad (3.20)$$

An additional constraint for the source zone is that

$$\alpha_f + \alpha_s + \alpha_l = 1. \quad (3.21)$$

Equations (3.13)-(3.21) provide a simple model for the continuous separation of a bidisperse suspension settling in a vertical settler in the absence of any lateral concentration gradients. The unknowns to be evaluated are $\{\alpha_p, \alpha_s, \alpha_l, U_{sO}, U_{lO}, U_{fO}, U_{sU}, U_{lU}, U_{fU}\}$. The feed stream flow rate and composition are specified together with the overflow (or underflow) stream flow rate.

The above equations were solved using a Gauss-Siedel iterative method. Once the source zone composition and the velocities at the two boundaries are determined, it is possible to evaluate the volume fractions of the short and long fibres in the overflow and underflow streams and they are given below.

$$\alpha_{sO} = -S U_{sO} \alpha_s / Q_O \quad (3.22a)$$

$$\alpha_{sU} = S U_{sU} \alpha_s / Q_U \quad (3.22b)$$

$$\alpha_{lO} = -S U_{lO} \alpha_l / Q_O \quad (3.22c)$$

$$\alpha_{lU} = S U_{lU} \alpha_l / Q_U \quad (3.22d)$$

Equations (3.16) and (3.19) indicate that there are three possible cases: (1) both fibres appear in the overflow stream, (2) only short fibres report to the overflow stream and no long fibres report to the overflow stream (i.e. $U_{lO} = 0$), (3) neither the short fibres

nor long fibres report to the overflow stream. For case I where both species appear in the overflow streams, combining equations (3.16) to (3.19) with (3.13) to (3.15) and (3.21) it is possible to show that the feed and source zone compositions are the same, i.e.

$$\alpha_f = \alpha_{fF}, \alpha_s = \alpha_{sF}, \alpha_l = \alpha_{lF}. \quad (3.23)$$

Finally an explicit expression for the fluid velocity in the overflow stream is given by

$$U_{fO} = -\frac{Q_O}{S} - \alpha_{sF} U_{As} - \alpha_{lF} U_{Al} \quad (3.24)$$

Combine (3.18), (3.19), (3.22a), (3.22c) and (3.24), the fraction ratio of short fibres in the overflow stream is given by the following equation:

$$\frac{\alpha_{sO}}{\alpha_{sO} + \alpha_{lO}} = \frac{\left[\frac{Q_O}{Q_F} \times \frac{Q_F}{S} \times \alpha_{sF} - U_{As} \alpha_{sF} \right]}{\left[\frac{Q_O}{Q_F} \times \frac{Q_F}{S} \times (\alpha_{sF} + \alpha_{lF}) - \alpha_{sF} U_{As} - \alpha_{lF} U_{Al} \right]} \quad (3.25)$$

3.3 EXPERIMENTAL SET-UP

The experimental set-up (Figure 3.3) consists of a settler, a holding tank equipped with a stirrer and two peristaltic pumps. The plexiglas settler was mounted in a vertical position on a steel stand and had 8 cm-width, 3 cm-depth, 40 cm-length

inner dimensions. The top and bottom ends of the settler were conical in shape to eliminate any dead zones where the fibres might accumulate. The feed was introduced at the middle of the settler by a peristaltic pump. The second peristaltic pump was used to control the overflow withdrawal flow rate. Both the overflow (Q_O) and underflow (Q_U) streams were returned to the holding tank for remixing.

The bidisperse suspension used in the present study were made up of 20% 1 mm fibre ($L_1 = 1.0 \times 10^{-3}$ m, $D_1 = 2.0 \times 10^{-5}$ m, $\rho_1 = 1.13 \times 10^3$ kg/m³) by weight and 80% 3 mm fibre ($L_2 = 3.0 \times 10^{-3}$ m, $D_2 = 2.0 \times 10^{-5}$ m, $\rho_2 = 1.13 \times 10^3$ kg/m³) by weight in water solution ($\mu_w = 1.0 \times 10^{-3}$ Pa·s, $\rho_w = 1.0 \times 10^3$ kg/m³).

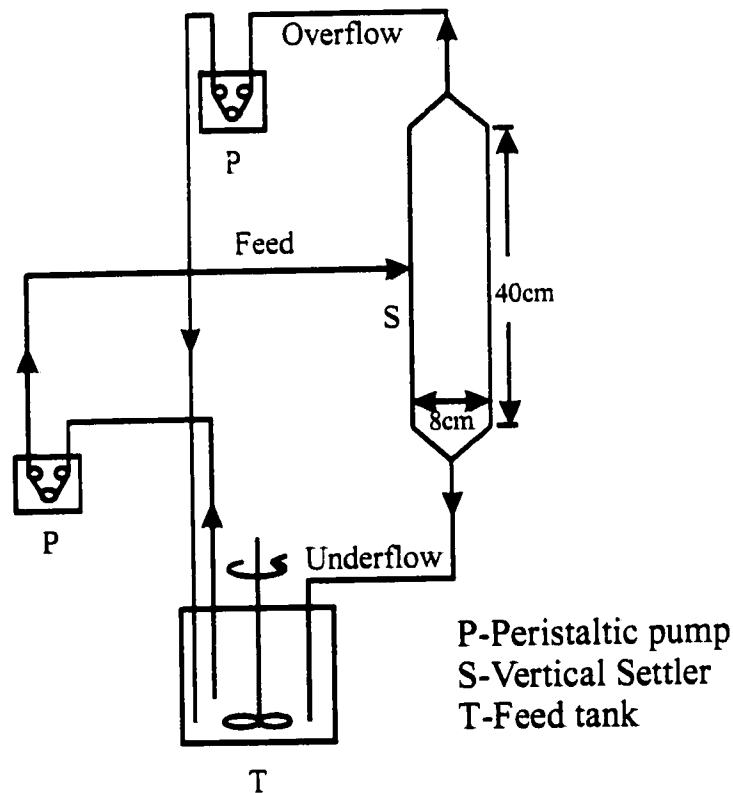


Figure 3.3 Vertical settler experimental set-up

As nylon fibres are hydrophobic in nature, few drops of Triton X-100 were added to obtain homogeneous nylon fibre-water suspension. Experimental observations showed that a 0.07% surfactant concentration gave good fibre suspension. Below this concentration, the surfactant was not sufficient to disperse the nylon fibres, however, at much higher concentrations, long fibres could get entrapped by large air bubbles and finally be floated. For each experiment, the feed flow rate was kept constant. The split ratio could be changed by a peristaltic pump pulling suspension from the top of the column. The time allowed to reach steady state condition was approximately 20-30 minutes. After reaching steady state conditions, samples from the overflow and underflow stream were taken separately. FQA was used to measure the sample mean length and the numbers of fibre measured for a certain amount of fibre suspension.

3.4 RESULTS AND DISCUSSIONS

3.4.1 Effect of split ratio

The effect of split ratio (Q_O/Q_F) was studied at a feed flow rate (Q_F) of $2.819 \times 10^{-6} \text{ m}^3/\text{s}$, feed consistency (X) 0.01%. The split ratio varied from 0.14 to 0.63. Variations of the average fibre length (length weighted mean length, L_L , and arithmetic mean length, A_L) for overflow and underflow streams shown in Figure 3.4.1a. Figure 3.4.1a indicates that the mean length of samples in overflow increased with an increase in the split ratio. However, practically no change was observed in fibre length in the underflow stream. Overflow fibre length distributions at different split ratios are also shown in Figure 3.4.1b.

At a given feed flow rate, for small split ratios, the upward fluid velocity is small as compared to the settling velocity of long fibre, therefore most of the short fibres come out in the overflow stream and reduce the average fibre length. As the split ratio is increased, the upward fluid velocity increases and starts to carry long fibres out in the overflow stream leading to an increase in the average fibre length. This suggests that by selecting a desired split ratio, a vertical settler is capable of fractionating fibres according to their length. The results are in agreement with our theoretical predictions.

From the Figure 3.4.1a, one can observe that the average fibre length of underflow stream is close to the feed mean length. This can be explained by considering the quantity of fibre suspension in the overflow stream. The consistency data for each sample from the overflow stream is given in table 3.4.1. At lowest split ratio 0.14, the consistency observed is 2.46×10^{-4} (% w/w), which is quite low compared to the feed consistency 1.0×10^{-2} (% w/w). It indicates that the actual amount of fibres removed from the overflow stream is too small to influence the average fibre length of underflow stream. Similar observations can be made at other split ratios. At the highest split ratio of 0.63, even though the consistency of overflow suspension increases significantly, there is no change in the average fibre length as compared to the feed stream. As a result, within the range of split ratios studied, the average length of the underflow stream hardly changes.

The above observations suggest that a vertical settler is capable of fractionating fibres of a given diameter by length, but the small difference in the settling velocity between the 3 mm fibres and 1 mm fibres limits the efficiency of the separation system.

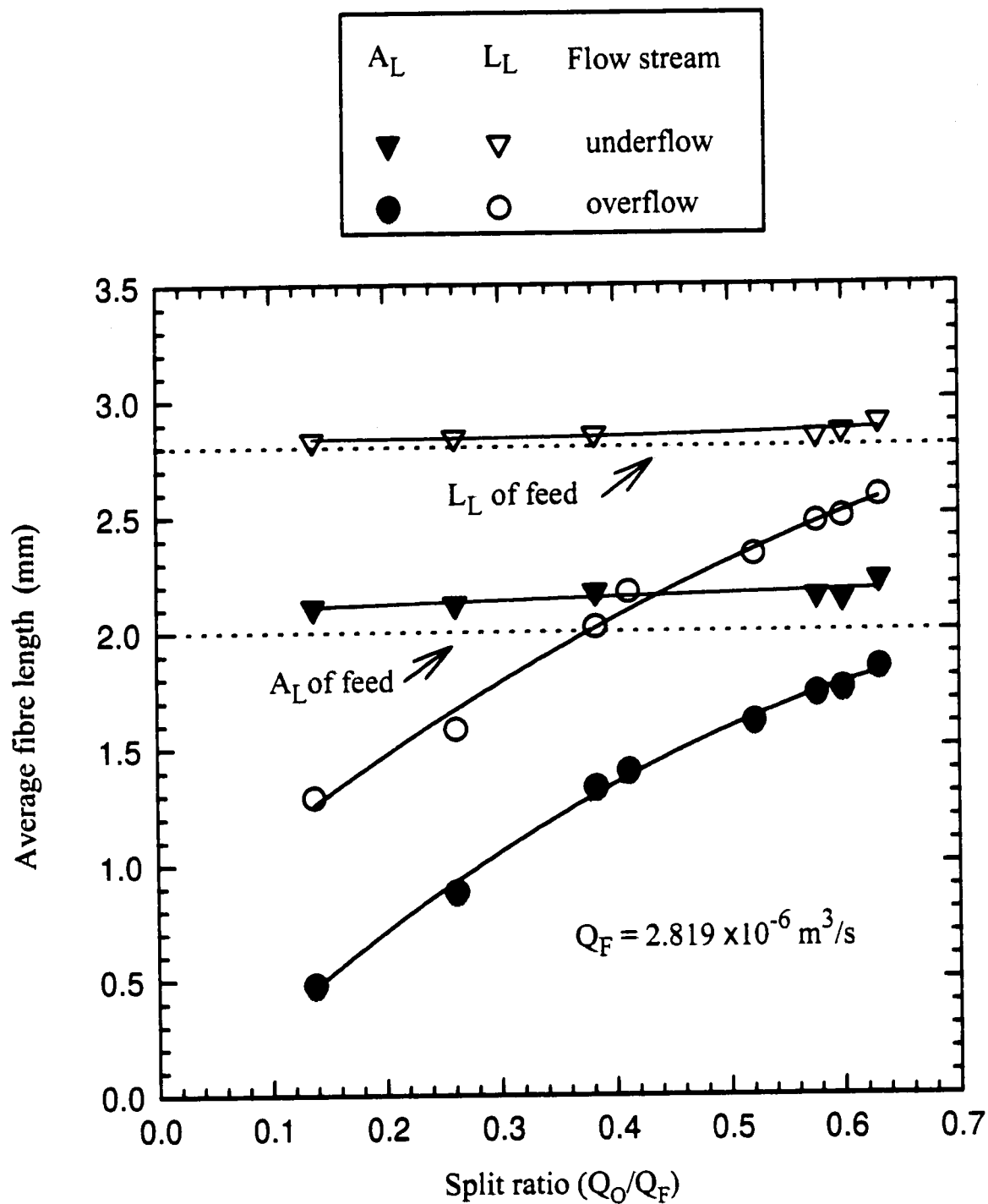


Figure 3.4.1a Variation of average fibre length in the overflow and underflow streams with split ratio

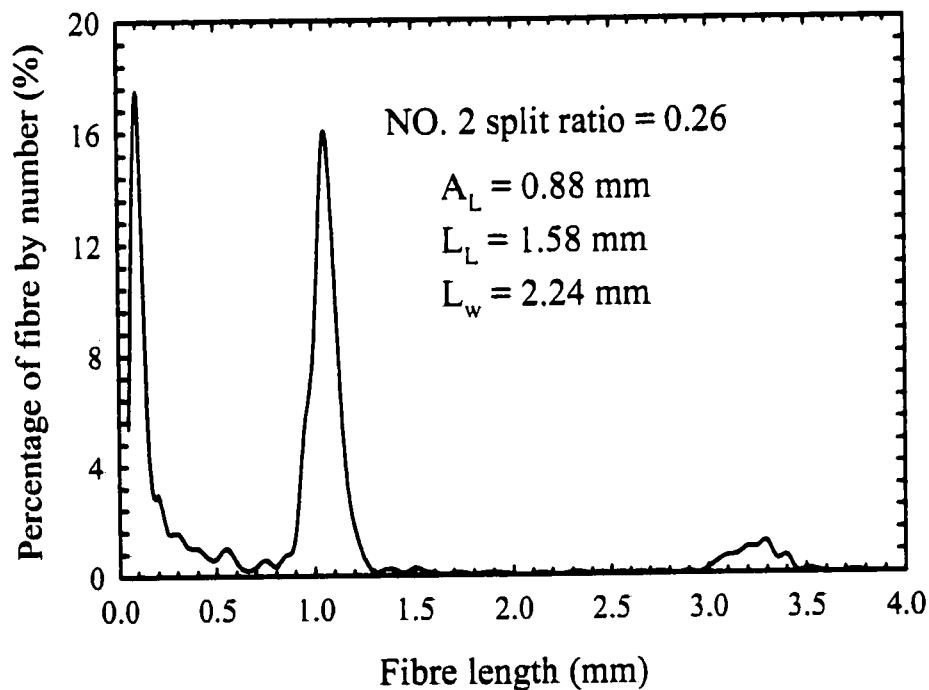
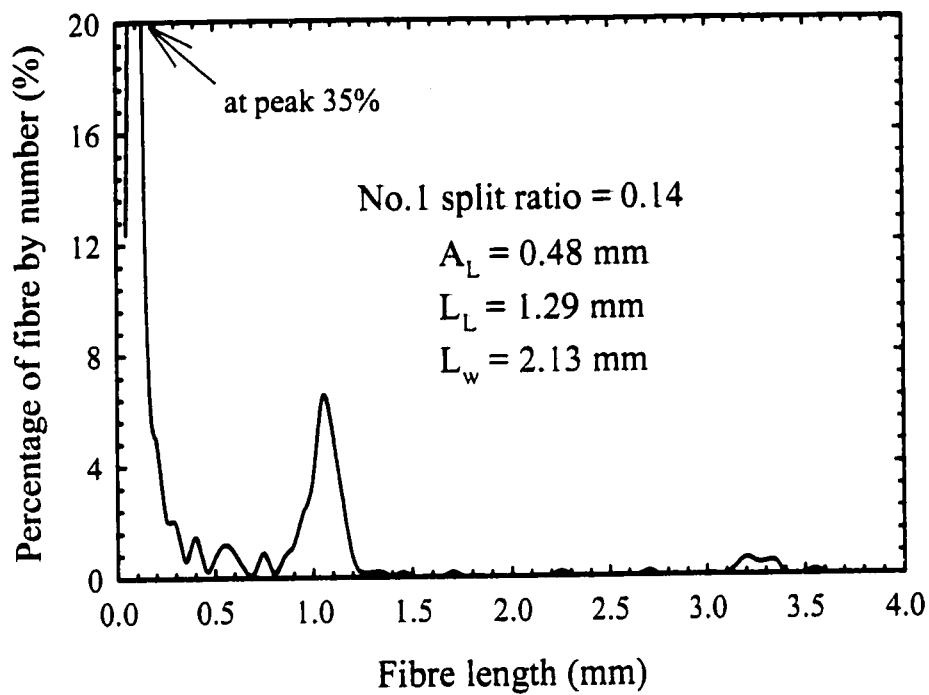


Figure 3.4.1b Overflow fibre length distributions at different split ratios
 $Q_F = 2.819 \times 10^{-6} \text{ m}^3/\text{s}$, $X = 0.01\%$
 Part 1

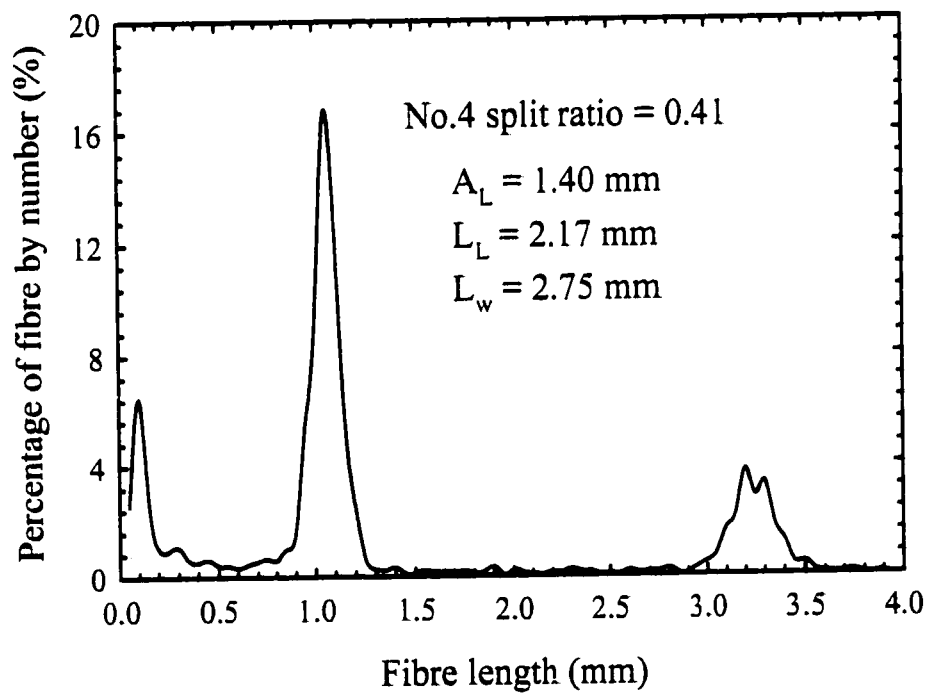
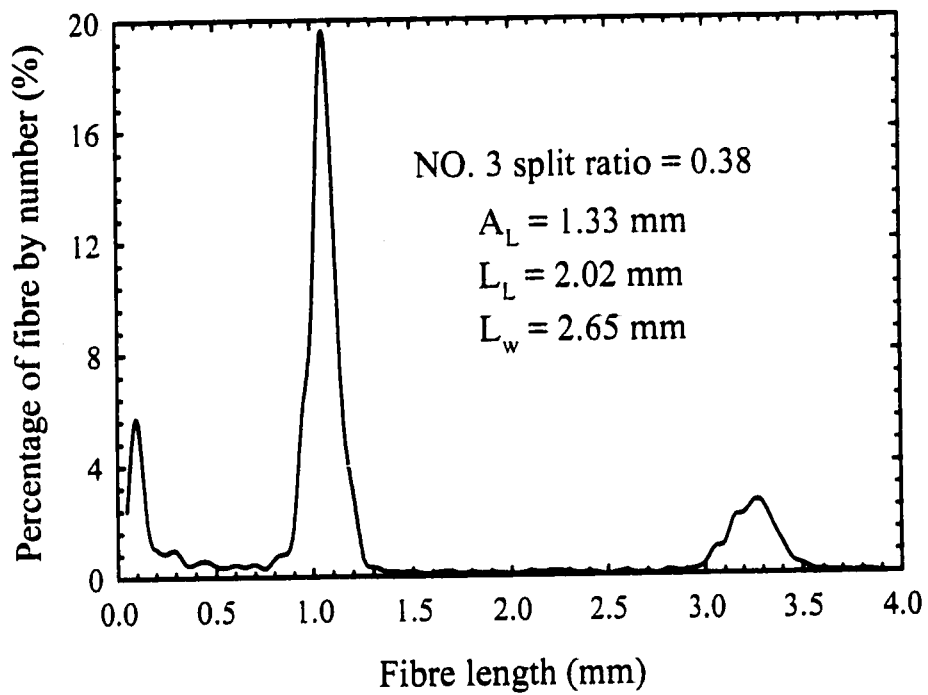


Figure 3.4.1b Overflow fibre length distributions at different split ratios
 $Q_F = 2.819 \times 10^{-6} \text{ m}^3/\text{s}$, $X = 0.01\%$
 Part 2

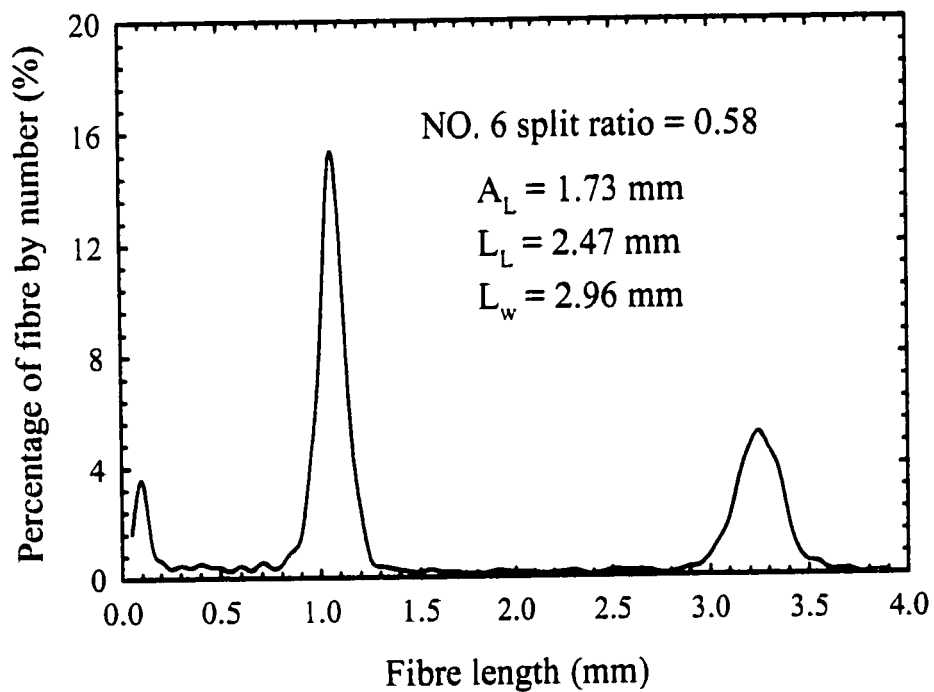
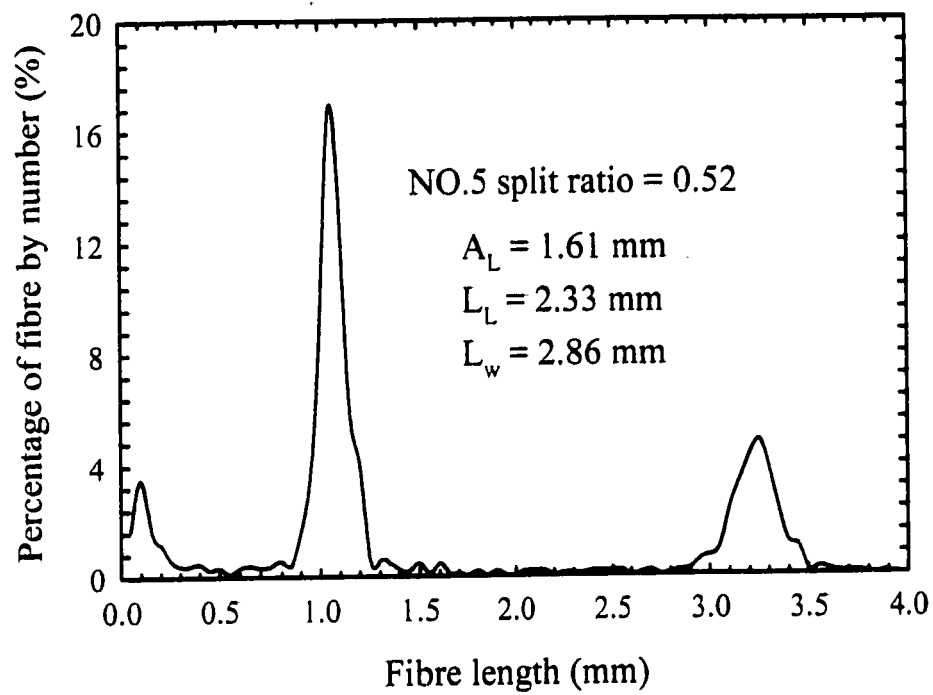


Figure 3.4.1b Overflow fibre length distributions at different split ratios
 $Q_F = 2.819 \times 10^{-6} \text{ m}^3/\text{s}$, $X = 0.01\%$
 Part 3

Overflow Sample	No.1	No.2	No.3	No.4	No.5	NO.6	No.7
Split Ratio	0.14	0.26	0.38	0.41	0.52	0.60	0.63
A_L (mm)	0.48	0.88	1.33	1.4	1.61	1.75	1.84
$X \times 10^4$ (%)	2.46	9.77	59.6	107	207	221	297

Table 3.4.1 Approximate consistency and average fibre length for each overflow stream sample corresponding to various split ratios at $Q_F = 2.819 \times 10^{-6} \text{ m}^3/\text{s}$.

3.4.2 Effect of feed flow rate

The effect of feed flow rate was studied for a feed consistency of 0.01%. Three feed flow rates were selected: 2.819×10^{-6} , 4.657×10^{-6} and $9.077 \times 10^{-6} \text{ m}^3/\text{s}$. Variations of the average fibre length (L_L and A_L) in the overflow stream with the different split ratios at various feed flow rates are shown in Figure 3.4.2a & b.

Figures 3.4.2a & b show that the average fibre length in the overflow stream for a given feed flow rate increased with an increase in the split ratio. It also can be observed that for each curve, there always exists a range of split ratio within which fractionation occurs. This range decreases with an increase in the feed flow rates. This means that the average fibre length in the overflow stream approaches the feed fibre length earlier at a higher feed flow rate. At the same split ratio, an increase in the feed flow rate leads to a higher overflow flow rate, i.e. the upward fluid velocity increases with an increase in the feed flow rate. As a result, more long fibres are carried away with the overflow stream whereby reducing the fractionation performance.

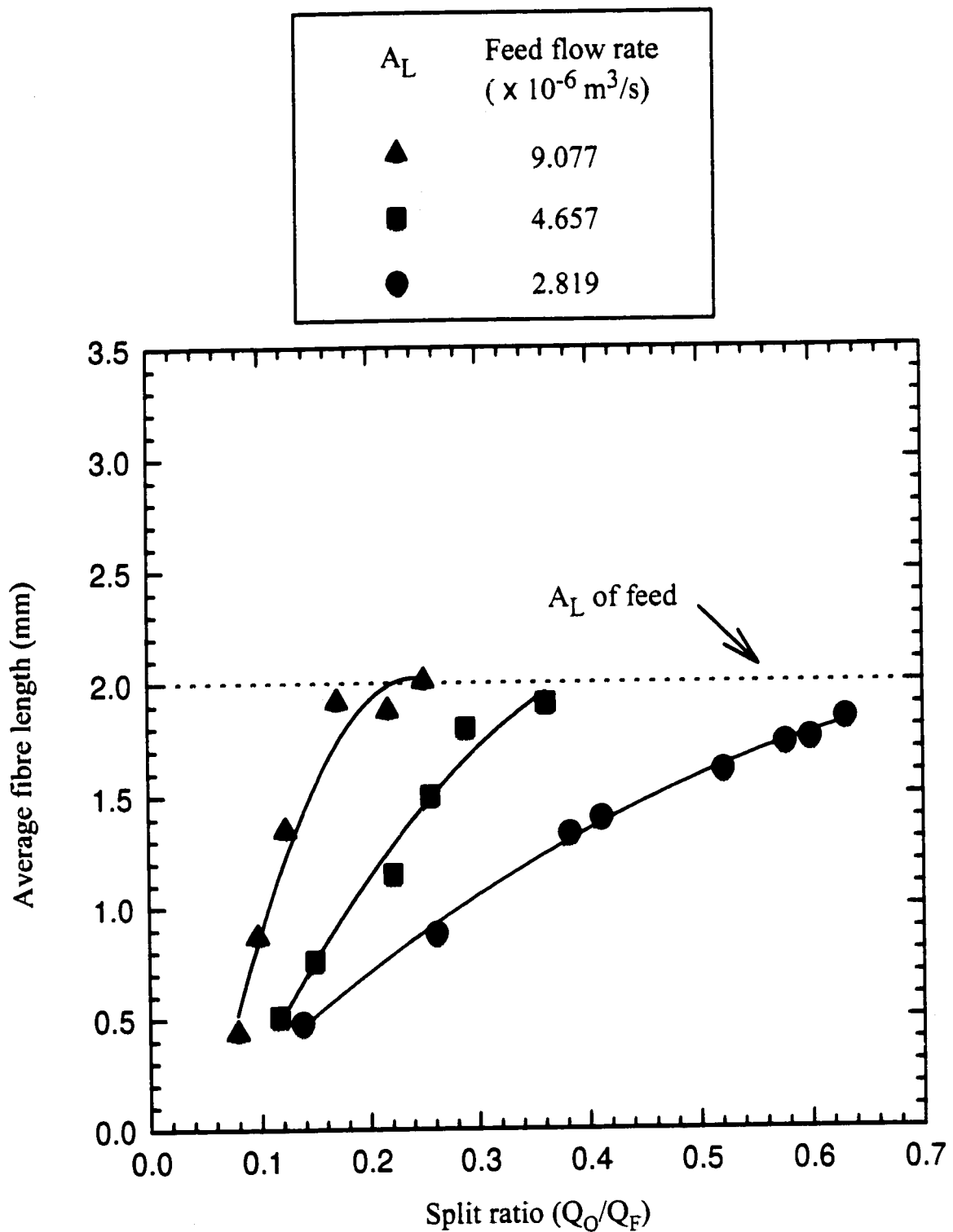


Figure 3.4.2a Variation of the arithmetic average fibre length with split ratio at different feed flow rates

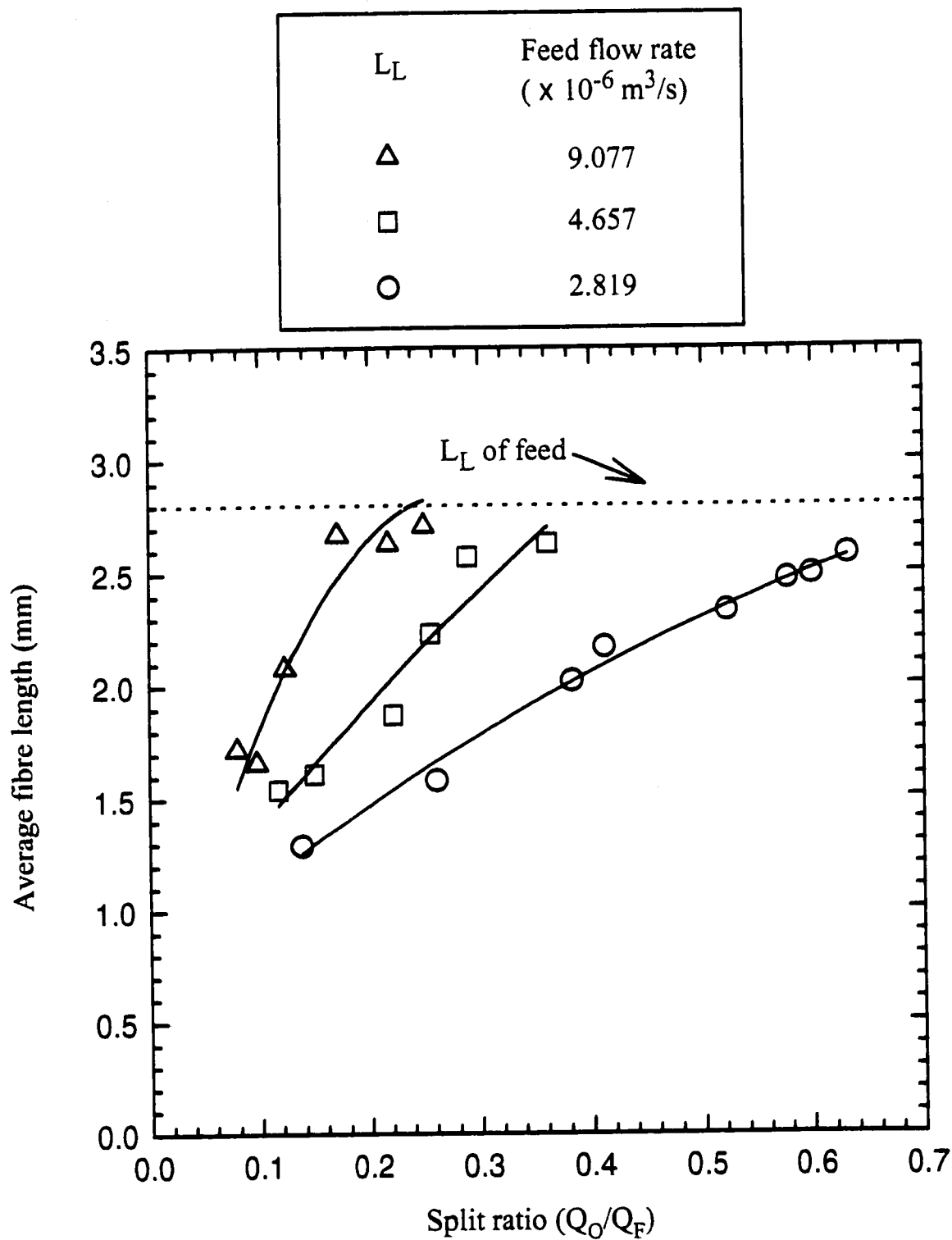


Figure 3.4.2b Variation of the length weighted average fibre length with split ratio at different feed flow rates

According to the definition, it is clear that upward fluid velocity can be expressed as $U_{fO} = (Q_F \times \text{split ratio})/S$. By converting the experiment data into upward fluid velocities, one can also plot the variation of the average fibre length in the overflow stream at different upward fluid velocities shown in Figure 3.4.2c. It can be observed that the average fibre length in the overflow stream increased with an increase in the upward fluid velocity and that the experimental data collapsed together for all the different feed flow rates. Based on the theoretical discussion in the previous section, it is known that the performance of fractionation in a vertical settler depends on upward fluid velocity for given feed consistency and composition. Figure 3.4.2c also indicates fairly good reproducibility of vertical settler method.

To compare the experimental data with the theoretical model, the average fibre length has to be converted in terms of fraction ratio of short fibres in overflow stream ($\alpha_{sO}/(\alpha_{sO} + \alpha_{lO})$). The conversion is shown in Appendix II.

The experimental results and model prediction are shown in Figures 3.4.2d-f. From these figures, one can observe that model predictions are better at $Q_F = 4.657 \times 10^{-6}$ and $9.077 \times 10^{-6} \text{ m}^3/\text{s}$ flow rates. However, large deviation is observed at the lowest feed flow rate of $2.819 \times 10^{-6} \text{ m}^3/\text{s}$.

From Figures 3.4.2d-f, one can always observe that there exists a range of split ratio below which both short and long fibres are carried in the underflow stream and above which both fibre types are carried out with the overflow stream. Calculations for this specific range of split ratio are discussed below.

Overflow fluid velocity (U_{fO}) was compared with the settling velocities of the fibres (U_{As} for 1 mm fibre and U_{Al} for 3 mm fibre). Theoretically, when $U_{fO} < U_{As}$, no

fibres report to the overflow stream; when $U_{As} < U_{f0} < U_{Al}$, only short fibres can be carried with the overflow stream; when $U_{f0} > U_{Al}$, both short and long fibres will come out along in the overflow stream. Therefore, the ideal condition for fibre fractionation will be $U_{As} < U_{f0} < U_{Al}$. From equation 3.11, the settling velocities for 1 mm and 3 mm fibres in water in axial flow can be calculated as 2.61×10^{-4} m/s and 3.31×10^{-4} m/s. The ranges of split ratio for the three different feed flow rates, $Q_F = 2.819, 4.657$ and 9.077 ($\times 10^{-6}$ m³/s) are (0.22 - 0.28), (0.14 - 0.17) and (0.07 - 0.09), respectively, which also shows that the range and absolute value of split ratios increase with a decrease in feed flow rate.

A_L	L_L	Feed flow rate ($\times 10^{-6} \text{ m}^3/\text{s}$)
▲	△	9.077
■	□	4.657
●	○	2.819

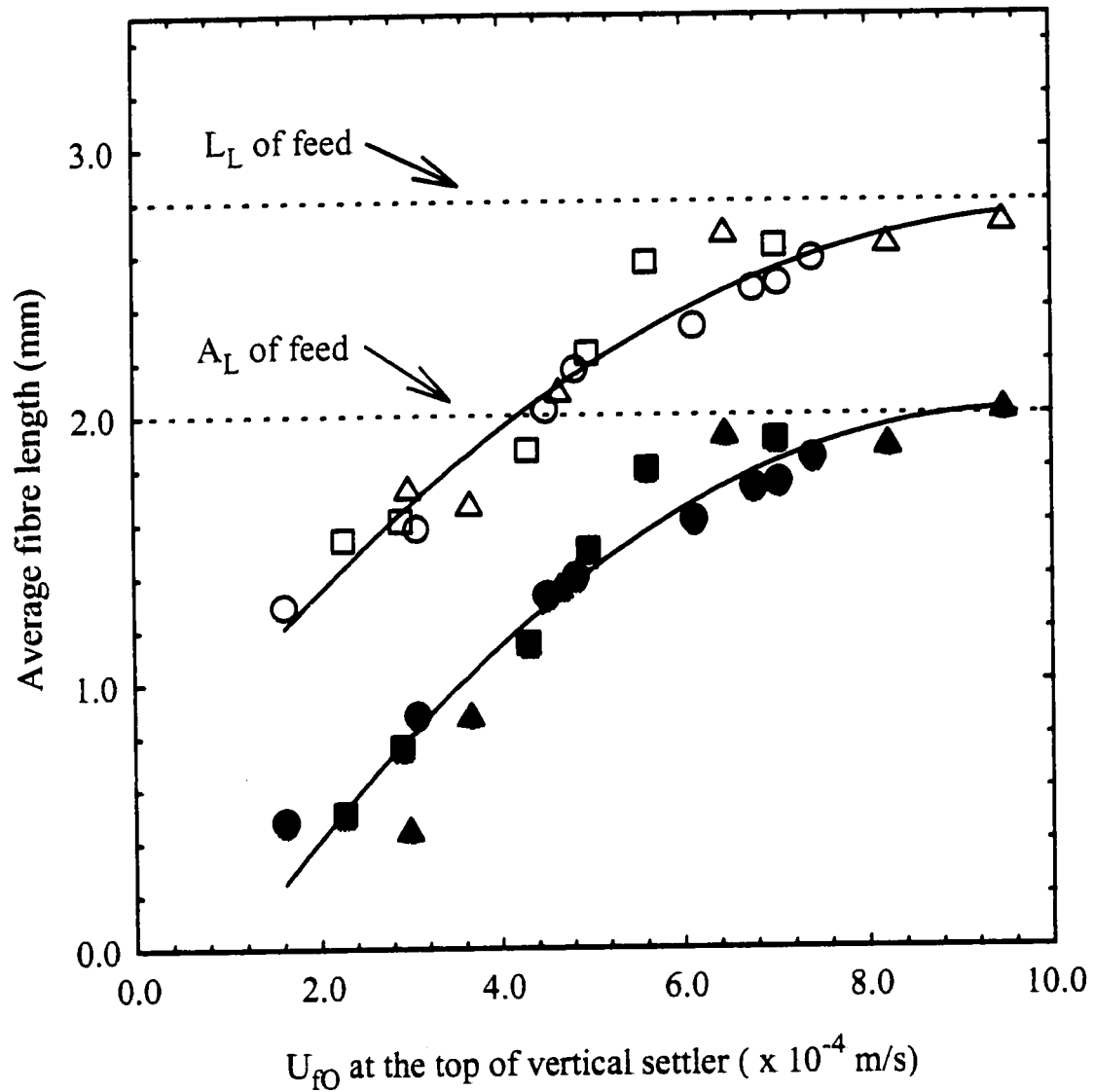


Figure 3.4.2c Variation of the average fibre length at different upward fluid velocities

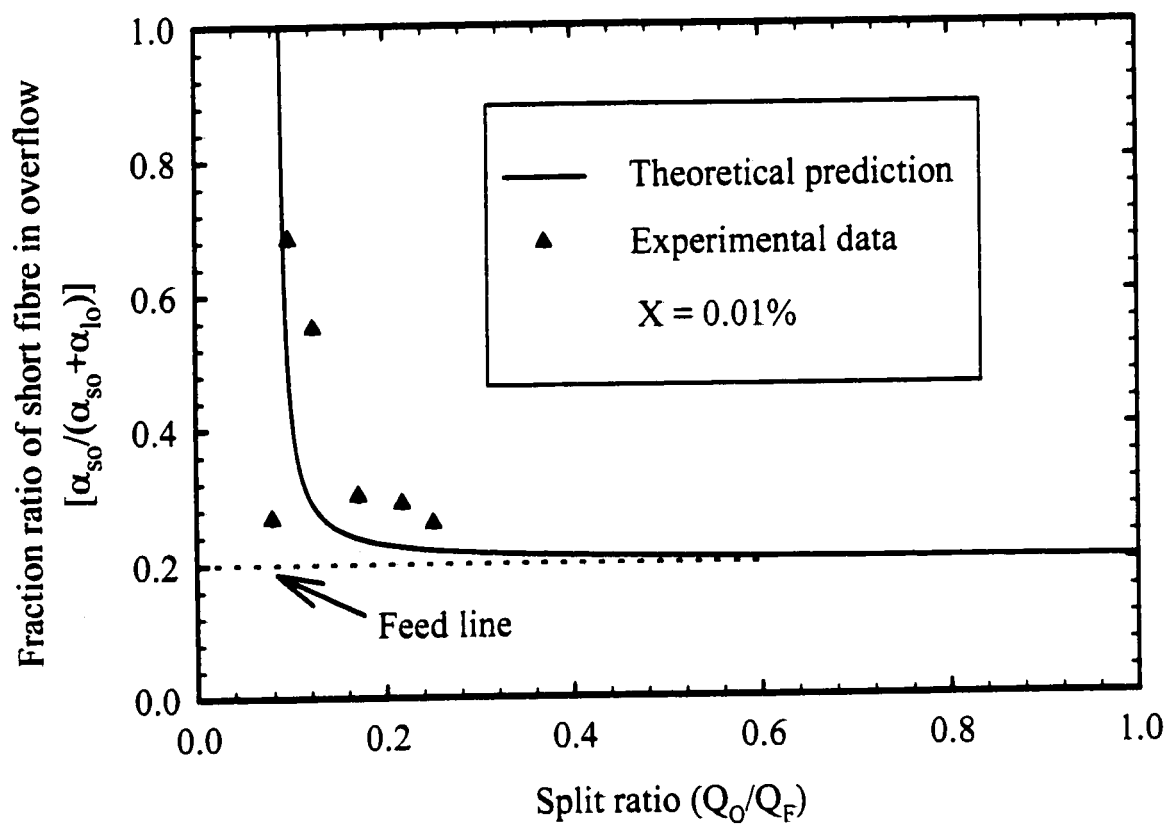


Figure 3.4.2d Comparison between theoretical model and experimental data for a feed flow rate of $9.077 \times 10^{-6} \text{ m}^3/\text{s}$

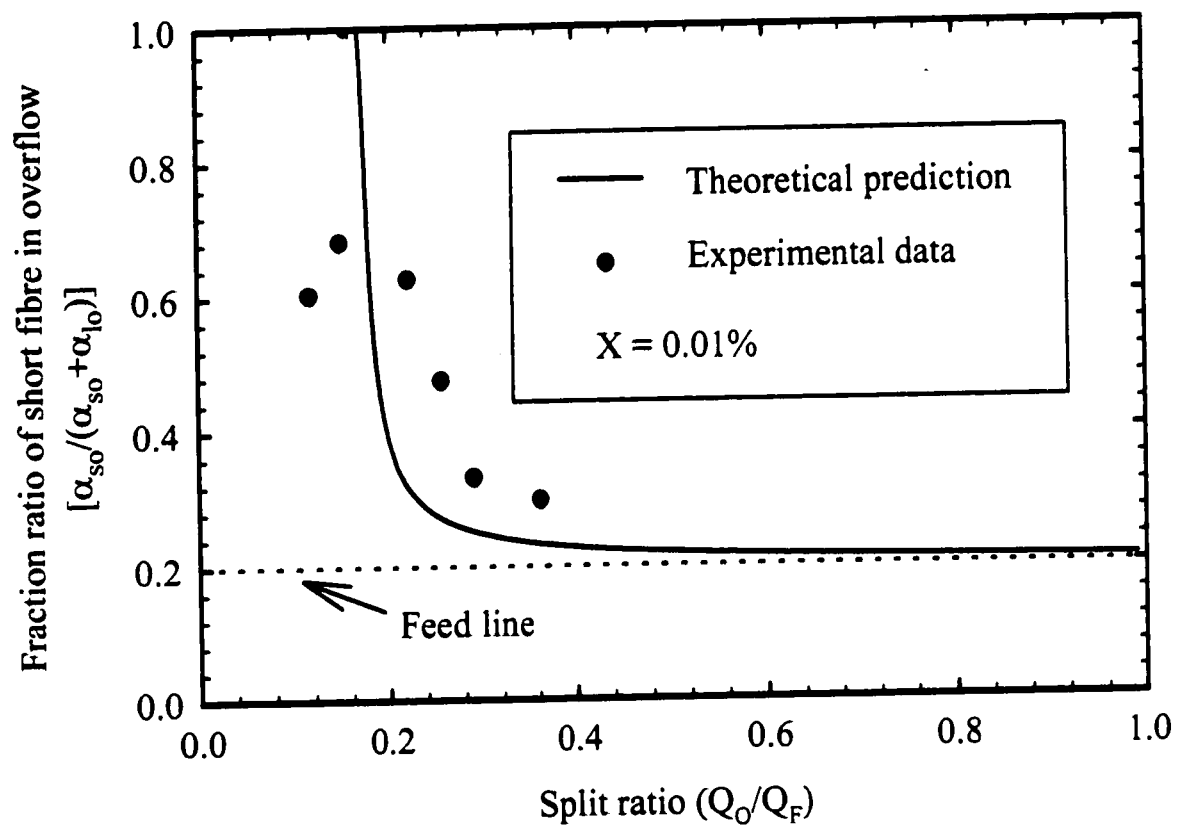


Figure 3.4.2e Comparison between theoretical model and experimental data for a feed flow rate of $4.657 \times 10^{-6} \text{ m}^3/\text{s}$

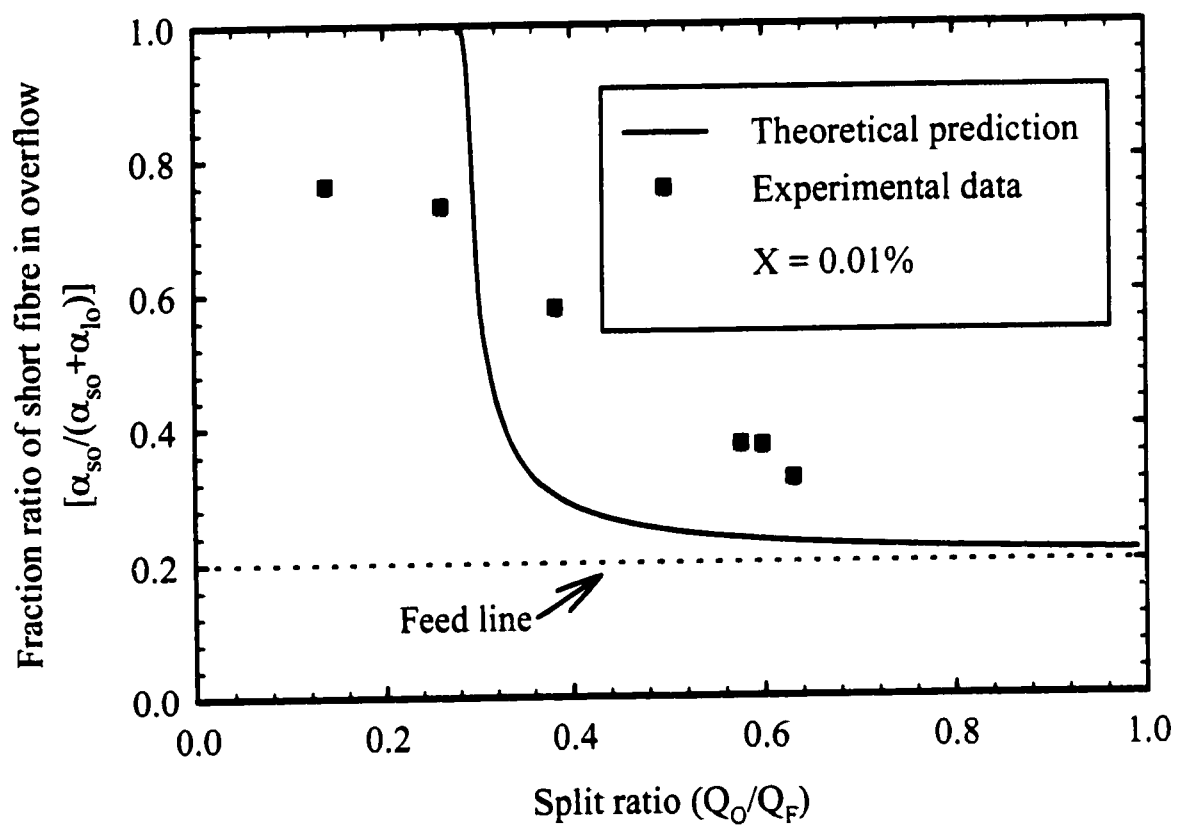
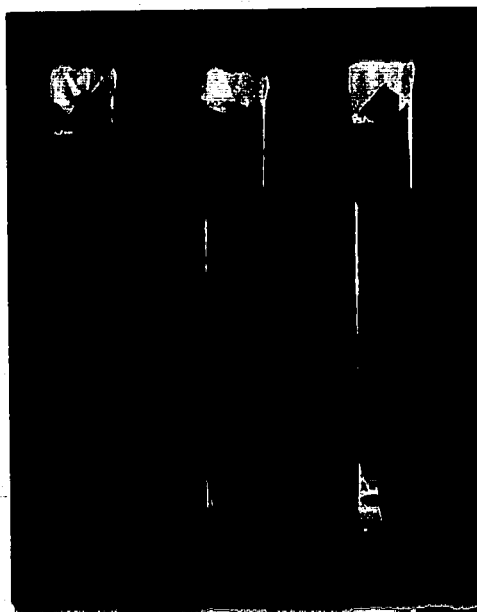


Figure 3.4.2f Comparison between theoretical model and experimental data
 for a feed flow rate of $2.819 \times 10^{-6} \text{ m}^3/\text{s}$

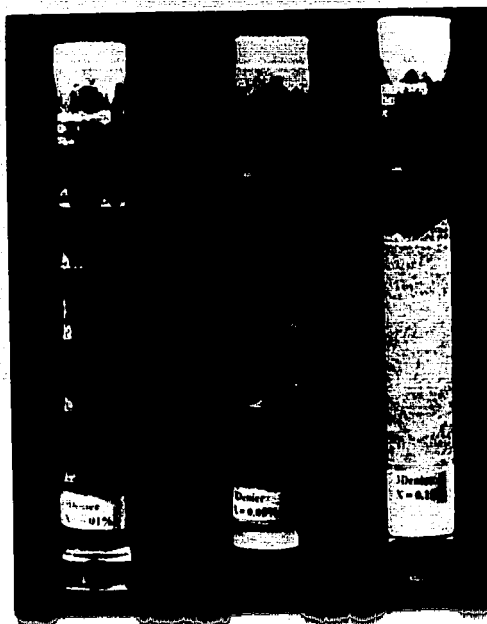
3.4.3. Effect of feed consistency

The effect of feed consistency was studied at a feed flow rate (Q_F) of $4.657 \times 10^{-6} \text{ m}^3/\text{s}$. The feed consistencies studied were 0.01%, 0.05% to 0.15%. Although the absolute values of the feed consistencies are very low, the presence of the fibre is visually evident. Photographs 3.4.3 (i) and 3.4.3 (ii) show the three suspensions when the fibres are settled at the bottom of a graduated cylinder and when they are in suspension, respectively. At $X = 0.15\%$, plugging by fibres occurred in the connecting tubing. Compared to $X = 0.15\%$, the other two are sufficiently dilute to avoid the plugging problem.

Variations of the average fibre length (L_L and A_L) in the overflow stream with split ratio for two feed consistencies are shown in Figure 3.4.3a. It can be observed that the average fibre length effects for $X = 0.01\%$ and 0.05% are similar, thereby supporting the assumption made for the theoretical model that there is no hindered settling due to extreme dilution. The modified experimental results in terms of fraction ratio of short fibres in the overflow ($\alpha_{sO}/(\alpha_{sO} + \alpha_{lO})$) and model predictions for both feed consistencies are shown in Figure 3.4.3b. The comparison of fractionation ratio of short fibre in overflow stream between model prediction and experimental data shows fairly good agreement. The results indicate that the model can be applied up to the highest feed consistencies employed in this study.



(i) Height of fibre bed under settle conditions



(ii) Well dispersed fibre suspensions

Photograph 3.4.3 Fibre suspensions at different consistencies of 0.01%, 0.05% and 0.15%

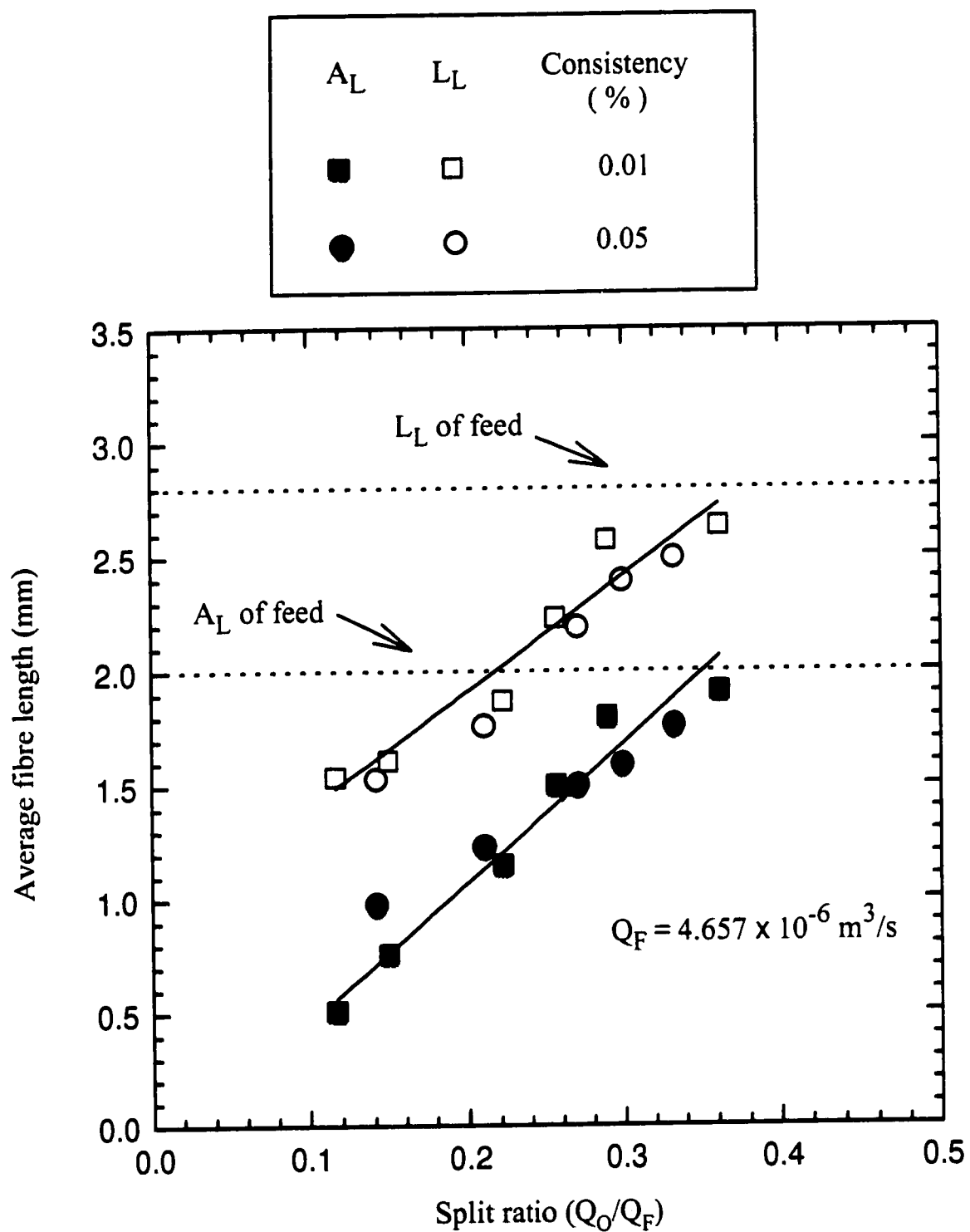


Figure 3.4.3a Variation of average fibre length at different feed consistencies

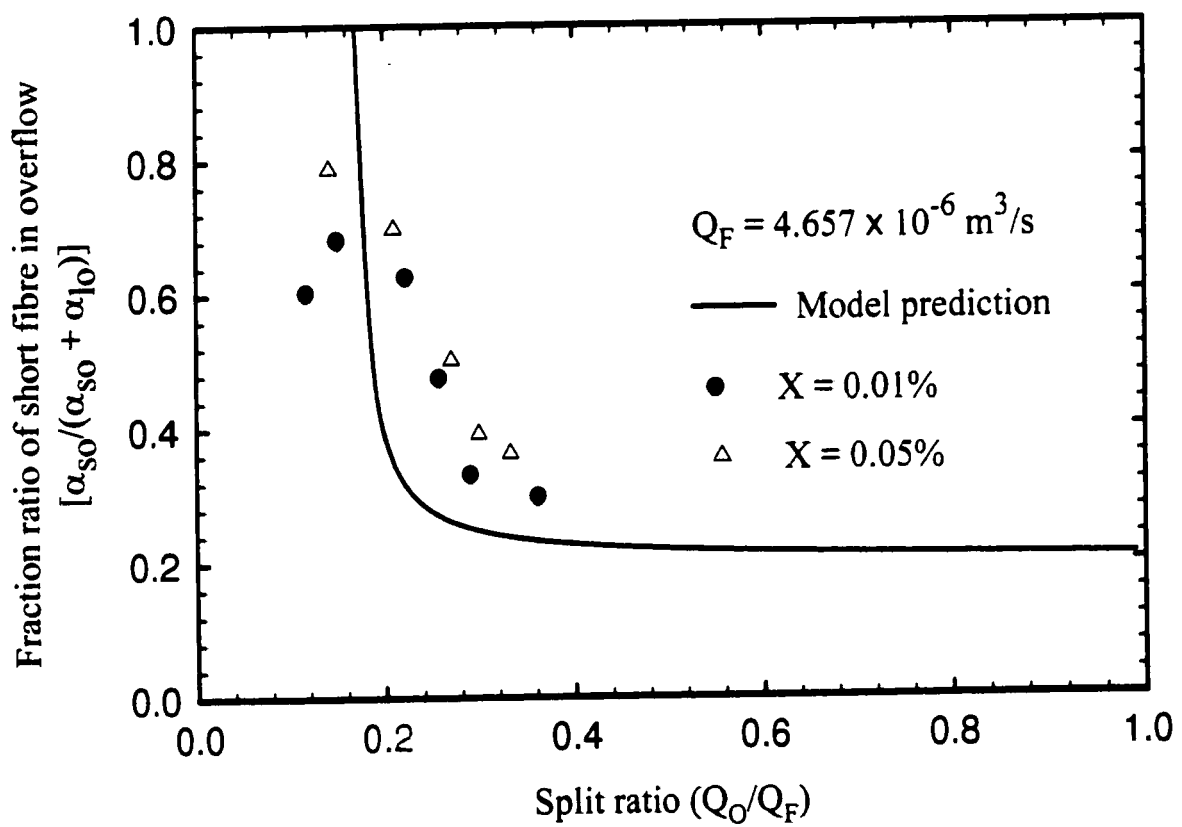


Figure 3.4.3b Comparison between theoretical model and experimental data for two feed consistencies

3.4.4 Effect of fibre diameter

Two different experiments were carried out using 14 μm and 20 μm diameter fibre suspensions. One mixture was made up of a suspension having 1 mm and 3 mm long fibres with a diameter of 14 μm . The other suspension had 1 mm and 3 mm long fibres with a diameter of 20 μm . Both suspensions were evaluated at a consistency of 0.01% and the composition of the feed suspension was 20% of 1 mm and 80% of 3 mm fibres. Their length distributions are shown in Figures 2.2e & f. Although the same mass ratio of the 1 to 3 mm fibres is used, the value of A_L for the 14 μm diameter suspension is 1.59 mm, which is different from that for the 20 μm diameter suspension which is 1.98 mm. This is simply due to the difference in the individual size distribution of fibres as shown in Figures 2.2a-d.

Variations of the average fibre length in the overflow stream with the split ratio at various feed flow rates are shown in Figure 3.4.4a for 20 μm diameter fibres and in Figure 3.4.4b for 14 μm diameter fibres. The feed flow rate was kept constant as $2.819 \times 10^{-6} \text{ m}^3/\text{s}$ for both experiments. In Figure 3.4.4b, the average length (L_L and A_L) plots of samples in the overflow stream for the 14 μm fibres are very close to their respective average feed lengths, which indicates small fibre fractionation. On the other hand, in Figure 3.4.4a for the 20 μm fibres, it can be observed that the average fibre length decreases with a decrease in the split ratio. Excellent fractionation is found at a low split ratio.

From section 3.2.1.2, the settling velocity of a fibre in axial flow is given by

$$U_A = \frac{D^2 \Delta \rho g \left[\ln\left(\frac{L}{D}\right) + 0.19315 \right]}{8\mu} \quad (3.11)$$

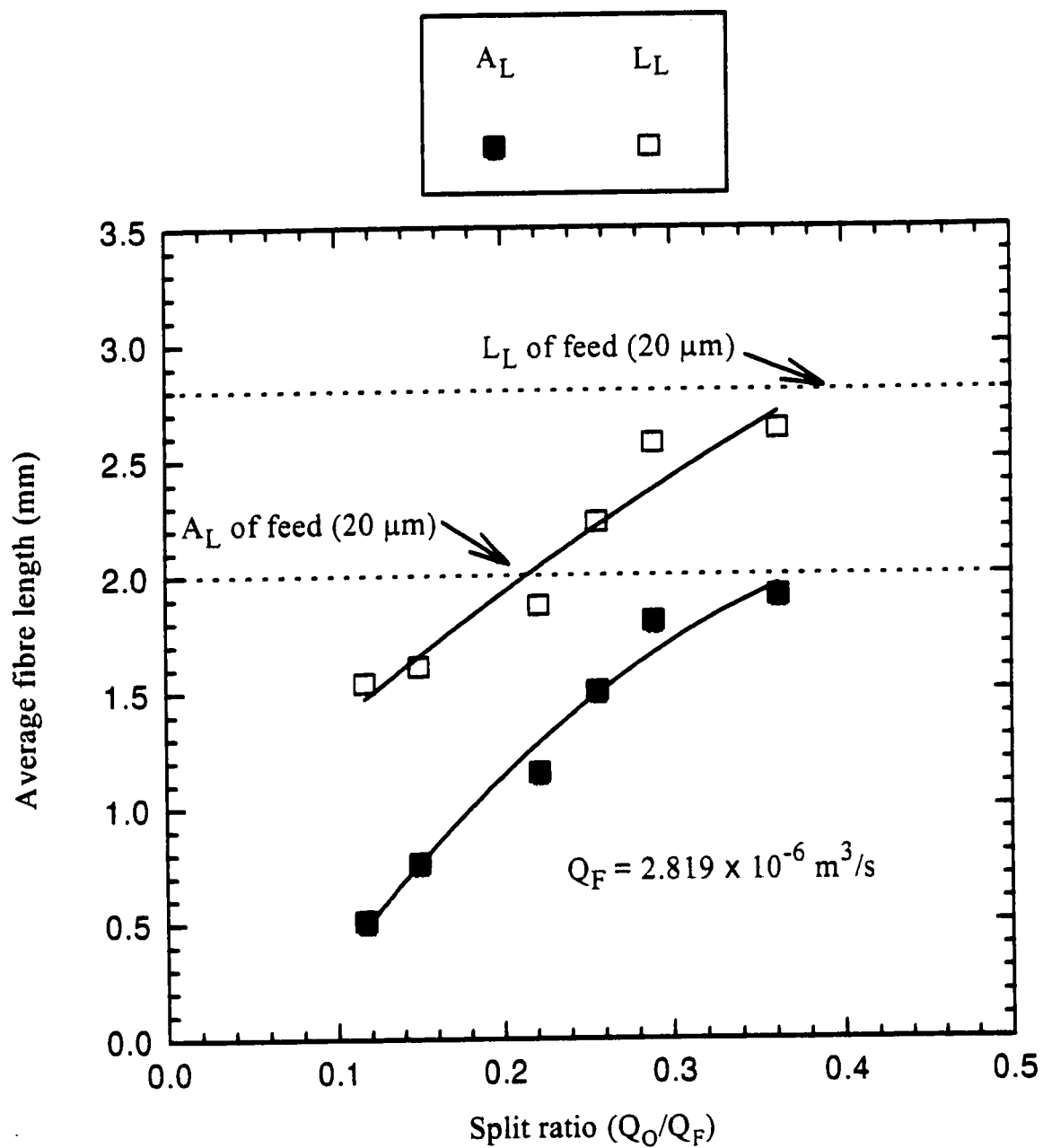


Figure 3.4.4a Variation of average fibre length with split ratio for a $20\ \mu\text{m}$ fibre diameter

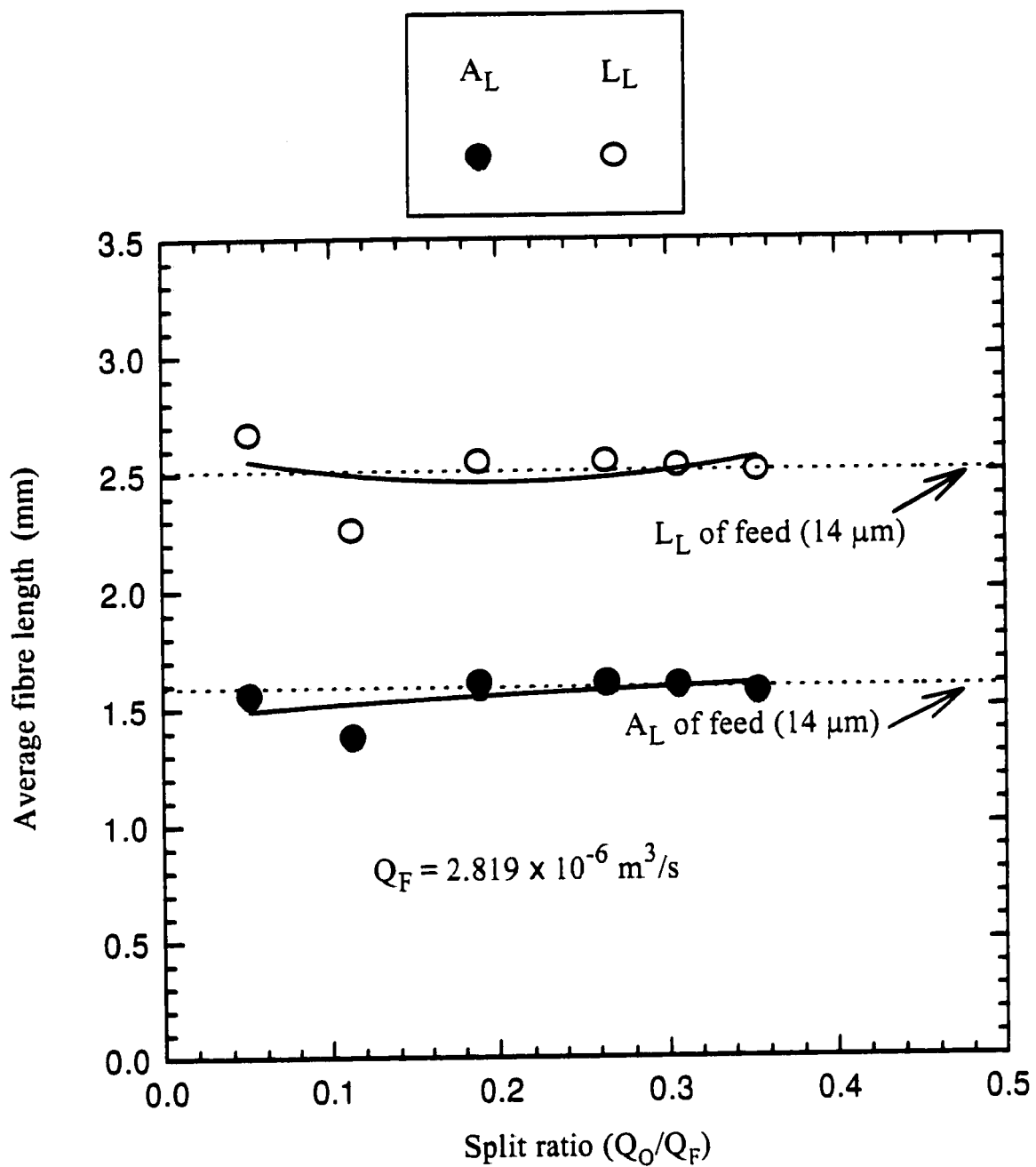


Figure 3.4.4b Variation of average fibre length with split ratio for a $14\ \mu\text{m}$ fibre diameter

Equation 3.11 indicates that the settling velocity of a fibre in axial flow depends on both the fibre length and its diameter. Figure 3.4.4c shows the variation of the settling velocity of individual fibres in axial flow with fibre diameter for 1 mm and 3 mm long fibres.

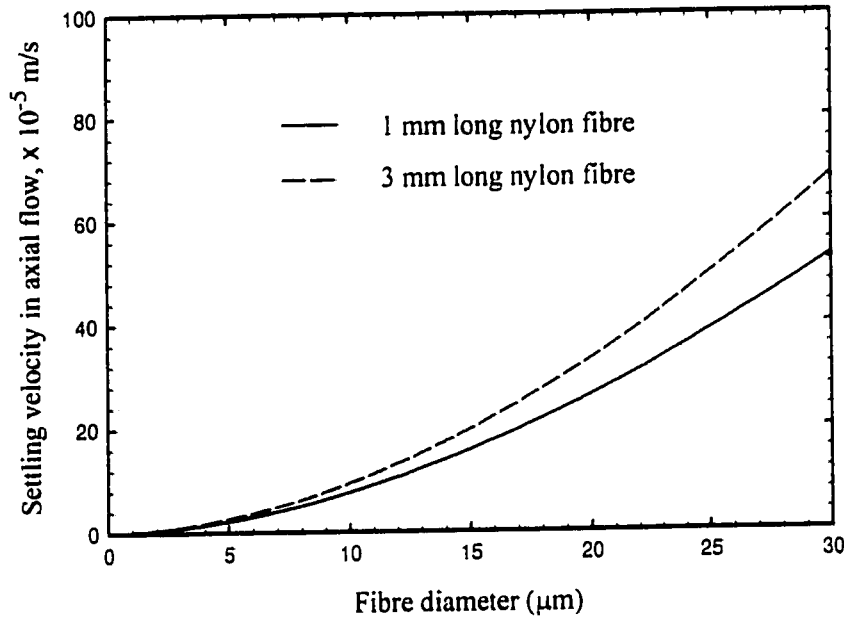


Figure 3.4.4c Variation of the settling velocity of individual fibres in axial flow with fibre diameter for 1 mm and 3 mm long fibres

From Figure 3.4.4c, it is clear that the settling velocity of fibre in axial flow increases with an increase in fibre diameter as well as with fibre length. Another important observation from this figure is that the difference of the settling velocity between 1 mm and 3 mm fibres decreases with a decrease in fibre diameter. For the 20 μm fibre diameter, the settling velocities of 1 mm and 3 mm are 2.61×10^{-4} and 3.31×10^{-4} m/s, respectively, and for the 14 μm fibre diameter, the settling velocities of 1 mm and 3 mm are 1.39×10^{-4} and 1.74×10^{-4} m/s, respectively. The difference between the settling velocities for 1 mm and 3 mm fibre with 14 μm fibre diameter is

only 49.0% that of 20 μm fibre diameter. For the same consistency, there is as twice number of fibres in 14 μm diameter fibre suspension as in 20 μm diameter fibre suspension. Therefore, the interactions among the fibres are much more in 14 μm diameter fibre suspension. These indicate that it is more difficult to separate fibres with 14 μm diameter than with 20 μm diameter. As one increases the fibre diameter, the difference in the settling velocity increases, and fractionation becomes more evident.

One can conclude that the difference in the settling velocities of fibres decreases with a decrease in fibre diameter, whereby fractionation becomes worse at small fibre diameters, and vice versa.

3.5 CONCLUSIONS

Due to the difference in the settling velocities, both theoretical analysis and experimental results suggested that a vertical settler is capable of fractionating fibres having identical diameters according to fibre length.

One can conclude that

- Fibre fractionation occurs only in a certain range of split ratios, within which the fractionation performance decreases with an increase in the split ratio.
- A range of split ratios, below and beyond which no fractionation can occur, decreases with an increase in the feed flow rate.
- For very dilute suspensions, feed consistency has no effect on fibre separation.
- Fibre fractionation performance is better for 20 μm fibre diameter than for 14 μm at the same fibre length due to its higher settling velocity.

A theoretical model, based on volumetric balance and slip velocity, agrees fairly well with the experimental results. From the theoretical model, fibre fractionation performance can be improved with an increase in fibre diameter.

CHAPTER 4

ROTATING CONE FRACTIONATOR

4.1 INTRODUCTION

Rotating cone fractionator (RCF) is a technique developed for fibre fractionation based on similar principles as that of a plate atomizing wheel. A literature survey on plate atomizing wheel is summarized in Table 4.1.

Moller et al. (1979) developed the technique of a plate atomizing wheel for fibre fractionation which could use feed consistency as high as 3% ~ 6%. The equipment consisted mainly of an atomizing wheel and a collection chamber as shown in Figure 4.1.

Source	Moller et al. (1979)	Moller et al. (1980)	Oroskar and Corosy (1984)	Oroskar and Corsby (1986)
Fibre Type	Ground wood Pulp fibres	50% TMP & 50% Kraft pulp, CSF = 350ml	Natural fibre; diameter = 18 & 54 microns length = 3mm	Softwood, Hardwood and Synthetic fibres of 54 & 18 microns 3mm long
Disk Design	Inverted plate	Inverted plate	Wide lip disk	Vaneless & Conical bowl with horizontal skirt
Disk Diameter (mm)	120	150, 210, 400, 550, 750	150	200
Lip Angle(degree), Lip Length (mm)	—	—	22 ^{1/2} , 45, 67 ^{1/2} , 90, 135 lip length = 50, 40	67 ^{1/2} , 45, 22 ^{1/2} , lip length = 50
Disk Speed (rpm)	20,000	850-4200	13080, 9620, 8420	6000, 9400, 4200, 2740, 1920
Feed Consistency (%) and Flow rate	3% 10.5 L/min	3-6% 1.1-10.2 ton/day	1.0% 3 L/min	1.6% 4 & 22 L/min
Remarks	Five fractions having different properties were collected from a given feed.	Power consumption has been measured and correlated for scale-up purpose.	Lip angle 67.5° and 45° are best for fractionation. No fractionation occurs with 135° lip angle. The amount of overlap between the collector zones increases with a decrease in the lip length.	Higher disk diameter and larger lip angle facilitate detachment of specific fibre diameter

Table 4.1 Literature survey on fibre fractionation using a plate atomizing wheel

(Rewatkar and Masliyah, 1996)

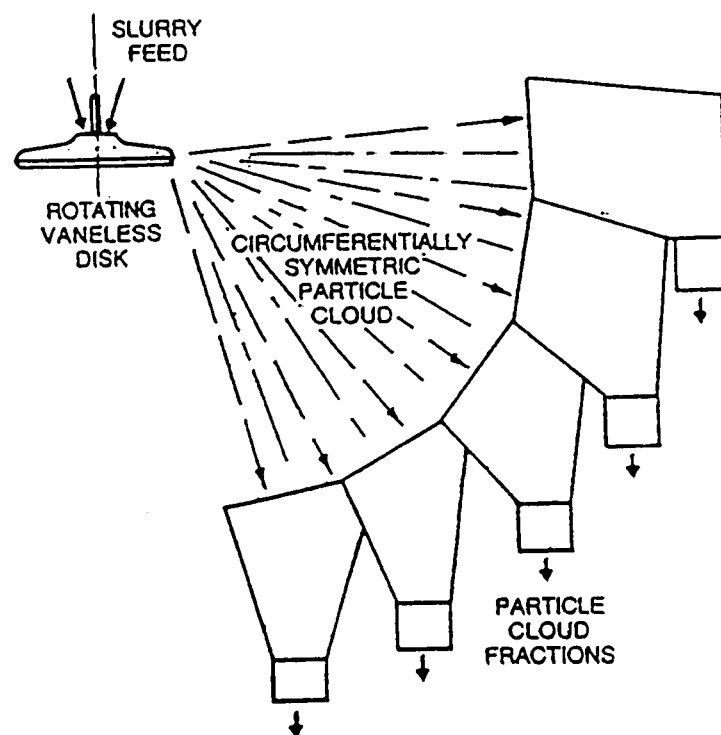


Figure 4.1 Axial zone collection of particle cloud near a rotating vaneless disk
(Oroskar and Crosby, 1986)

They used the saucer type plate for atomizing suspensions in a similar way to that of a spray dryer. A strong shear field within the suspension film on the plate assisted in fractionating the fibres.

Oroskar and Crosby (1986) studied the various design and operating parameters responsible for fibre fractionation. They recommended that a shallow disk

having keen-edged chambers with lips of extreme widths gives sharp fractionation. They explained the phenomenon of fibre separation on the basis of a force balance. The fibres in the liquid film passing over the disk surface move toward the disk periphery. At the corner of the disk, fibres migrate toward the free film surface and are subjected to two forces simultaneously: an inertial force, resulting from the change in direction of the fibres at the corner, and a centrifugal force resulting from the disk rotation. The detachment of a fibre from the liquid film surface, at the disk corner occurs, when the kinetic energy of the fibre becomes greater than the surface energy associated with fibre disengagement.

After reviewing the previous literature, Rewatkar and Masliyah (1997) designed a new fractionator named rotating cone fractionator (RCF). The unique feature of the rotating cone fractionator adopted in their study was that its surface was constructed from a sieve mesh, thereby introducing a "rough" surface, and the feed pipe was located at an off-centre position to the axis of rotation. Details for RCF set-up are given in section 4.2. The fractions were collected at different angular locations. By using 100% hardwood thermo-mechanical pulp, they showed that this technique was able to fractionate fibre according to fibre length. The performance of RCF was found strongly dependent on the roughness of cone surface, rotational cone speed, feed flow rate and pulps feed consistency.

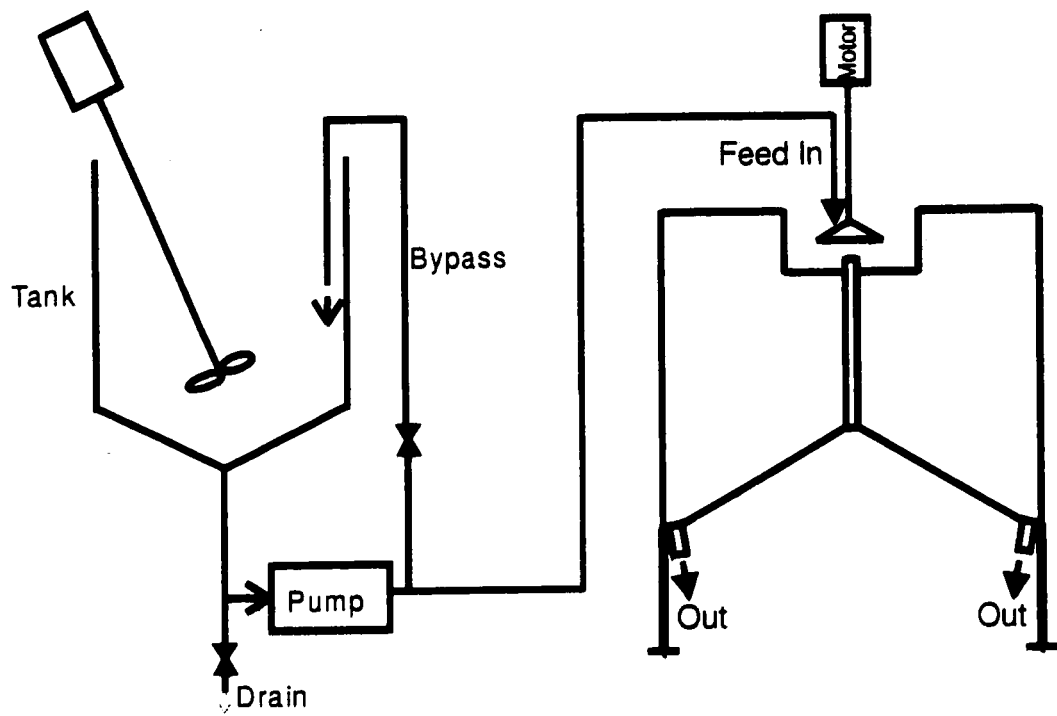
Plate atomizing wheel developed by Oroskar and Crosby (1986) indicated that separation was much more sensitive to fibre diameter than fibre length, which was supported by their experiment. Since the previous study on RCF was carried out using natural wood fibre, it was difficult to decide whether separation occurs due to difference in fibre length or diameter. In the present study, two nylon fibres with the same diameter but different length were used to determine fractionation sensitivity to fibre length. As well, some new parameters were studied, such as the location of the

distributor. The details of the synthetic fibres and suspensions are given in the previous sections 2.2 and 3.3.

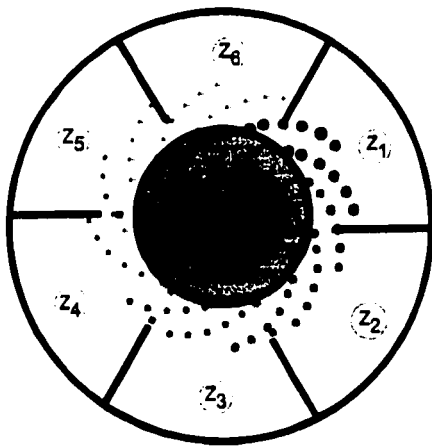
4.2 EXPERIMENTAL SET-UP AND PROCEDURE

4.2.1 Experimental set-up

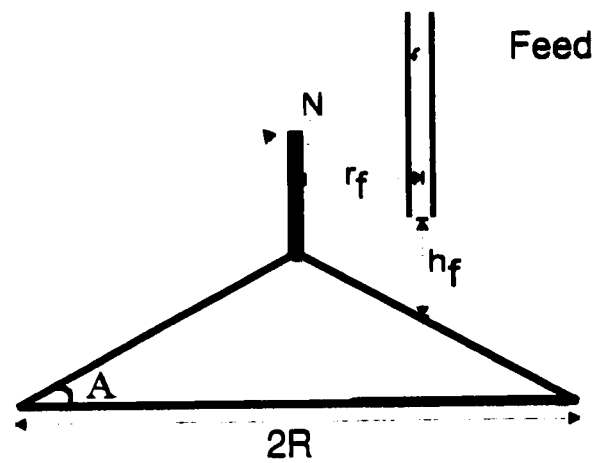
A schematic diagram of the experimental set-up used in this study is shown in Figure 4.2. The fibre suspension was prepared in the feed holding tank and was kept in a well-mixed condition with the help of a stirrer. The fibre suspension was pumped using a peristaltic pump that was pre-calibrated. In all cases, the feed delivery point was displaced from the axis of rotation of the cone. The feed fibre suspension flowed over the conical surface and finally at the rim of the cone it was dispersed into the air. The dispersed spray was collected in a circumferential collection assembly, whose top view is shown in Figure 4.2 (B). Circumferential collection assembly was made of six equally divided compartments built within a cylindrical vessel. Each compartment was provided with its own outlet at the bottom of the vessel. Collection zone numbers were selected according to the transition boundary of suspension film appearing on the conical surface. All the experiments were carried out by adjusting the collection assembly in such a way that the dispersed spray originating from the transition boundary at the rim of the cone was captured by the first zone as shown in Fig 4.2 (B). The subsequent zone numbers were assigned based on their angular location compared with the location of the first collection zone. Therefore, the fibre suspension collected at a lower number zone comes out of cone surface earlier than fibre suspension collected at a higher number zone. Figure 4.2 (C) shows the design details of the rotating cone and feed distributor.



(A) RCF Set-up



(B) Top View of Collection Tank



(C) Rotating cone

Figure 4.2 RCF experimental set-up

4.2.2 Experimental procedure

The experimental conditions in this study are shown in Table 4.2.2.

PARAMETERS	RANGE OF VALUE STUDIED
Cone angle (A)	30°
Cone radius (R, mm)	60 and 90
Roughness of cone surface	smooth, 32-mesh and 20-mesh
Distributor location (r_p , mm)	16.5, 25.5 and 40.5
Feed flow rate ($Q_p \times 10^{-5} \text{ m}^3/\text{s}$)	1.955 to 4.755
Rotational cone speed (N, rpm)	450 to 2500
Feed consistency (X, %)	0.025 to 0.1

Table 4.2.2 Range of parameters studied for RCF

The stepwise procedure to carry out fibre fractionation using RCF is as follows:

1. Prepare the fibre suspension of known consistency in the feed tank.
2. Pre-set the experimental condition, including the cone design, feed flow rate and rotational cone speed.
3. Pass the fibre suspension onto the rotating cone, observe the transition boundary and align collection assembly in such a way that the dispersed spray aligned with the transition boundary falls into the first zone.
4. Clean the collection assembly with water.
5. Run the test under the same pre-decided conditions for about 5 minutes.
6. Measure the mass and the average fibre length of the suspensions collected in each zone.

The feed consistency used in this study was very low, and hence, it was difficult to measure accurately the consistency of a suspension collected in a given zone. In order to obtain a measure of the amount of fibres collected in each zone, an approximate method was used as discussed earlier in section 2.3. In the present study, the amount of fibres collected in each zone is reported only for one set of experiments. However, the variation of average fibre length with different collection zones has been reported for all the tests.

4.3 VISUAL OBSERVATIONS

In a conventional spinning disk atomizer (feed location is at the rotational axis), depending on the flow rate and rotational speed, atomization takes place in three different forms: direct drop formation, ligament formation and film formation. Several investigators (Fraser et al, 1963, Matsumoto et al., 1974) studied this aspect in detail and proposed various semi-empirical equations to predict these modes of atomization for a single phase flow.

When a fibre suspension is introduced onto the rotating cone surface but at a position off-centre from vertical axis of rotating cone, the suspension is dragged in the angular direction with the rotating surface due to the no-slip condition. Due to the centrifugal force, the suspension flows in the radial direction until it reaches the rotating cone rim. At the rim, it detaches from the cone surface. At the detachment point, the suspension flows into the air in the form of droplet or a film. The state of the flow depends on the experimental conditions, such as cone roughness, feed flow rate, rotational cone speed, the location of distributor, feed consistency, etc. Various modes of atomization can simultaneously occur at different angular locations on the cone rim as shown in Figure 4.3.

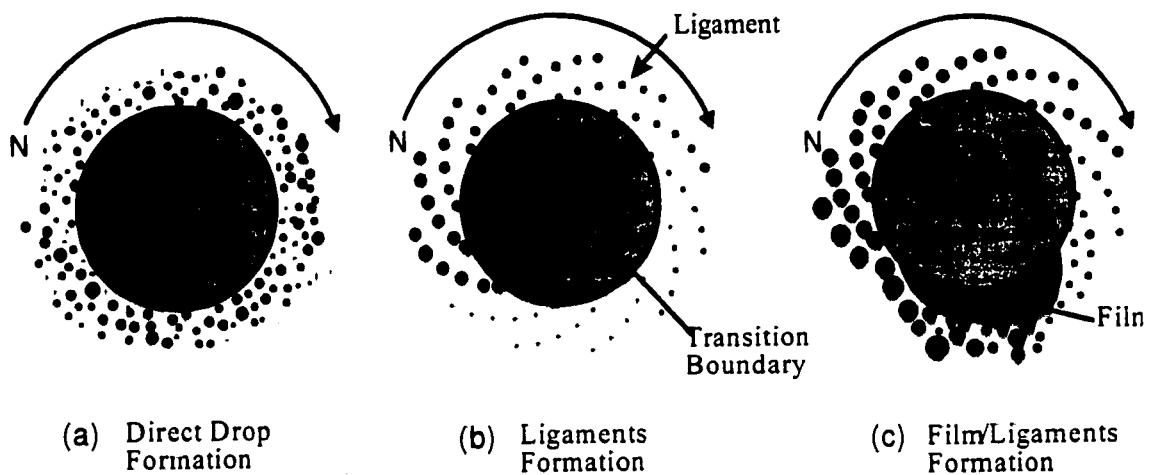


Figure 4.3 Three different atomization modes for RCF

At a constant rotating cone speed, there are three different atomization modes that can be observed with an increase in feed flow rate: direct drop formation, ligament formation and film / ligament formation. Similar phenomena were reported by Rewatkar and Masliyah (1997). They concluded that the performance of fractionation varied from mode to mode and ligament formation showed excellent fibre fractionation according to length. In the present study, an attempt was made where most of the experiments were carried out under film/ligament formation.

4.4 POSSIBLE FRACTIONATION MECHANISM

Oroskar and Crosby (1986) carried some theoretical analysis on vaneless disk fractionation. From their point of view, the fibres tend to become disentangled and orient themselves in the radial direction because of the intense shear in the film. Any

difference between fibre and liquid density coupled with centrifugal forces arising from tangential motion results in the fibres and the fluid having different radial velocities. At the disk periphery, detachment occurs when the kinetic energy of a fibre in terms of its normal velocity component equals or exceeds the surface energy involved in the process. As fibres exit at various depths within the film, their detachment occurs over at least a portion of the lip surface instead of exactly at the upstream edge of the lip. Based on disk geometry and dimensions, operation conditions, and properties of the slurry components, an approximate performance model was developed and agreed reasonably well with their experiments.

In order to illustrate a possible mechanism of fibre fractionation using nylon fibres by RCF, some results on suspended particle flow under laminar flow conditions by previous researchers are discussed below.

Starkey (1956), Saffman (1956) and Bretherton (1962) observed that during laminar flow of a suspension through a tube, a suspended particle would follow a path adjacent to an equilibrium radial position between the tube axis and tube wall. Karnis et al. (1966) further concluded that in Poiseuille flow:

- the rate of migration increased with increasing particle size
- the equilibrium radial position depended on particle size, decreasing as the particle size is increased.
- rigid cylinders and spheres, drifted radially either inward or outward to the equilibrium position.
- elastomer filaments, which were deformed by the shear field, migrated to the tube axis.

According to Matsumoto et al. (1973) and Bruin (1969) (cited from Oroskar, 1981), for a given radial position, the radial velocity U within a suspension film is

parabolic with a zero radial velocity at the cone surface and a maximum at the free surface. The tangential velocity is constant given by V . The field is shown in Figure 4.4a. It is clear then that the fluid experiences little shear rate in the angular direction as the shear effect is in mainly normal (lateral) to the cone surface, i.e. Z direction. Consequently, particle migration occurs in the lateral direction only.

Based on previous results, we can predict that for rod-like particles, rods having larger aspect ratios migrate faster toward the equilibrium position and concentrate nearer the center of film than rods having a smaller ratio. Unlike rigid particle, flexible rods migrate toward an equilibrium position of zero shear, i.e. free surface of the film. In our study, feed suspension includes 1 mm and 3 mm nylon fibres with the same diameter of $20\text{ }\mu\text{m}$, therefore their aspect ratios are 50 and 150,

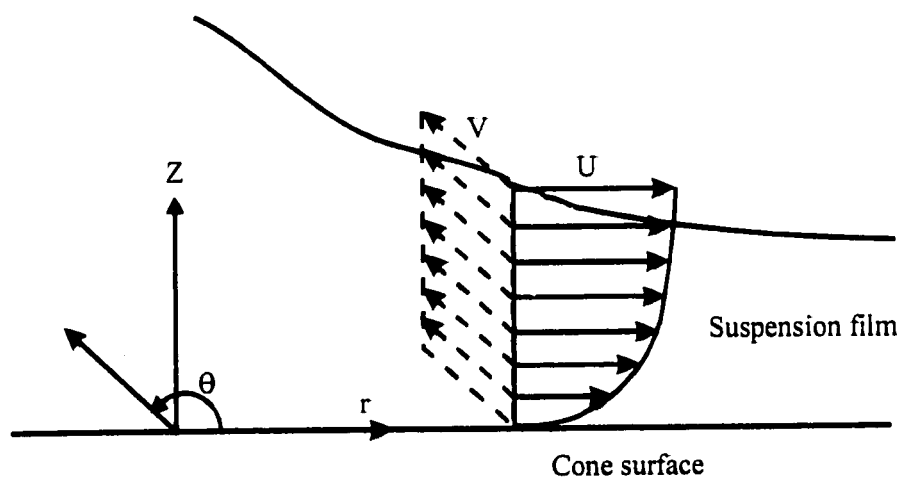


Figure 4.4a Flow of fibre suspension over the cone surface showing radial and tangential velocity profile

respectively. Due to the difference in the aspect ratio, we can assume that, within the film of fibre suspension flowing over the conical surface, the 1 mm fibre migrates like a rigid particle, however, 3 mm fibre is more like a flexible particle. Hence, within the flowing film, the 3 mm fibres move faster to the equilibrium position of zero shear

(top surface of suspension film) than the 1mm fibres to their equilibrium position (the centre of film). This means that there is a gradual separation of larger particles from the smaller ones as the edge of the disk is approached. In short, we can conclude that this preferential migration of the long fibres away from the cone surface towards the film free surface results in the formation of a fibre length gradient within the flowing suspension in a direction perpendicular to the cone surface.

The radial and tangential velocity components of a fibre flowing in the suspension depend on the location of the fibre within the film. Oroskar and Crosby (1986) found that fibres close to the free surface (long fibres in the present study) have a higher radial velocity than fibres close to the disk surface (short fibres and fines in the present study). The difference in the radial component of velocities of long and short fibres helps in the separation of these fibres in the angular direction. This can be explained with the help of Figure 4.4b. In Figure 4.4b, U and V are the

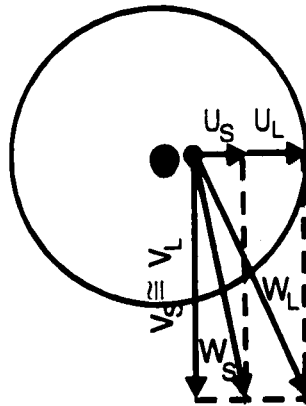


Figure 4.4b Schematic view of fibre migration velocities over a conical surface

radial and tangential velocities of a fibre, respectively. Subscripts S and L denote short and long fibres, respectively. One can safely assume that $U_S < U_L$ and $V_S \cong V_L$,

and the resultant velocity vectors for short (W_s) and long fibres (W_L) can be drawn shown in Figure 4.4b. From the resultant velocity vectors, long fibres, having been residing close to the surface of the film flowing over the cone, would reach the cone's rim earlier than the short fibres. Hence, fractionation will occur in the angular direction.

4.5 RESULTS AND DISCUSSIONS

Various designs and operating parameters affect the flow condition on and around the cone. For example, roughness of the cone surface and cone speed can change the shear rate within the suspension film over the cone surface, feed flow rate can change the thickness of the suspension film, feed consistency can strongly influence the interaction between the fibres and cone diameter affects the residence time for fibres on the cone surface, etc. In the following sections, the effects of these parameters on fractionation are studied in some details.

4.5.1 Variation of average fibre length and amount of fibres with collection zone

In this experiment, only one condition was chosen to present the variation of average fibre length and amount of fibres collected in different collection zones. The feed consistency was 0.01% (w/w). Triton X-100 with concentration of 0.07% (w/w) was added to keep fibre suspended. Feed flow rate and rotational speed of the cone were $1.955 \times 10^{-5} \text{ m}^3/\text{s}$ and 450 rpm, respectively. A 30° cone having a 90 mm radius and smooth surface was used. The location of the feed distributor, r_f was 10.5 mm away from the axis of rotation, and the vertical location, h_f was 5 mm high from the cone surface.

Variation of the average fibre length with the location of a collection zone is shown in Figure 4.5.1a. From this figure, it can be observed that the fibre mean length of each sample continuously decreases with increasing collection zone number, i.e. with angular position. As discussed earlier, the long fibres would come out of cone surface earlier than the short fibres. Therefore the suspension with a lower number zone has more long fibres and the suspension in a higher number zone has more short fibres. The length distributions of suspension from different collection zones are shown in Figure 4.5.1b.

Variation of percentage of amount fibres collected in different collection zones is presented in Figure 4.5.1c. It can be observed that in general, the amount of fibres collected in each zone decreased rapidly with increasing zone number from zone 1 to zone 4. However, it remains nearly constant for zone 4, 5 and 6. In zone 1, the percentage of fibres collected is 53.2%, which is almost 50 times as that of zone 6 (1.1%). This indicates that the amount of short fibres removed from the feed is very small, so the mean length of the fibres in the first zone is close to the feed value.

Overall, the results from this experiment suggest that fibres having the same diameter could be fractionated according to their length. The effect of various experimental designs and other operating parameters of RCF has been tested and the results are given in the following section.

4.5.2 Effect of surface roughness

Rewatkar and Masliyah (1997) studied the effect of surface roughness on fractionation of hardwood fibres. They concluded that a rotating cone having a rough surface gave better fractionation performance, at lower rotational speeds and higher

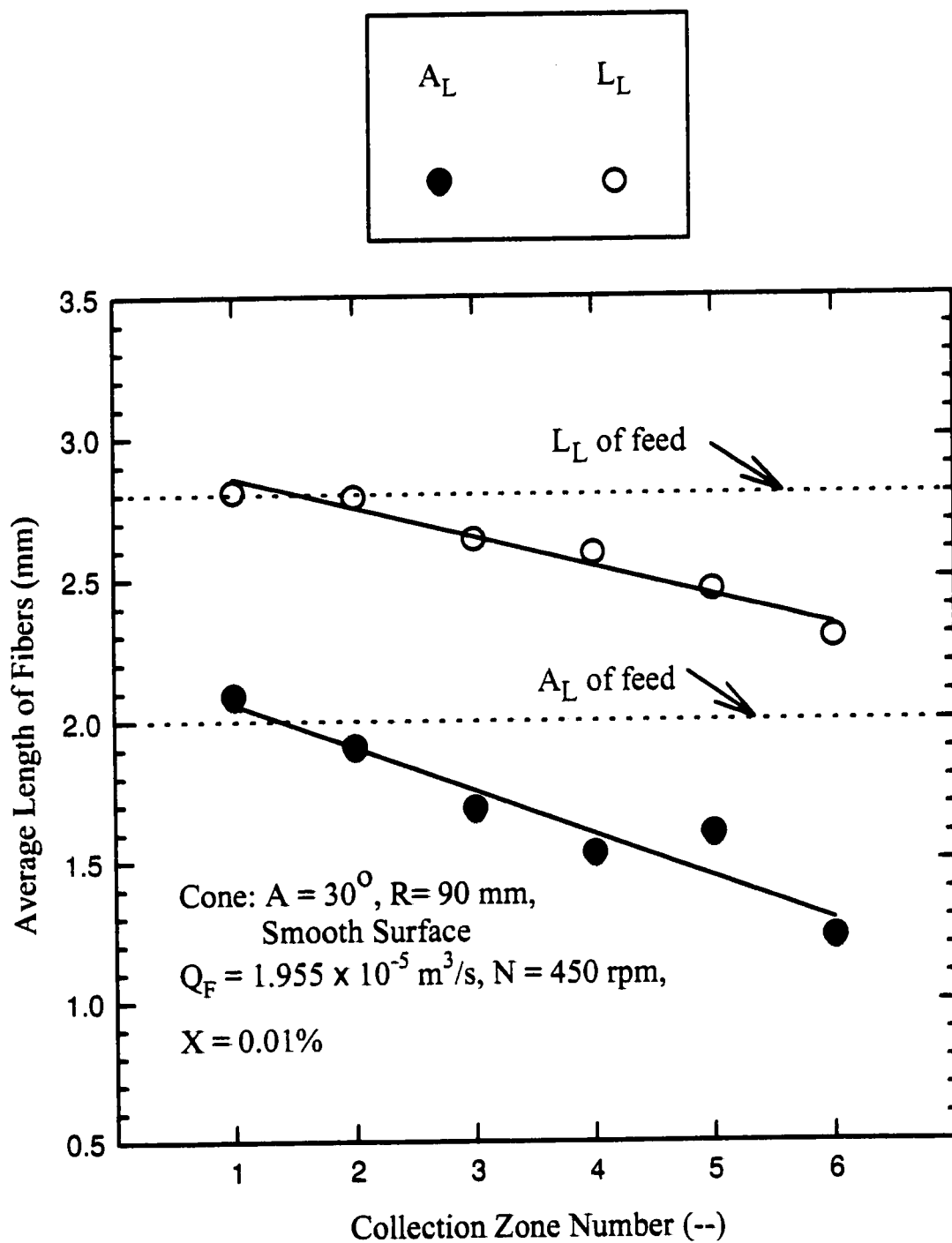


Figure 4.5.1a Variation of average fibre length at different collection zones

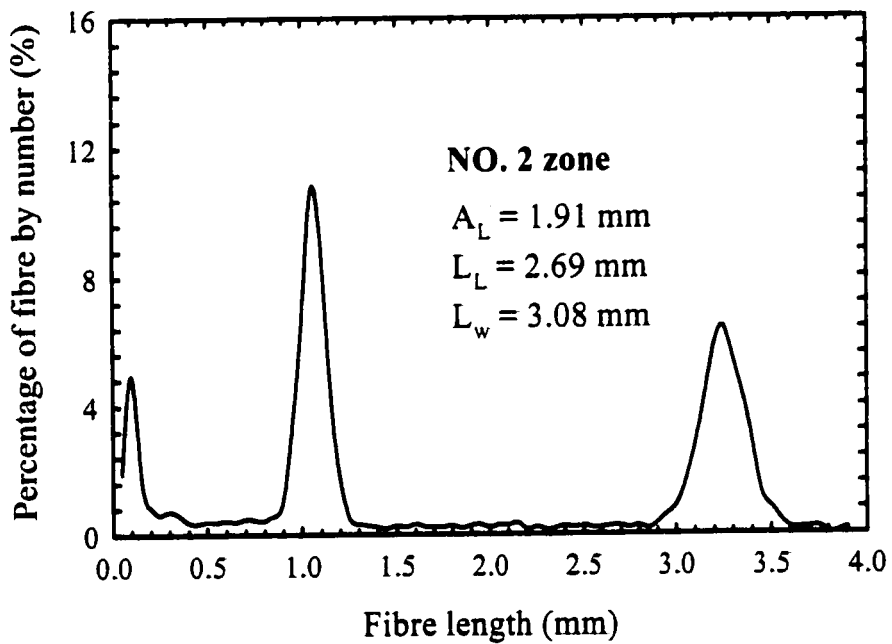
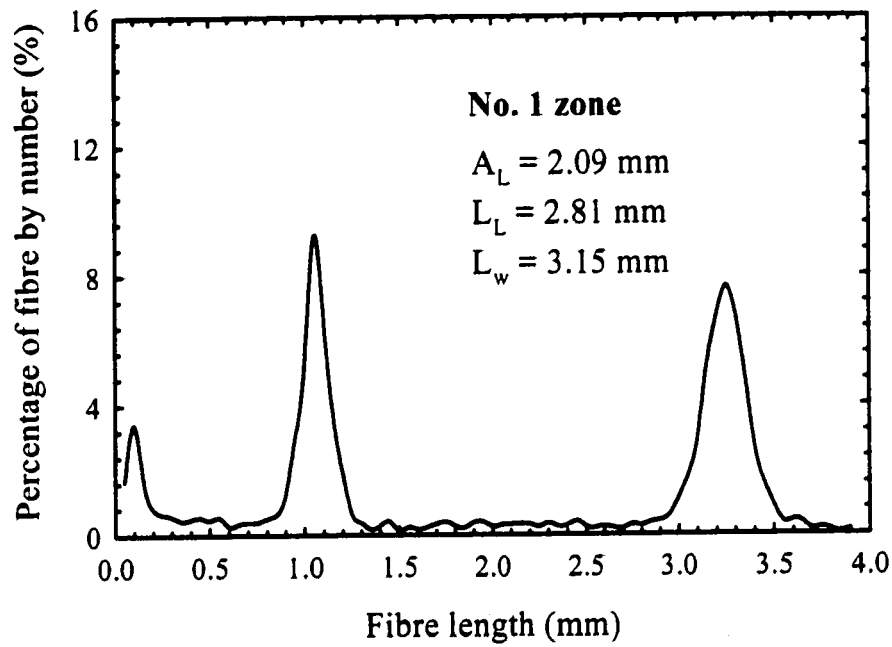


Figure 4.5.1b Length distributions of suspension from different collection zones (Part 1)

Cone: $A = 30^\circ$, $R = 90 \text{ mm}$, Smooth surface; $X = 0.01\%$;
 $Q_F = 1.949 \times 10^{-5} \text{ m}^3/\text{s}$, $N = 450 \text{ rpm}$.

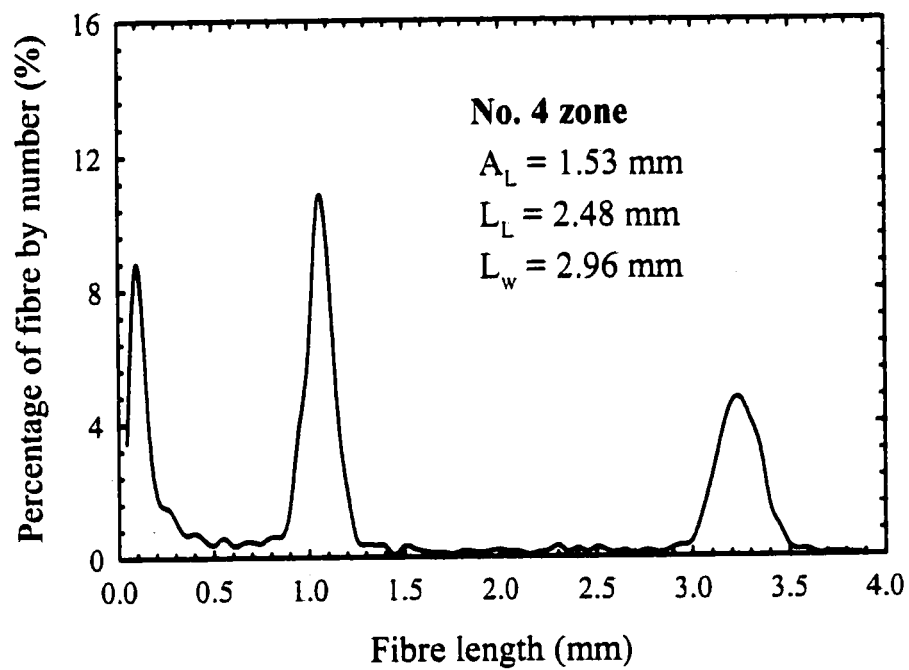
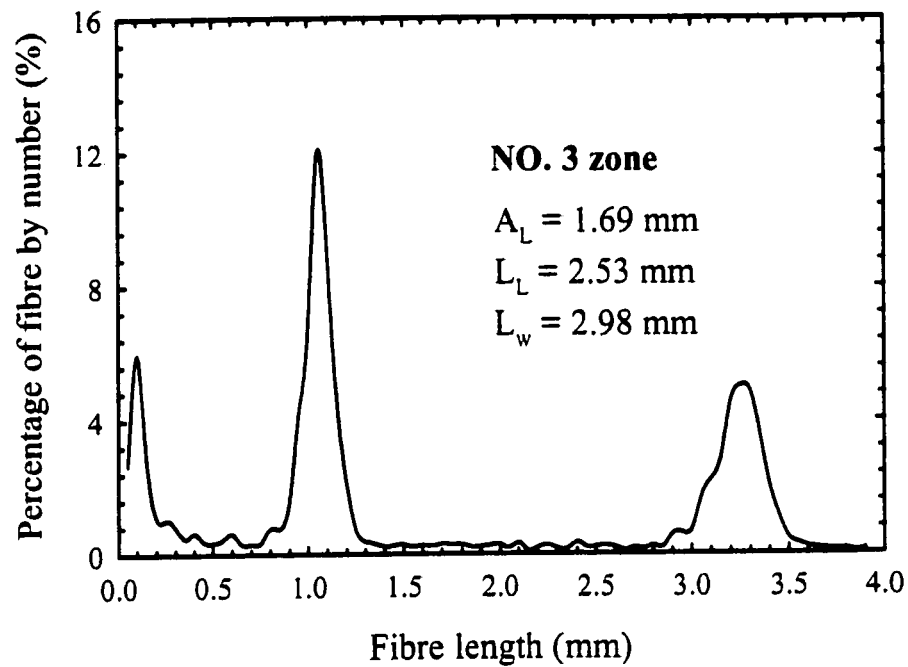


Figure 4.5.1b Length distributions of suspension from different collection zones (Part 2)

Cone: $A = 30^\circ$, $R = 90 \text{ mm}$, Smooth surface; $X = 0.01\%$;
 $Q_F = 1.949 \times 10^{-5} \text{ m}^3/\text{s}$, $N = 450 \text{ rpm}$.

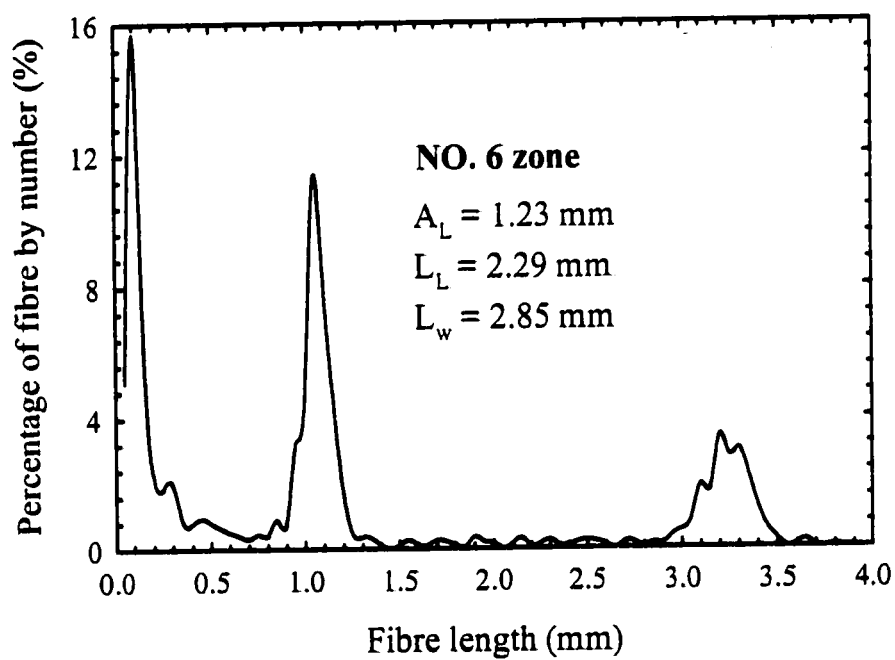
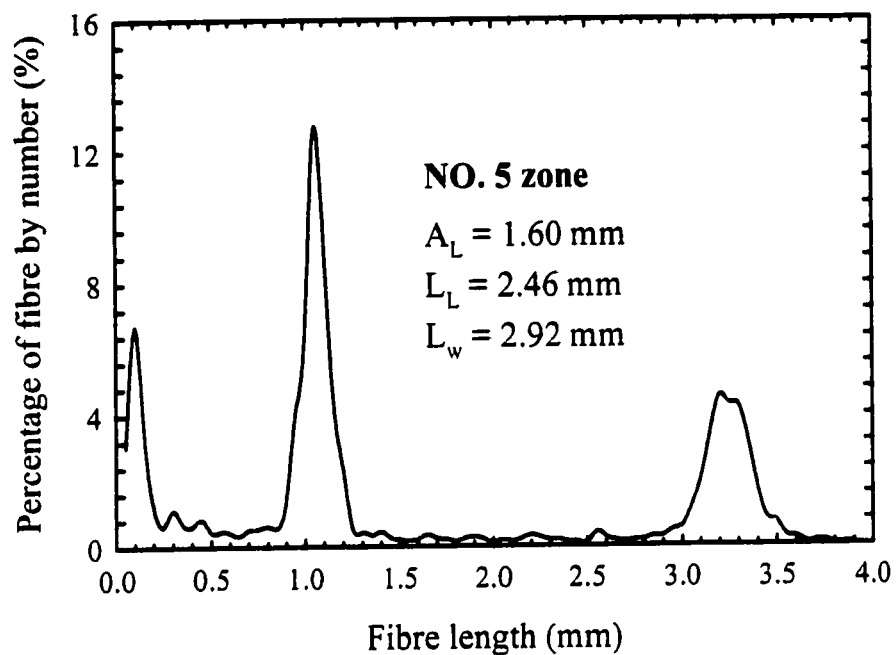


Figure 4.5.1b Length distributions of suspension from different collection zones (Part 3)

Cone: $A = 30^\circ$, $R = 90 \text{ mm}$, Smooth surface; $X = 0.01\%$;

$Q_F = 1.949 \times 10^{-5} \text{ m}^3/\text{s}$, $N = 450 \text{ rpm}$.

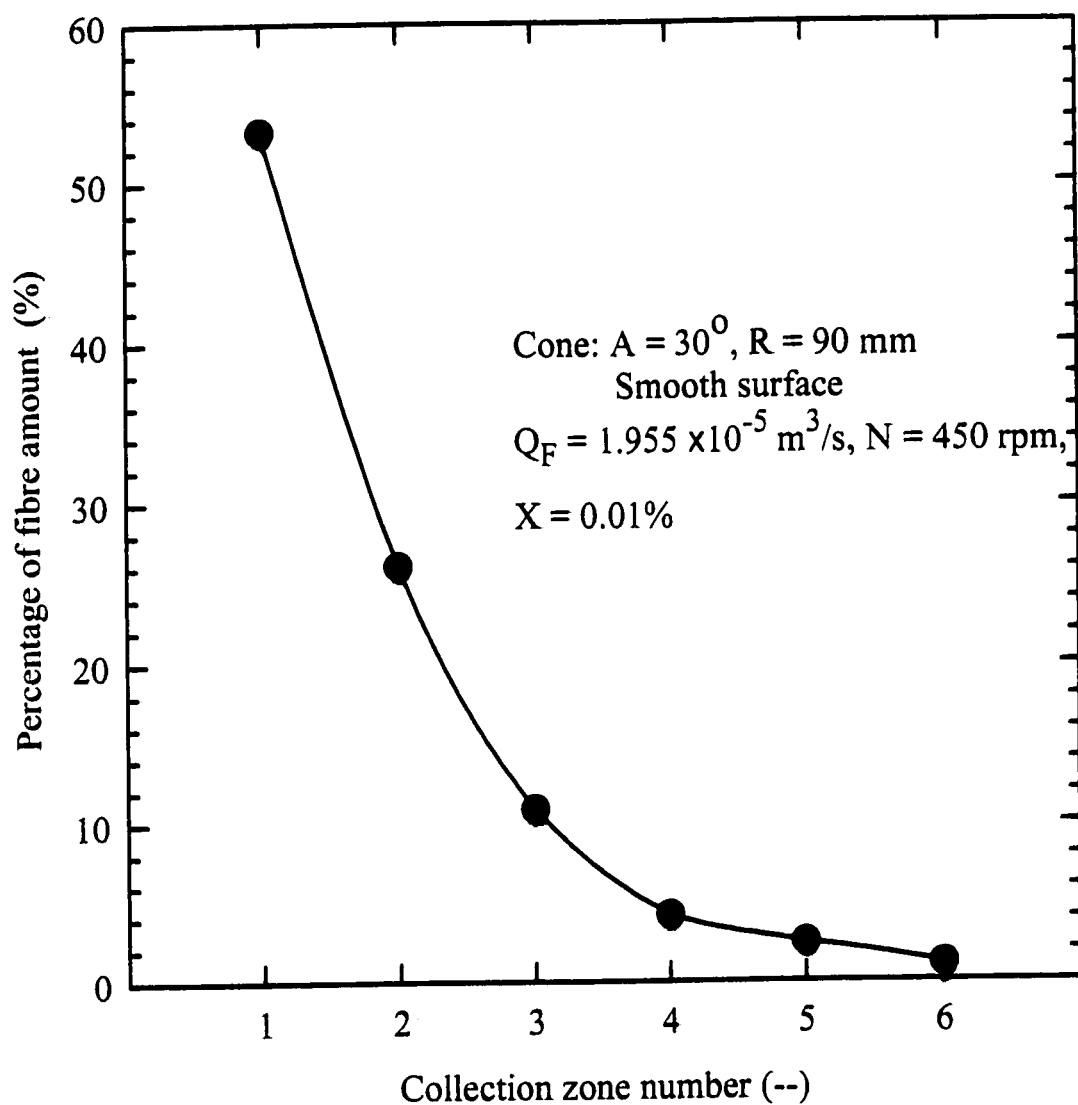


Figure 4.5.1c Variation of percentage of fibre weight with collection zone

feed flow rates, as compared to a rotating cone having a smooth surface. The optimum rough surface was found to be dependent on feed fibre length.

In the present study, nylon fibres were used to study the effect of surface roughness. Cones having smooth, 12-, 20- and 32- mesh surfaces were used. Cones with a rough surface were fabricated using sieve screens. The details of wire size and opening for these mesh sieve screens are given in Table 4.5.2a. The openings of the mesh sieves were blocked using adhesive tape on the lower side of the cone surface, such that no suspension can directly pass through the openings. In the tests, the feed pipe was located 10.5 mm away from the axis of rotation.

Screen Size	Wire Diameter (μm)	Opening (μm)
12-mesh	600	1710
20-mesh	474	798
32-mesh	237	553

Table 4.5.2a Details of wire size and openings of the different screens

At the beginning of the experimental procedure, "much better" fractionation performance was obtained for 20-mesh surface cone as compared to smooth surface cone. However, experimental observation showed that most of the nylon fibres deposited on the rough screen and did not flow along with the suspension. This is shown in Photograph 4.5.2 for the 20-mesh surface cone. It was also found that fibre deposition became more apparent with an increase in the surface roughness. However, there were no fibres depositing on the smooth surface at all. As a result, the reproducibility of the experiments using rough surface cone was very poor. This problem was eliminated by using a smooth surface cone. The fibre suspension flows easily on smooth cone surface up to the rim of cone where it is dispersed. The



Photograph 4.5.2 Photograph of suspension flow on a rough surface cone

Cone: $A = 30^\circ$, 20-mesh, $R = 90$ mm, $N = 450$ rpm,
 $Q_F = 3.804 \times 10^{-5} \text{ m}^3/\text{s}$, $X = 0.01\%$, $r_f = 16.5$ mm

transition boundary formed over the smooth surface cone was quite distinct, helping in the alignment of the collection assembly.

Two sets of experiments were carried out to test the reproducibility of the experiment. The experimental conditions are shown in Table 4.5.2b. Each experiment was repeated twice. The results of the reproducibility test are shown in Figure 4.5.2a and Figure 4.5.2b for a smooth and rough surface, respectively.

Parameters	Figure 4.5.2a	Figure 4.5.2b
Roughness of cone surface	Smooth	20-mesh
Cone angle (A)	30°	30°
Cone radius (R , mm)	90	90
Distributor location (r_p , mm)	16.5	16.5
Feed flow rate ($Q_f, \times 10^{-5} \text{ m}^3/\text{s}$)	1.955	3.804
Rotational cone speed (N , rpm)	450	450
Feed consistency (X , %)	0.01	0.01

Table 4.5.2b Experimental conditions for reproducibility tests

From Figure 4.5.2a and 4.5.2b, it can be observed that the difference in the experimental results from the two sets of experiments for the smooth surface cone is almost negligible. However, for the 20-mesh surface cone, the deviations of fibre mean length collected in different collection zones for the two experimental runs are quite different, even though they are under the same experimental conditions. Other experiments under different conditions also indicate ill reproducibility for the 20-mesh surface. The reason for the ill reproducibility is that the nylon fibres

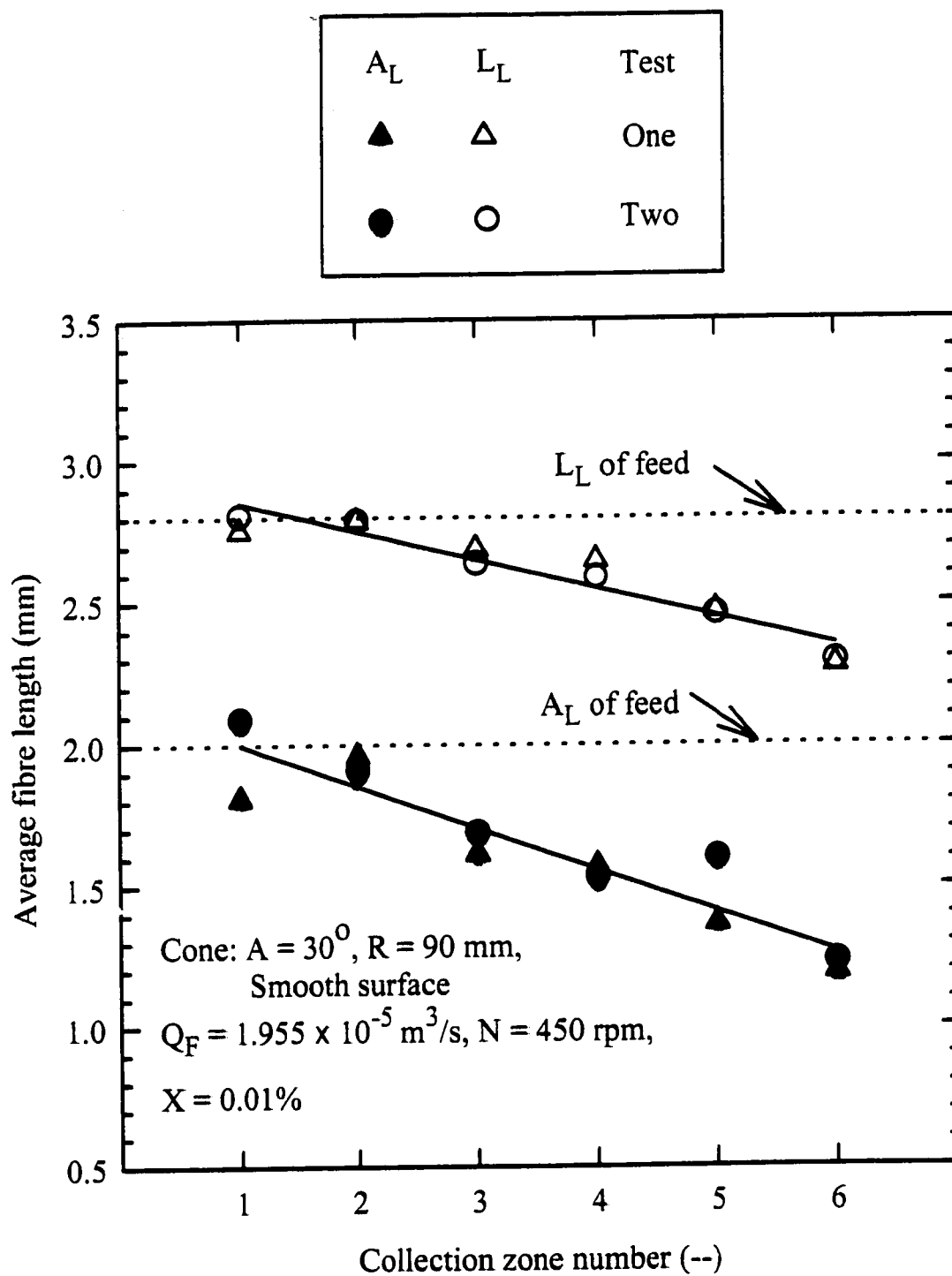


Figure 4.5.2a Reproducibility test for a smooth surface cone

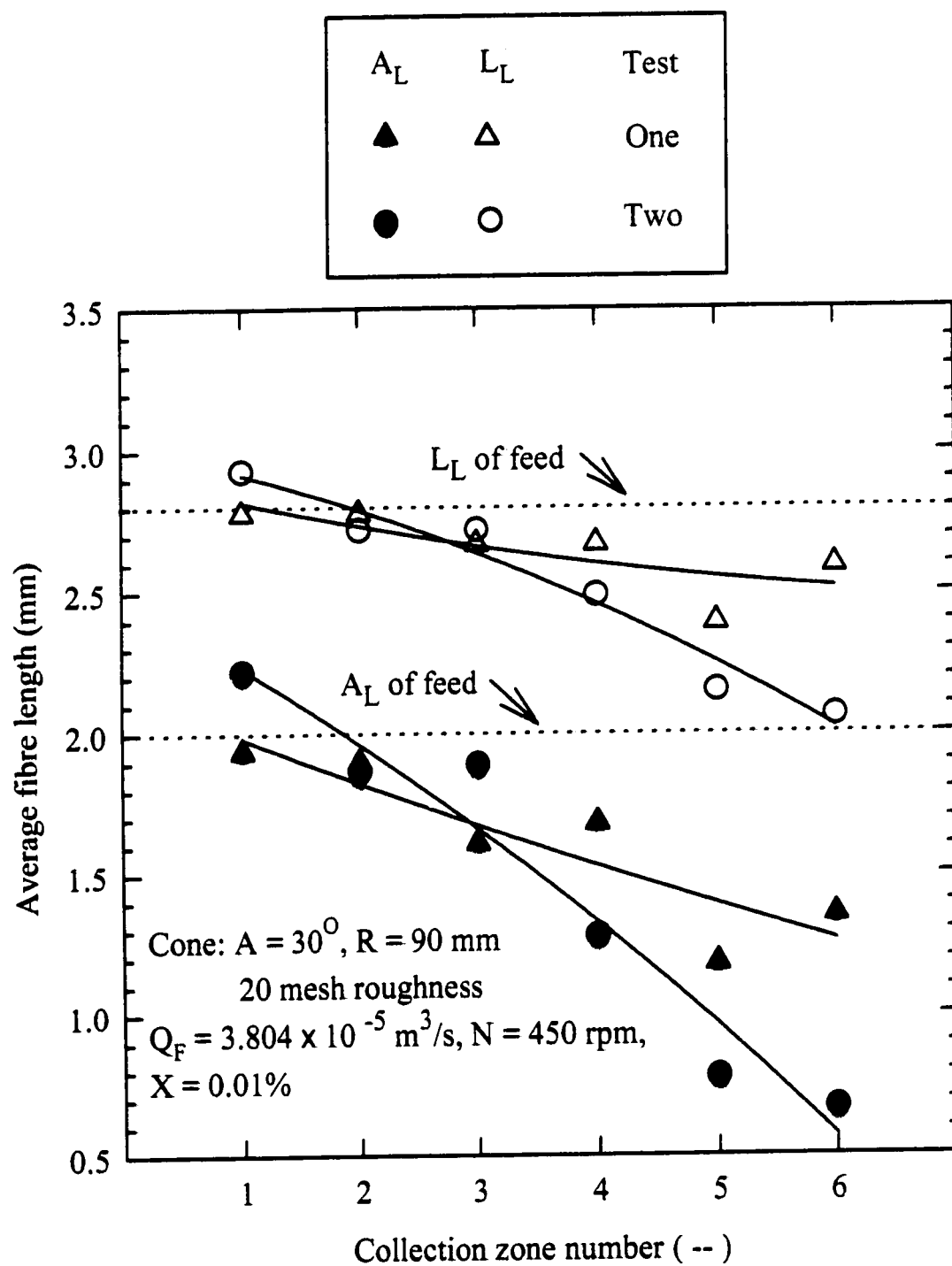


Figure 4.5.2b Reproducibility test for a 20-mesh surface cone

accumulated on the rough surface. As a result, experiments to study the effect of cone roughness can not be carried out for nylon fibres. For the rest of study, only a smooth surface cone was used.

4.5.3 Effect of radial location of feed distributor

The effect of feed distributor radial location was studied at $1.955 \times 10^{-5} \text{ m}^3/\text{s}$ feed flow rate and 450 rpm rotational cone speed. A smooth cone having 30° cone angle and 90 mm radius was used. Three different feed distributor radial locations were tested, namely, 16.5, 25.5 and 40.5 mm. The vertical location of the distributor was kept 5 mm above the cone surface.

Variation of the average fibre length with collection zone location for different feed distributor locations is shown in Figure 4.5.3a. It can be observed that the average fibre length for both 16.5 mm and 40.5 mm decreases continuously with increasing collection zone number. However, for the 25.5 mm location, average fibre length decreases from zone 1 to 3 following by an increase at zone 4, and then decreases again till zone 6.

Schematic flow patterns on the cone and along the cone's rim for various distributor locations were sketched in Figure 4.5.3b. It is clear that two transition boundaries were observed over the cone surface for the 25.5 mm and 40.5 mm locations, however, only one simple transition boundary was observed for 16.5 mm location.

In this study, the distinct wave pattern in average fibre length and zone number was only observed for 25.5 mm radial location of feed distributor. A good explanation for this observation has not been found yet. However, the thickness,

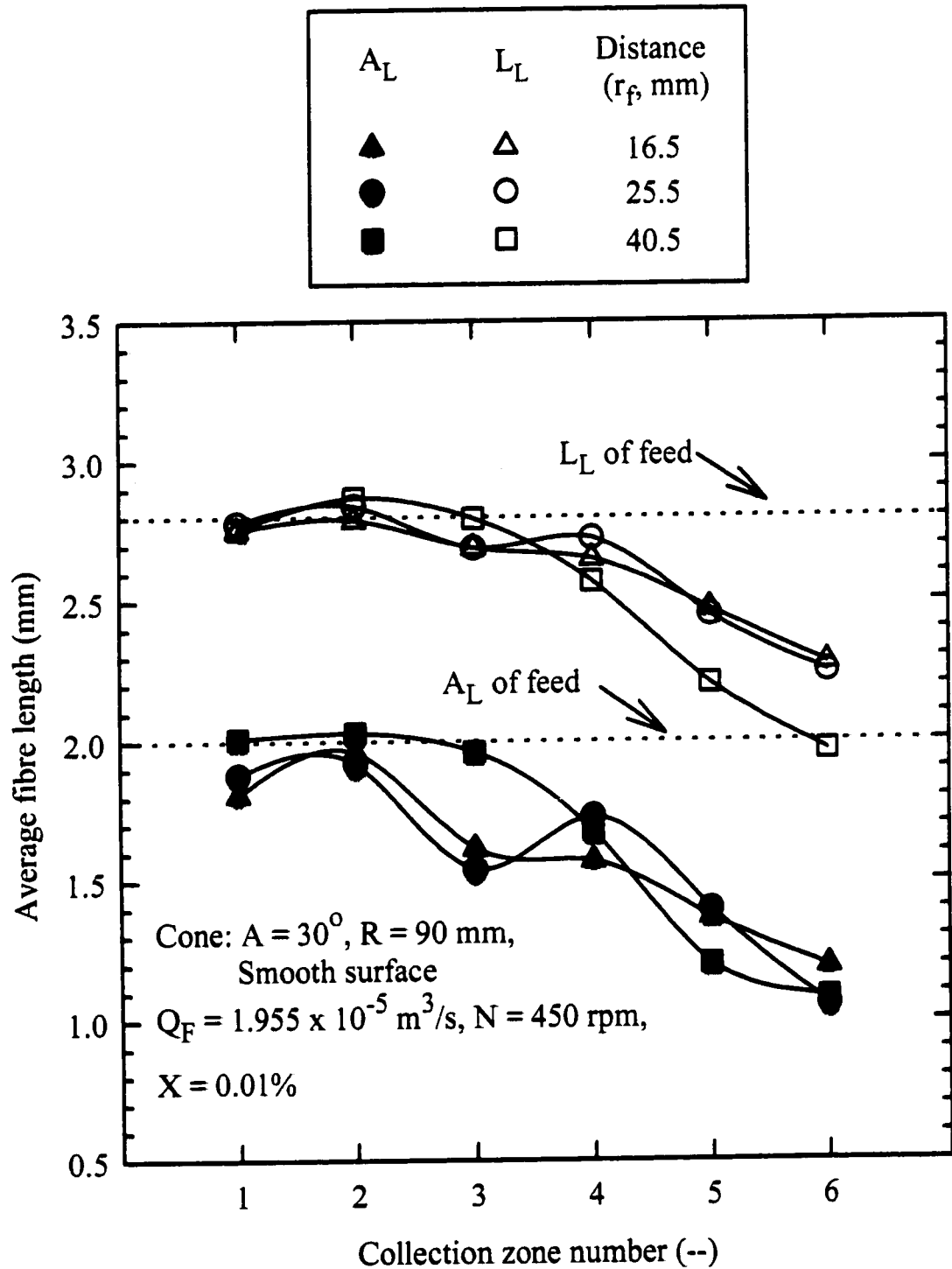


Figure 4.5.3a Variation of average fibre length at different radial locations of feed distributor

continuity, and area of suspension film over the cone surface might be the cause for such a wave-like variation. This phenomenon has been further studied for 25.5 mm radial location at various cone speeds, 300 rpm, 450 rpm, 670 rpm and 850 rpm. The other experimental conditions remained the same. Variation of average fibre length at different rotational cone speeds for 25.5 mm radial location are shown in Figure 4.5.3c. It can be observed that the wave pattern is diminished at the high rotational cone speed of 850 rpm, and there is no large difference among 300 rpm, 450 rpm and 670 rpm cases.

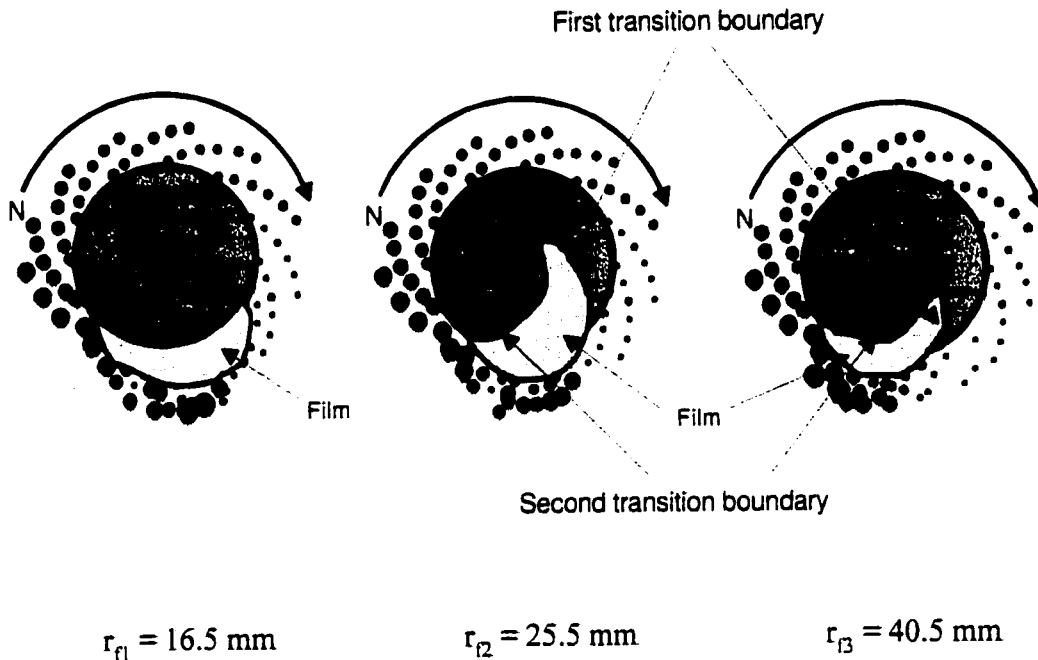


Figure 4.5.3b Effect of radial location of feed distributor on flow pattern

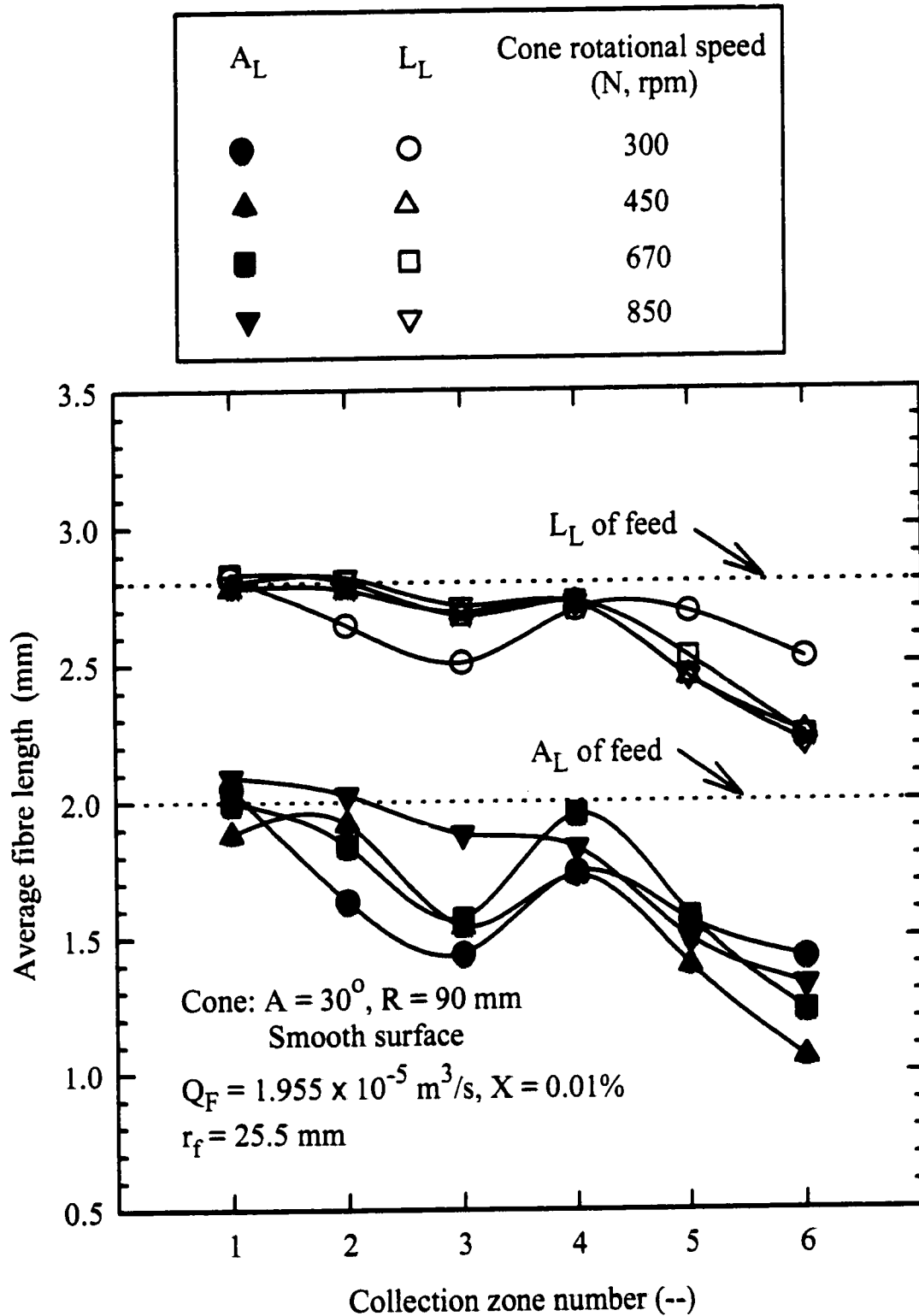


Figure 4.5.3c Variation of average fibre length at different rotational cone speeds at $r_f = 25.5$ mm

4.5.4 Effect of feed flow rate

The effect of feed flow rate was studied for a smooth rotating cone surface having 90 mm radius. The feed flow rates were varied from $1.955 \times 10^{-5} \text{ m}^3/\text{s}$ to $4.755 \times 10^{-5} \text{ m}^3/\text{s}$, at a constant rotational speed of 450 rpm. The radial location of feed distributor r_f was 10.5 mm and the feed consistency was 0.01% (w/w). Variation of the average fibre length at different collection zones at various flow rates is shown in Figure 4.5.4. It can be observed that in the range of feed flow rate studied, the fibre mean length continuously decreases with increasing collection zone number. However, within the range studied, no effect of feed flow rate was observed on the fibre fractionation performance.

Photographs for $1.955 \times 10^{-5} \text{ m}^3/\text{s}$ and $4.755 \times 10^{-5} \text{ m}^3/\text{s}$ feed flow rates are shown in Photograph 4.5.4. It is observed that fractionation for both feed flow rates takes place in the form of film/ligament. The size of the film formed at the lower feed flow rate was larger than that at the higher value. In general, the performance of fractionation varied with the mode of atomization (Rewatkar and Masliyah, 1997). In the present study, only one mode of atomization was obtained within the range of the flow rates studied and consequently the experimental results show no difference in fractionation performance.

4.5.5 Effect of rotational cone speed

The effect of rotational cone speed was studied for a smooth cone having 60 mm radius. The cone speed was varied from 450 rpm to 2500 rpm, at a constant feed flow rate of $1.955 \times 10^{-5} \text{ m}^3/\text{s}$ with a feed consistency at 0.01% (w/w). The

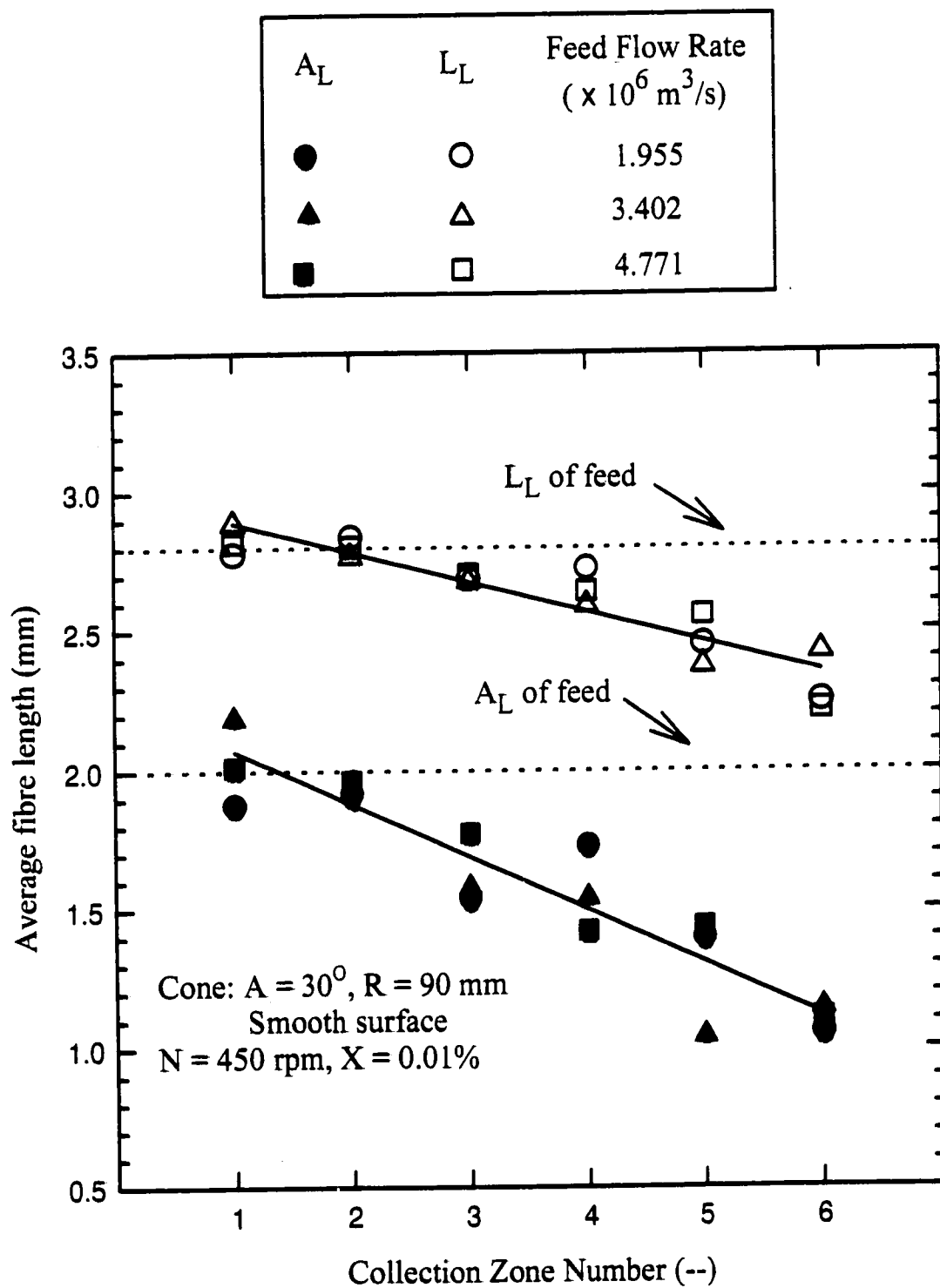
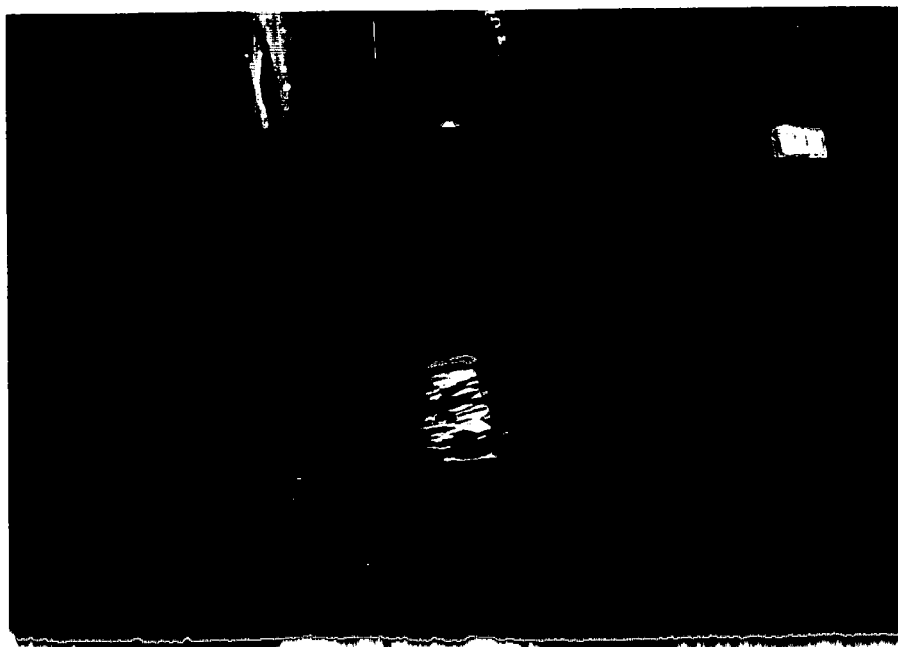
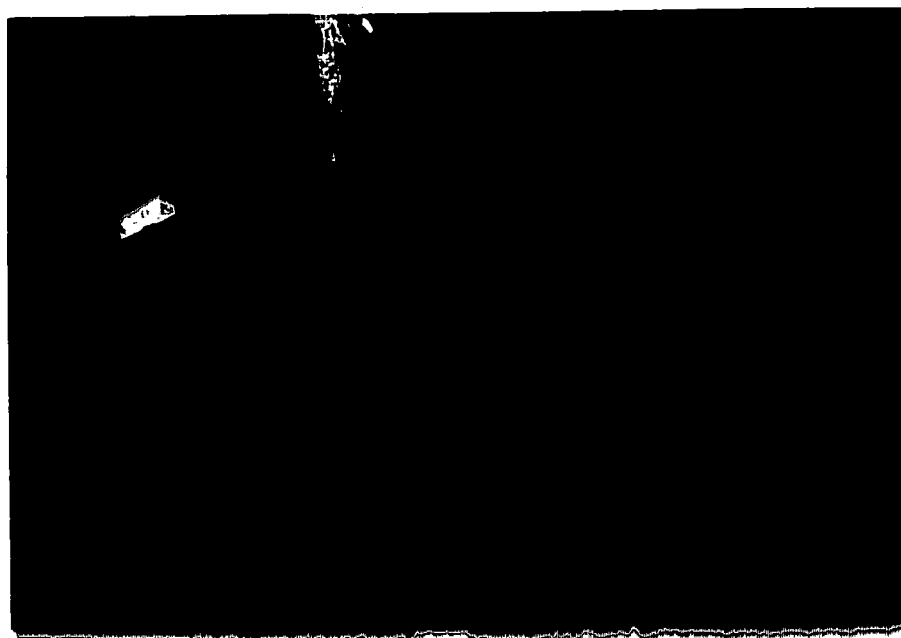


Figure 4.5.4 Variation of average fibre length at different feed flow rates



$1.955 \times 10^{-5} \text{ m}^3/\text{s}$



$4.755 \times 10^{-5} \text{ m}^3/\text{s}$

Photograph 4.5.4 Photographs of suspension flow at two different feed flow rates

Cone: $A = 30^\circ$, $R = 90 \text{ mm}$, $N = 450 \text{ rpm}$, $X = 0.01$, $r_f = 16.5 \text{ mm}$

feed distributor was located 10.5 mm away from the axis of the rotation. Variations of the average fibre length with the location of collection zone are shown in Figure 4.5.5. It is observed that the fractionation performance improves with an increase in rotational cone speed from 450 rpm to 670 rpm. However, with a further increase in the rotational cone speed to 2500 rpm, fractionation performance deteriorates. This indicates the necessity of an optimal rotational cone speed for improved fibre fractionation.

Photographs of the suspension flow pattern for various rotational cone speeds are shown in Photograph 4.5.5. The flow pattern observed was that of film/ligament formation, except at the high rotational cone speed of 2500 rpm, where drop/ligament formation was observed. The photographs also show that, as the rotational cone speed increases from 450 rpm to 670 rpm, the suspension film along the rim of the rotating cone shifts towards the rotational direction. When the rotational cone speed reaches 2500 rpm, the suspension film can be dragged back to the feed point where mixing with the feed occur. Such mixing reduces fractionation efficiency. This phenomenon can be observed in the photograph for 2500 rpm. Therefore, among the range of rotational cone speeds studied, the worst fractionation performance occurs at 2500 rpm.

Overall, for the best fractionation performance, there is an optimal cone speed before the overlapping between the fractionated suspension and the feed takes place. For rough surface cone, Rewatkar and Masliyah (1997) found that the mode of atomization changes dramatically with an increase in rotational cone speed. They recommended an optimal rotational cone speed for fibre fractionation.

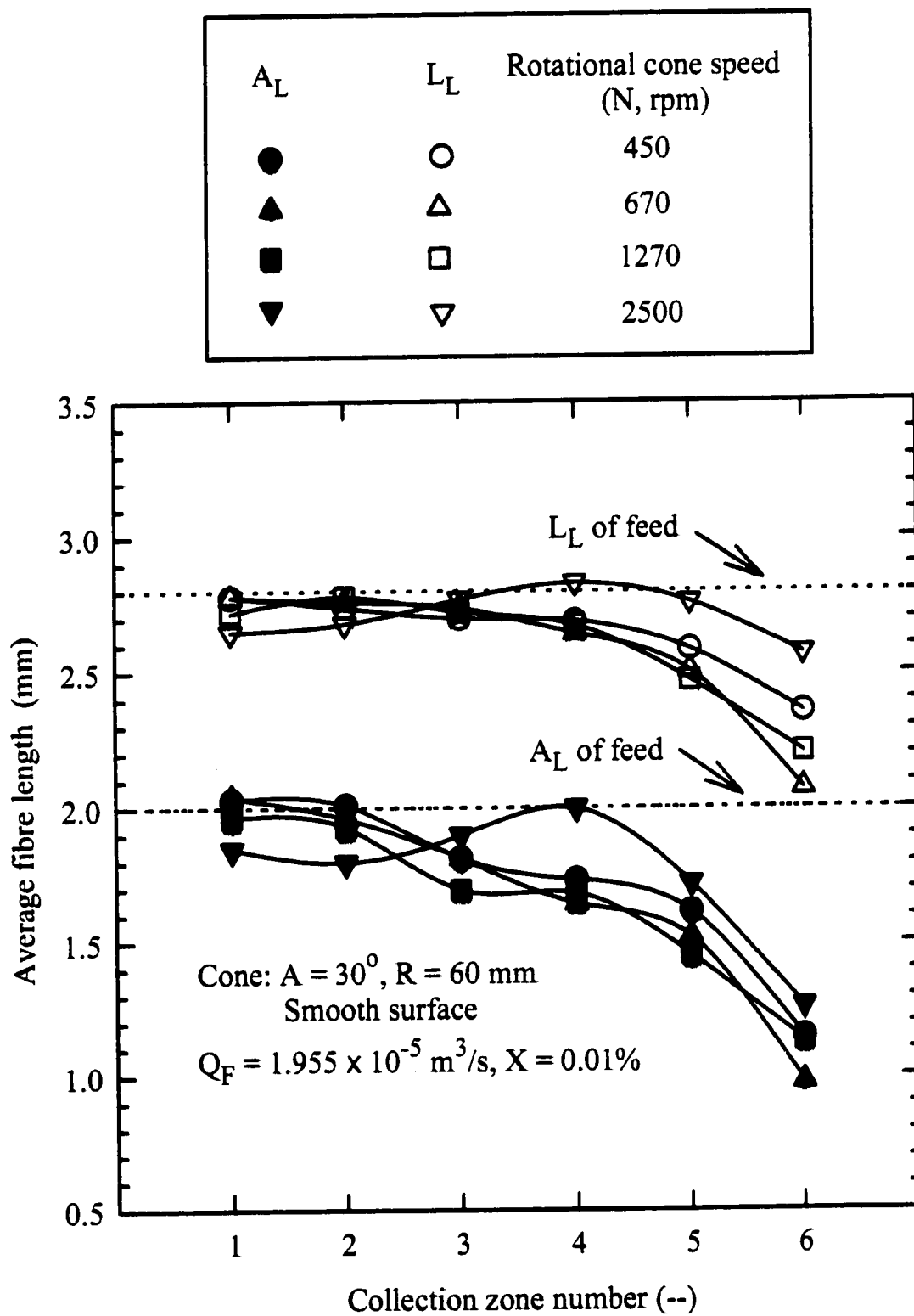


Figure 4.5.5 Variation of average fibre length at different rotational cone speeds



450 rpm



670 rpm



2500 rpm

Photograph 4.5.5 Photographs of suspension flow at three different rotational cone speeds

Cone: $A = 30^\circ$, $R = 60$ mm, $Q_F = 1.955 \times 10^{-5}$ m³/s, $X = 0.01\%$,
 $r_f = 16.5$ mm

4.5.6 Effect of feed consistency

The effect of feed consistency was studied for a 90 mm cone radius. The feed consistency was varied from 0.01 to 0.1 (% w/w). The feed flow rate and rotational cone speed were $1.955 \times 10^{-5} \text{ m}^3/\text{s}$ and 450 rpm, respectively. The feed distributor was located 10.5 mm away from the axis of the rotation. Variation of the average fibre length with the location of collection zone at various feed consistencies is shown in Figure 4.5.6. It is observed that within the range studied, fractionation performances are very similar according to the value of the length weighted average length. However, the value of the arithmetic average length does show that the better fractionation performance occurs at 0.01% feed consistency.

Kerekes (1992) provided an equation for calculating the value of crowding factor (M) which is a measure of the fibre entanglement.

$$M = \frac{2}{3} C_v \left(\frac{L}{D} \right)^2 \quad (4.1)$$

where C_v - volumetric concentration of fibres,

L - fibre length,

D - fibre diameter.

The value of the crowding factor (M) increases as the consistency of fibre suspension increases. They concluded that when $M < 1$, the fibres are free to move relative to one another in translation with occasional collision, and they may remain temporarily together. As M increases from 1 to 60, more collisions take place through translation and then eventually through rotation. For $M > 60$, the fibres become restrained in rotation relative to one another through three-point contact.

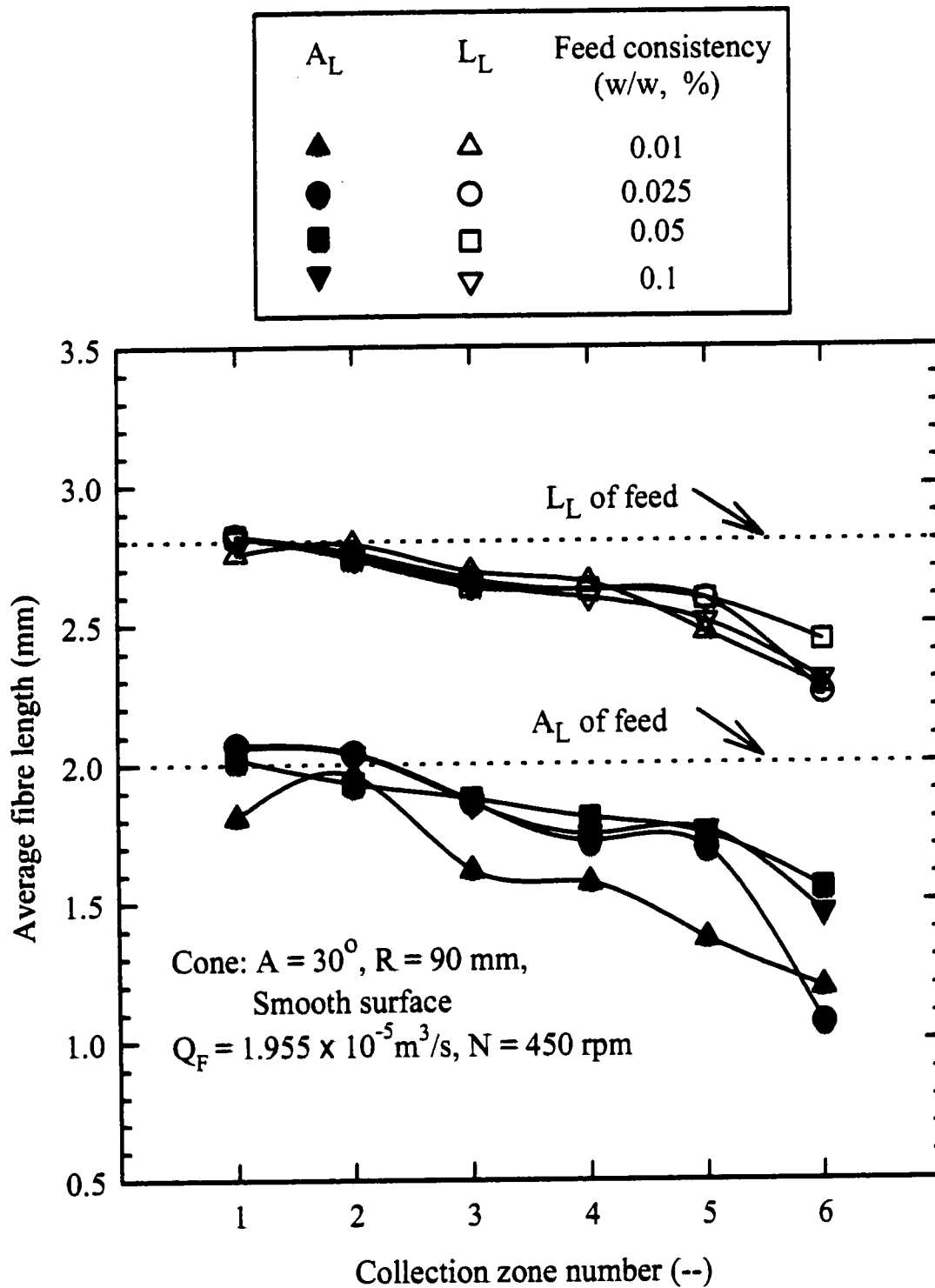


Figure 4.5.6 Variation of average fibre length at different feed consistencies

In the present study, $A_L = 2.00$ mm and $D = 0.02$ mm. Since the density of nylon fibres used is very close to that of the water, for we can approximately use the feed consistency, X (w/w) as being the volumetric concentration of fibres, C_v . Therefore, the crowding factor can be obtained using equation 4.1. They are 0.67, 1.67, 3.33, and 6.67 for consistency 0.01%, 0.025%, 0.05% and 0.1%, respectively. It is clear that only at $X = 0.01\%$, the crowding factor ($M = 0.67$) is in the range of $M < 1$, in which fibres are free to move. For the experimental runs of $X > 0.01\%$, the value of the crowding factors is in the range $1 < M < 60$, in which more collisions occur to obstruct the fractionation performance. Therefore, the better fractionation performance should be expected in the lower consistency because of the fewer interactions among the fibres. This prediction agrees with the experimental results that the better fractionation performance occurs at the low feed consistency of 0.01%.

4.5.7 Effect of cone size

The effect of cone radius was studied at 450 rpm and 670 rpm rotational cone speeds. Two smooth cones having 60 mm and 90 mm cone radii were used. A feed flow rate of $1.955 \times 10^{-5} \text{ m}^3/\text{s}$ and a feed consistency of 0.01% were kept constant. The feed distributor was located 10.5 mm away from the axis of the rotation. Variation of the average fibre length with the location of collection zones at the two different cone diameters are shown in Figure 4.5.7a and Figure 4.5.7b. At 450 rpm, the cone having 90 mm radius gives slightly better fractionation performance than the cone having 60 mm radius. However, both cones give similar fractionation at 670 rpm. Two photographs taken for the 60 mm and 90 mm cone radii at 450 rpm rotational cone speed are shown in Photograph 4.5.7.

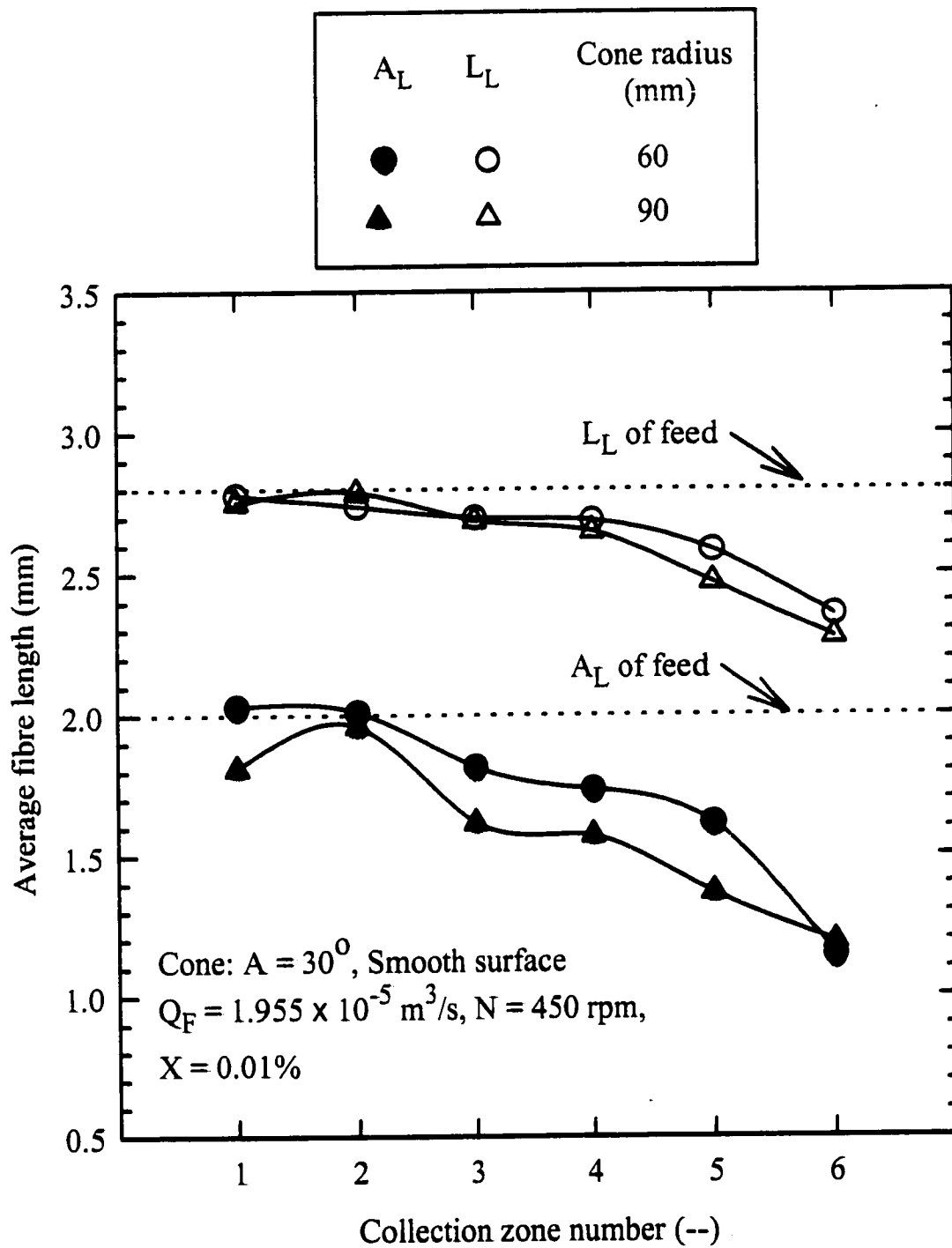


Figure 4.5.7a Variation of average fibre length at different cone radii at $N = 450 \text{ rpm}$

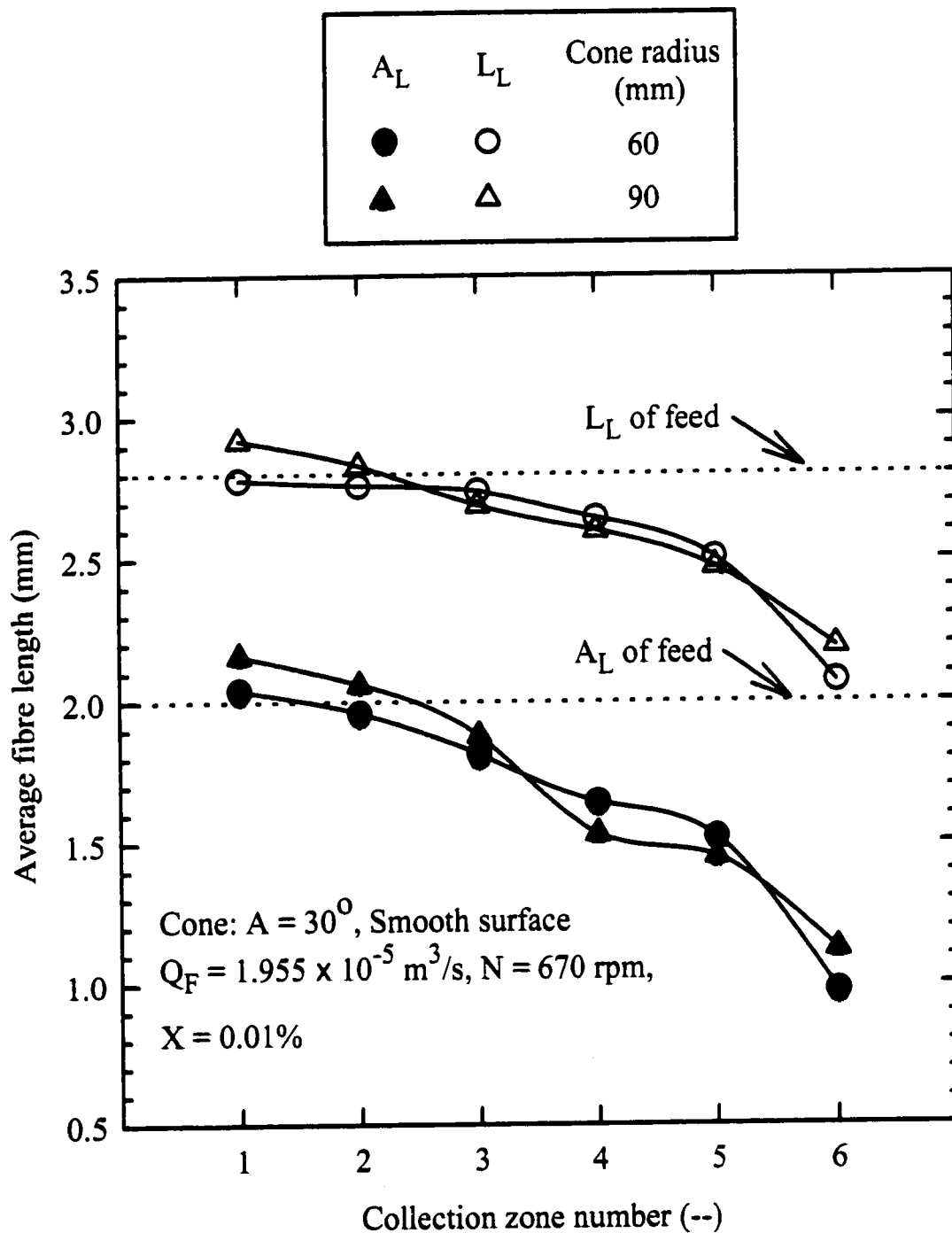


Figure 4.5.7b Variation of average fibre length at different cone radii at $N = 670 \text{ rpm}$



60 mm



90 mm

Photograph 4.5.7 Photographs of flow pattern at two different cone radii

Cone: $A = 30^\circ$, $N = 450$ rpm, $X = 0.01$, $Q_F = 1.955 \times 10^{-5} \text{ m}^3/\text{s}$,
 $r_f = 16.5$ mm

4.6 CONCLUSIONS

For a given fibre diameter, it was found that a rotating cone fractionator fractionates nylon fibres according to fibre length difference. The effect of various parameters studied was found to influence the fractionation performance. The conclusions are as follows:

- A rough surface-rotating cone can not be used to fractionate nylon fibres due to the operating problems associated with it.
- The flow pattern on and around a rotational cone changes with the location of feed distributor.
- Within the experimental range studied, feed flow rate shows no effect on the fractionation performance.
- It has been found that there is an optimal rotational cone speed for a better fractionation performance.
- Feed consistency influences fractionation due to the interaction among the fibres in the suspension. Low feed consistency favors better fractionation.

CHARTPER 5

SUMMARY

The demand for fibre fractionation is increasing due to raw-material shortage, environmental protection demands, and minimizing energy costs. Various studies have been carried out successfully in this area. However, as natural fibres have different fibre length and diameter, it is difficult to assess whether a given fractionation takes place due to different length or diameter. The objective of this study is to determine whether fractionation is due to the fibre length or diameter. Nylon fibres, having the same diameter but different lengths of 1 mm and 3 mm, were used to achieve the goal in the present study. Two methods were used: a vertical settler and a rotating cone fractionator.

A vertical settler, which has previous been used for fractionation of spherical particles, was found to be very successful. It was used in this study to fractionate fibres of the same diameter by their length difference. As the fibre had an orientation parallel to the flow direction, fractionation can take place according to length and

diameter. Experiments were conducted to separate fibres of the same diameter but of different length. A theoretical model has been developed and it agrees fairly well with the experimental results. Various parameters have been studied and the results show that the performance of fibre fractionation decreases with an increase in overflow stream flow rate. Under extreme dilution used in this study there is no effect of feed consistency. The theoretical model expression and experimental results also indicate that fibre fractionation performance improves for larger fibre diameter.

A rotating cone fractionator, which was designed to study hardwood fibre fractionation by Rewatkar and Masliyah, also proved to be capable of fractionating nylon fibres of the same diameter by their length difference. Visual observations, photographs and fibre length measurements suggested that fibre fractionation performance strongly depended on the flow characteristics formed on and surrounding the rotating cone. The study of the various operating parameters showed that the performance of fibre fractionation increases with a decrease in feed consistency. However, there was no effect of feed flow rate within the range studied. It was also found that there was an optimal rotational cone speed for a better fractionation performance. Possible fractionation mechanism was provided based on the literature study.

In the present study, our objective has been well achieved in that nylon fibres of the same diameter can be fractionated according to their length difference.

CHARTPER 6

RECOMMENDATIONS FOR FUTURE WORK

1. In the present study, only few experiments have been carried out to measure the consistency of the fractionated streams. This is due to the very high dilution used in the feed stream. Methods to evaluate consistencies at high dilution should be investigated.
2. In all the experimental tests conducted, fibres of different lengths were tested. However, no experimental tests were conducted on fibres having the same length but different diameters. The difficulty in conducting such tests is that even though fibre quality analyzer can measure both fibre length and coarseness, the accuracy for coarseness measurement is always unsatisfactory due to various problems, such as debris and mass of fibres. Recently, Seth and Chan (1997) studied a new procedure for the measurement of fibre coarseness with optical fibre length analyzers.
3. More efforts should be made to resolve the mechanism as to why fibre fractionation occurs using the RCF method.

REFERENCES

1. Anczurowski, E. and Mason, S. G., "The Kinetics of Flowing Dispersions: II. Equilibrium Orientation of Rods and Discs (Theoretical)", *J. Colloid Interface Sci.* **23**, 522-532 (1967)
2. Batchelor, G. K. and Janse Van Rensburg, R. W., "Structure Formation in Bidisperse Sedimentation", *J. Fluid. Mech.* **166**, 379-407 (1986)
3. Bretherton, F. P., *J. Fluid Mech.* **14**, 284 (1962)
4. Bruin, S., *Chem. Eng. Sci.* **24**, 1647(1969)
5. Clark, J. d'A., "Effect of Fibre Coarseness and Length", *TAPPI* **45** (8), 628 (1962b)
6. Clark, J. d'A., "The Measurement and Influence of Fibre Length", *Paper Trade J.* **115** (26), 36 (1942)
7. Davis, R. H., "Sedimentation of Axisymmetric Particles in Shear Flows", *Phys. Fluids* **A3**, 2051-2060 (1991)
8. Dixon, D. C., "Momentum-Balance Aspects of Free Settling Theory – II. Continuous, Steady-State Thickening", *Separation Sci.* **12**, 193-203 (1977)
9. Eckert, W., Masliyah, J. H. and Afacan, A., "Fractionation of Softwood TMP by Flotation", *TAPPI J.*, **80**, No. 5, 210-216 (1997)
10. Fessas, Y. P. and Weiland, R. H., "Convective Solids Settling Induced by a Buoyant Phase – a New Method for the Acceleration of Thickening", *Resources Conserv.* **9**, 87-93 (1982)
11. Fessas, Y. P. and Weiland, R. H., "The Settling of Suspensions Promoted by Rigid Buoyant Particles", *Int. J. Multiphase Flow* **10**, 485-507 (1984)
12. Forgacs, O. C., "The Characterization of Mechanical Pulps", *Pulp and Paper Magazine of Canada* **64**, T-89 (1963)

13. Fraser, R. P., Dombrowski, P. N. and Routley, J. H., "The Filming of Liquids by Spinning Cups", *Chem. Eng. Sci.* **18**, 323-337 (1963)
14. Happel, J. and Brenner, H., "Low Reynolds Number Hydrodynamics with Special Applications to Particulate Media", Second Edition, Martinus Nijhoff Publishers: The Hague, The Netherlands (1983).
15. Jeffery, G. B., "The Motion of Ellipsoidal Particles Immersed in a Viscous Fluid", *Proc. R. Soc. Lond. Ser. A*, **102**, 161-179 (1922)
16. Karnis, A., Goldsmith, H. L., and Mason, S. G., "The Flow of Suspensions Through Tubes: V. Inertial Effects", *Can. J. Chem. Eng.* **44**, 181-193 (1966)
17. Kerekes, R. J., and Schell, C. J., "Characterization of Fibre Flocculation Regimes by a Crowding Factor", *Journal of Pulp and Paper Science* **18**, J32-38 (1992)
18. Kynch, G. J., "A Theory of Sedimentation", *Trans. Faraday Soc.* **48**, 166-176 (1952)
19. Law, D. H.-S., Masliyah, J. H., MacTaggart, R. S. and Nandakumar, K., "Gravity Separation of Bidisperse Suspensions: Light and Heavy Particle Species", *Chem. Engng. Sci.* **42**, 1527-1538 (1987)
20. Masliyah, J. H., "Hindered Settling in a Multi-Species Particle System", *Chem. Engng. Sci.* **34**, 1166-1168 (1979)
21. Masliyah, J. H., Kwong, T. K. and Seyer, F. A., "Theoretical and Experimental Studies of a Gravity Separation Vessel", *Ind. Engng. Chem. Process Des. Dev.* **20**, 154-160 (1981)
22. Masliyah, J. H., Nasr-El-Din, H., and Nandakumar, K., "Continuous Separation of Bidisperse Suspensions in an Inclined Channel", *Int. J. Multiphase Flow* **15**, 815-829 (1989)
23. Matsumoto, S., Saito, K., and Takashima, Y., "Phenomenal Transition of Liquid Atomization From Disk", *J. Chem. Eng. Japan* **7**(1), 13-19 (1974)
24. Matsumoto, S., Saito, R. and Takashima, Y., *J. Chem. Eng. Japan* **6**(6), 503(1973)

25. Moller K., De Ruvo, A., Norman B., and Felsvang, K., "Screen, Cleaning and Fractionation with an Atomizer", Paper Technology and Industry **20** (3), 110 (1979)
26. Nasr-El-Din, H., Masliyah, J. H., and Nandakumar, K., "Continuous Gravity Separation of Concentrated Bidisperse Suspensions in a Vertical Column", Chem. Engng. Sci. **45**, 849 (1990)
27. Nasr-El-Din, H., Masliyah, J. H., Nandakumar, K., and Law, H.-S., "Continuous Separation of a Bidisperse Suspension in a Vertical Column", Chem. Engng Sci. **43**, 3225-3234 (1988)
28. Nasr-El-Din, H., Masliyah, J. H., Nandakumar, K., and Law, H.-S., "Continuous Gravity Separation of Concentrated Bidisperse Suspension in an Inclined Plate Settler", Int. J. Multiphase Flow **16**, 909-919 (1990)
29. Oroskar, A. R. and Crosby, E. J., "Vaneless Disk Fractionation of Slurries", Industrial and Engineering Chemistry, Fundamentals, **25** (4), 483 (1986)
30. Oroskar, A. R., "Spray Fractionation", Ph.D. Thesis, University of Wisconsin-Madison, Madison, WI (1981).
31. Patwardhan, V. S. and Tien, C., "Sedimentation and Liquid Fluidization of Solid Particles of Different Sizes and Densities", Chem. Engng Sci. **40**, 1051-1060 (1985)
32. Pruppacher, H. R., LeClair, B. P. and Hamielec, A. E., J. Fluid Mech. **44**, 781-790 (1970)
33. Rewatkar, V. B. and Masliyah, J. H., "Hardwood Fibre Fractionation Using Rotating Cone", Can. J. Chem. Eng. **75**, 196-204 (1997)
34. Rewatkar, V. B. and Masliyah, J. H., "Wood Pulp Fibre Fractionation", in "Mixed-Flow Hydrodynamics", Advances in Engineering Fluid Mechanics Series, N. P. Cheremisinoff, Ed., Gulf Publishing Company, Houston, TX, 871-906 (1996)

35. Richardson, J. F. and Meikle, R. A., "Sedimentation and Fluidization Part III", Trans. Instn Chem. Engrs **39**, 348-356 (1961)
36. Romero, C., Agarwala, J. P. and Davis, R. H., "Separation and Classification of Axisymmetric Particles in an Inclined Settler", Int. J. Multiphase Flow **19**, 803-816 (1993)
37. Saffman, P. G., J. Fluid Mech., **1**, 540 (1956)
38. Selim, M. S., Kothari, A. C. and Turian, R. M., "Sedimentation of Multisized Particles in Concentrated Suspension", A.I.Ch.E. J. **29**, 1029-1038 (1983)
39. Seth, Rajinder S. and Chan, Ben K., "Measurement of Fibre Coarseness with Optical Fibre Length Analyzers", TAPPI. J. **80**, 217-219 (1997)
40. Smith, T. N. "The Differential Sedimentation of Particles of Two Different Species", Trans. Instn Chem. Engrs **43**, T69-73 (1965)
41. Smook, G.A. "Hand Book for Pulp and Paper Technologists", Second Edition, Augus Wilde Publications (1992)
42. Starkey, T. V., "The Laminar Flow of Stream of Suspended Particles", Brit. J. Appl. Phys. **7**, 52-55 (1956)
43. Talmadge, W. P. and Fitch, E. B., "Determining Thickener Unit Areas", Ind. Engng Chem. **47**, 38-41 (1955)
44. Tarrer, A. R., Lim, H. C., Koppel, L. B. and Grady, C. P. L., "A Model for Continuous Thickening", Ind. Engng Chem. Process Des. Dev. **13**, 341-346 (1974)
45. Weiland, R. H. and McPherson R. R., "Accelerated Settling by Addition of Buoyant Particles", Ind. Engng Chem. Fundam. **18**, 45-49 (1979)
46. Weiland, R. H., Fessas, Y. P. and Ramarao, B. V., "On Instabilities Arising During Sedimentation of Two-Component Mixtures of Solids", J. Fluid Mech. **142**, 383-389 (1984)
47. Whitmore, R. L., "The Sedimentation of Suspensions of Spheres", Br. J. Appl. Phys. **6**, 239-245 (1955)

APPENDIX I

Data for all the figures included in this thesis.

1. Figure 3.4.1a Variation of average fibre length in the overflow and underflow streams with split ratio

Split ratio	Feed	0.14	0.26	0.38	0.41	0.52	0.58	0.60	0.63
A _{Lo} (mm)	2.00	0.48	0.88	1.33	1.40	1.61	1.73	1.75	1.84
L _{Lo} (mm)	2.80	1.29	1.58	2.02	2.17	2.33	2.47	2.49	2.58
A _{Lu} (mm)	2.00	2.11	2.12	2.17	2.16	2.15	2.15	2.14	2.22
L _{Lo} (mm)	2.80	2.83	2.84	2.85	2.84	2.85	2.84	2.86	2.90

where subscribe "O" represents overflow and "U" for underflow.

2. Figure 3.4.2a & b Variation of the arithmetic and the length weighted average fibre lengths with split ratio at different feed flow rates

Split ratio	Feed	0.14	0.26	0.41	0.52	0.60	0.63
A _{L1} (mm)	2.00	0.48	0.88	1.40	1.61	1.75	1.84
L _{L1} (mm)	2.80	1.29	1.58	2.17	2.33	2.49	2.58
Split ratio	Feed	0.12	0.15	0.22	0.26	0.29	0.36
A _{L2} (mm)	2.00	0.51	0.76	1.15	1.50	1.80	1.91
L _{L2} (mm)	2.80	1.54	1.61	1.87	2.23	2.57	2.63
Split ratio	Feed	0.08	0.10	0.12	0.17	0.22	0.25
A _{L3} (mm)	2.00	0.44	0.87	1.35	1.92	1.88	2.01
L _{L3} (mm)	2.80	1.72	1.66	2.08	2.67	2.63	2.71

where subscribe number represents different feed flow rate, "1" for $2.819 \times 10^{-6} \text{ m}^3/\text{s}$, "2" for $4.657 \times 10^{-6} \text{ m}^3/\text{s}$, and "3" for $9.077 \times 10^{-6} \text{ m}^3/\text{s}$.

3. Figure 3.4.3a Variation of average fibre length at different feed consistencies

Split ratio	Feed	0.12	0.15	0.22	0.26	0.29	0.36
A _{L1} (mm)	2.00	0.51	0.76	1.15	1.50	1.80	1.91
L _{L1} (mm)	2.80	1.54	1.61	1.87	2.23	2.57	2.63
Split ratio	Feed	0.14	0.21	0.27	0.30	0.33	
A _{L2} (mm)	2.00	0.98	1.23	1.50	1.59	1.76	
L _{L2} (mm)	2.80	1.53	1.76	2.19	2.39	2.49	

where subscribe number represents different feed consistency, "1" for 0.01% and "2" for 0.05%.

4. Figure 3.4.4a & b Variation of average fibre length with split ratio for 20 μ m and 14 μ m fibre diameters

Split ratio	Feed	0.12	0.15	0.22	0.26	0.29	0.36
A _{L1} (mm)	2.00	0.51	0.76	1.15	1.50	1.80	1.91
L _{L1} (mm)	2.80	1.54	1.61	1.87	2.23	2.57	2.63
Split ratio	Feed	0.05	0.11	0.19	0.26	0.31	0.35
A _{L2} (mm)	1.59	1.56	1.38	1.61	1.61	1.60	1.57
L _{L2} (mm)	2.51	2.67	2.26	2.55	2.55	2.53	2.51

where subscribe number represents different type of nylon fibres, "1" for 20- μ m fibre diameter and "2" for 14- μ m fibre diameter.

5. Figure 4.5.1a Variation of average fibre length at different collection zones

Source	Feed	Zone 1	Zone 2	Zone 3	Zone 4	Zone 5	Zone 6
A_L (mm)	2.00	2.09	1.91	1.69	1.53	1.60	1.23
L_L (mm)	2.80	2.81	2.79	2.64	2.59	2.46	2.29

where A_L represents arithmetic mean length and L_L for length weighted mean length.

6. Figure 4.5.1c Variation of percentage of fibre weight with collection zone

Source	Zone 1	Zone 2	Zone 3	Zone 4	Zone 5	Zone 6
fraction (%, w/w)	53.2	26.1	10.9	4.2	3.3	1.1

7. Figure 4.5.2a Reproducibility test for a smooth surface cone

Source	Feed	Zone 1	Zone 2	Zone 3	Zone 4	Zone 5	Zone 6
A_{L1} (mm)	2.00	2.09	1.91	1.69	1.53	1.60	1.23
L_{L1} (mm)	2.80	2.81	2.79	2.64	2.59	2.46	2.29
A_{L2} (mm)	2.00	1.81	1.96	1.62	1.57	1.37	1.19
L_{L2} (mm)	2.80	2.76	2.79	2.69	2.65	2.47	2.28

where "1" represents test 1 and "2" for test 2.

8. Figure 4.5.2b Reproducibility test for a 20-mesh surface cone

Source	Feed	Zone 1	Zone 2	Zone 3	Zone 4	Zone 5	Zone 6
A_{L1} (mm)	2.00	2.22	1.87	1.89	1.28	0.78	0.67
L_{L1} (mm)	2.80	2.93	2.72	2.72	2.49	2.15	2.06
A_{L2} (mm)	2.00	1.94	1.90	1.61	1.68	1.18	1.35
L_{L2} (mm)	2.80	2.78	2.78	2.67	2.67	2.39	2.59

where "1" represents test 1 and "2" for test 2.

9. Figure 4.5.3a Variation of average fibre length at different radial locations of feed distributor

Source	Feed	Zone 1	Zone 2	Zone 3	Zone 4	Zone 5	Zone 6
A_{L1} (mm)	2.00	1.81	1.96	1.62	1.57	1.37	1.19
L_{L1} (mm)	2.80	2.76	2.79	2.69	2.65	2.47	2.28
A_{L2} (mm)	2.00	1.88	1.92	1.54	1.73	1.40	1.06
L_{L2} (mm)	2.80	2.78	2.84	2.69	2.73	2.45	2.25
A_{L3} (mm)	2.00	2.01	2.03	1.96	1.68	1.20	1.08
L_{L3} (mm)	2.80	2.76	2.87	2.80	2.57	2.21	1.97

where subscript represents the radial location of feed distributor r_p , "1" for 16.5 mm, "2" for 25.5 mm and "3" for 40.5 mm.

10. Figure 4.5.3c Variation of average fibre length at different rotational cone speeds
at $r_f = 25.5\text{mm}$

Source	Feed	Zone 1	Zone 2	Zone 3	Zone 4	Zone 5	Zone 6
A_{L1} (mm)	2.00	2.05	1.64	1.44	1.74	1.56	1.43
L_{L1} (mm)	2.80	2.82	2.65	2.51	2.70	2.69	2.52
A_{L2} (mm)	2.00	1.88	1.92	1.54	1.73	1.40	1.06
L_{L2} (mm)	2.80	2.78	2.78	2.69	2.73	2.45	2.25
A_{L3} (mm)	2.00	2.00	1.84	1.57	1.96	1.58	1.23
L_{L3} (mm)	2.80	2.83	2.81	2.68	2.73	2.53	2.24
A_{L4} (mm)	2.00	2.09	2.03	1.88	1.83	1.50	1.33
L_{L4} (mm)	2.80	2.80	2.82	2.72	2.73	2.45	2.21

where subscribe represents different rotational cone speed, "1" for 300 rpm, "2" for 450 rpm, "3" for 670 rpm and "4" for 850 rpm.

11. Figure 4.5.4 Variation of average fibre length at different feed flow rates

Source	Feed	Zone 1	Zone 2	Zone 3	Zone 4	Zone 5	Zone 6
A_{L1} (mm)	2.00	1.88	1.92	1.54	1.73	1.40	1.06
L_{L1} (mm)	2.80	2.78	2.84	2.69	2.73	2.45	2.45
A_{L2} (mm)	2.00	2.19	1.95	1.58	1.54	1.04	1.14
L_{L2} (mm)	2.80	2.89	2.77	2.68	2.59	2.37	2.42
A_{L3} (mm)	2.00	2.01	1.97	1.78	1.42	1.44	1.11
L_{L3} (mm)	2.80	2.82	2.81	2.71	2.64	2.56	2.22

where subscribe number represents different feed flow rates, "1" for $1.955 \times 10^{-5} \text{ m}^3/\text{s}$, "2" for $3.604 \times 10^{-5} \text{ m}^3/\text{s}$, and "3" for $4.755 \times 10^{-5} \text{ m}^3/\text{s}$.

12. Figure 4.5.5 Variation of average fibre length at different rotational cone speeds

Source	Feed	Zone 1	Zone 2	Zone 3	Zone 4	Zone 5	Zone 6
A _{L1} (mm)	2.00	2.03	2.01	1.82	1.74	1.62	1.15
L _{L1} (mm)	2.80	2.78	2.74	2.70	2.69	2.59	2.36
A _{L2} (mm)	2.00	2.04	1.96	1.82	1.65	1.52	0.98
L _{L2} (mm)	2.80	2.78	2.76	2.74	2.65	2.51	2.07
A _{L3} (mm)	2.00	1.97	1.93	1.70	1.69	1.45	1.13
L _{L3} (mm)	2.80	2.72	2.78	2.73	2.68	2.47	2.21
A _{L4} (mm)	2.00	1.85	1.80	1.90	2.00	1.72	1.26
L _{L4} (mm)	2.80	2.65	2.68	2.77	2.83	2.76	2.57

where subscript represents different rotational cone speed, "1" for 450 rpm, "2" for 670 rpm, "3" for 1270 rpm and "4" for 2500 rpm.

13. Figure 4.5.6 Variation of average fibre length at different feed consistencies

Source	Feed	Zone 1	Zone 2	Zone 3	Zone 4	Zone 5	Zone 6
A _{L1} (mm)	2.00	1.81	1.96	1.62	1.57	1.37	1.19
L _{L1} (mm)	2.80	2.76	2.79	2.69	2.65	2.47	2.28
A _{L2} (mm)	2.00	2.07	2.04	1.87	1.72	1.70	1.07
L _{L2} (mm)	2.80	2.82	2.76	2.67	2.63	2.59	2.25
A _{L3} (mm)	2.00	2.02	1.93	1.88	1.81	1.75	1.55
L _{L3} (mm)	2.80	2.82	2.74	2.64	2.63	2.59	2.44
A _{L4} (mm)	2.00	2.06	2.04	1.86	1.75	1.76	1.46
L _{L4} (mm)	2.80	2.82	2.75	2.65	2.60	2.51	2.30

where subscript number represents different feed consistency, "1" for X = 0.01%, "2" for 0.025%, "3" for 0.05% and "4" for 0.1%.

14. Figure 4.5.7a Variation of average fibre length at different cone radii
at N = 450 rpm

Source	Feed	Zone 1	Zone 2	Zone 3	Zone 4	Zone 5	Zone 6
A_{L1} (mm)	2.00	2.03	2.01	1.82	1.74	1.62	1.15
L_{L1} (mm)	2.80	2.78	2.74	2.70	2.69	2.59	2.36
A_{L2} (mm)	2.00	1.81	1.96	1.62	1.57	1.37	1.20
L_{L2} (mm)	2.80	2.76	2.79	2.69	2.65	2.47	2.28

where subscript represents different cone radii, "1" for 60 mm "2" for 90 mm.

15. Figure 4.5.7b Variation of average fibre length at different cone radii
at N = 670 rpm

Source	Feed	Zone 1	Zone 2	Zone 3	Zone 4	Zone 5	Zone 6
A_{L1} (mm)	2.00	2.04	1.96	1.82	1.65	1.52	0.98
L_{L1} (mm)	2.80	2.78	2.76	2.74	2.65	2.51	2.07
A_{L2} (mm)	2.00	2.16	2.06	1.88	1.53	1.45	1.12
L_{L2} (mm)	2.80	2.92	2.83	2.69	2.60	2.47	2.19

where subscript represents different cone radii, "1" for 60 mm "2" for 90 mm.

APPENDIX II

Conversion for term $\alpha_{so}/(\alpha_{so} + \alpha_{lo})$

FQA can provide all the information about the number of fibres for each group ranging from to 4 mm or over (for example, 0.05 mm ~ 0.1 mm, 0.1 mm ~ 0.15 mm, 0.15 mm ~ 0.20 mm,..., 3.0 mm ~ 3.05 mm...etc..). Since the total amount of fibres measured (n) as well as the number of fibres in fibre length group (n_j) are known, the fraction of each group fibre length (α_j) can be calculated by the following equation:

$$\alpha_j = (n_j A_{Lj}) / (n A_L) \quad \text{where } j \text{ is the number of the fibre group}$$

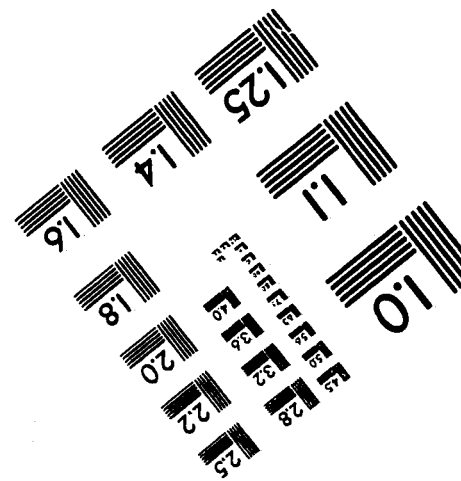
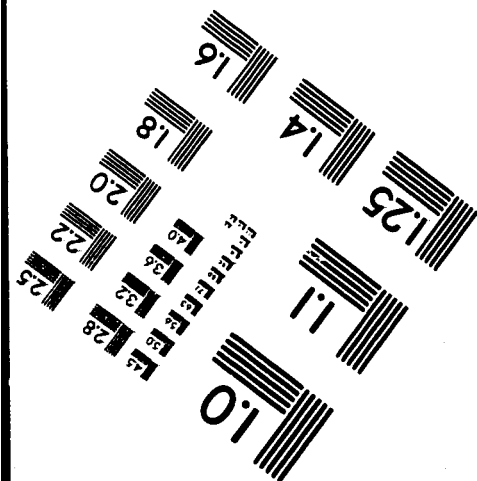
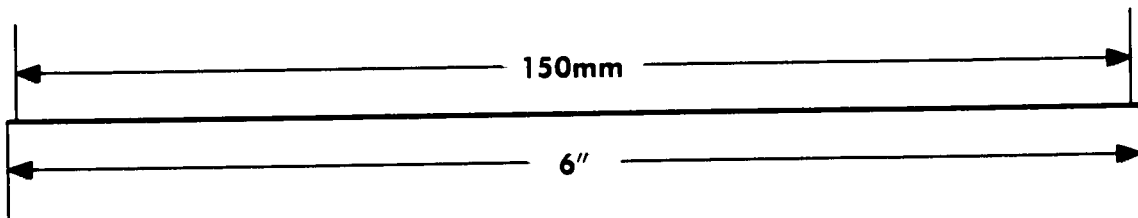
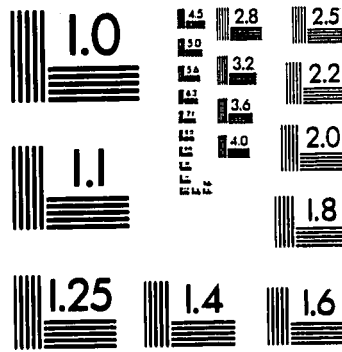
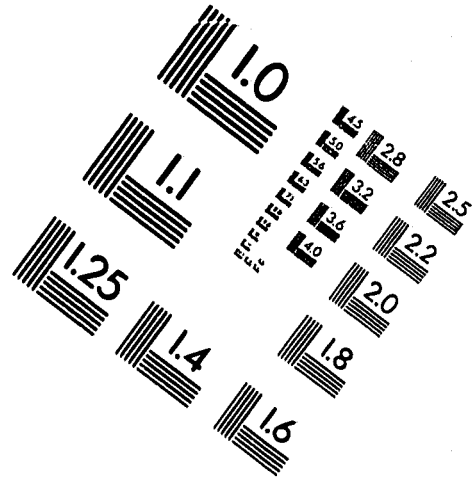
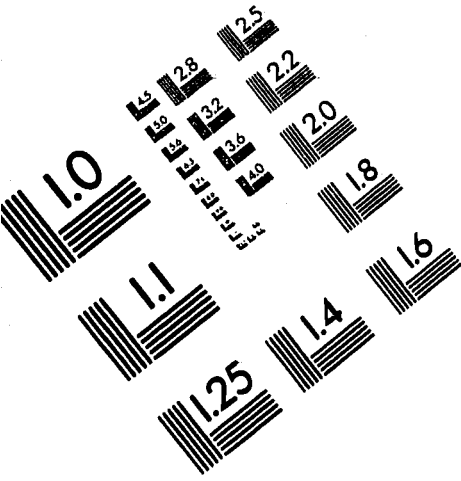
In the present study, the length range of short fibre and long fibre chosen are 0.8 mm ~ 1.2 mm and 2.8 mm ~ 3.2 mm, respectively. Fraction of them can be calculated by the following equations:

$$\alpha_{so} = \sum n_j A_{Lj} / (n A_L) \quad \text{where } j = 16, 17, \dots, 24.$$

$$\alpha_{lo} = \sum n_j A_{Lj} / (n A_L) \quad \text{where } j = 56, 57, \dots, 64.$$

Then, the term of fraction ratio of short fibre in overflow, $\alpha_{so}/(\alpha_{so} + \alpha_{lo})$, can be calculated.

IMAGE EVALUATION TEST TARGET (QA-3)



APPLIED IMAGE, Inc
1653 East Main Street
Rochester, NY 14609 USA
Phone: 716/482-0300
Fax: 716/298-5989

© 1993, Applied Image, Inc., All Rights Reserved